PROBING SUPRAMOLECULAR ASSEMBLIES
VIA
FLUORESCENT REPORTER MOLECULES

A Dissertation

Presented to

The Faculty of the Graduate School

University of Missouri – Columbia

In Partial Fulfillment

of the Requirements for the Degree

Doctor of Philosophy

---

by

DANIEL BOUTROS BASSIL

Dr. Sheryl A. Tucker, Dissertation Supervisor

MAY 2007

The undersigned, appointed by the Dean of the Graduate School, have examined the dissertation entitled

PROBING SUPRAMOLECULAR ASSEMBLIES
VIA
FLUORESCENCE REPORTER MOLECULES

Presented by Daniel B. Bassil

A candidate for the degree of Doctor of Philosophy

And herby certify that in their opinion it is worthy of acceptance.

Professor Sheryl Tucker

Professor Jerry Atwood

Professor Michael Greenlief

Professor Timothy Glass

Professor Youssef Saab

DEDICATION

I dedicate this work to: my father *Pierre*, my mother *Aurore*, my brother *Paul*, my sister *Carelle*, my uncle *Antoine*, my aunt *Mathilde* and her family, my aunt *Diamant*, my aunt *Carol* and her family, my late aunt *Loulou* and her family, my cousins *Saba*, *Bassil* and his family, *Marie José* and her family, and last but not least to the soul of my grand parents.

ACKNOWLEDGMENTS

First, I would like to express my gratitude to my supervisors, Dr. Sheryl A. Tucker for her encouragement, guidance, and friendship throughout my research. My appreciation goes to Dr. Jerry L. Atwood for his collaboration during this research, and to all their former and current group members.

My appreciation goes to all my friends that I met in the Chemistry Department. I am deeply grateful to the Department of Chemistry at the University of Missouri – Columbia (MU), for giving me this great opportunity to undertake my doctoral degree at this institution. My appreciation goes as well to Dr. Elias, Dr. Youssef Saab and their families for persuading me to continue my studies at MU.

Finally, the support and encouragement from my family and friends have given me the impetus to accomplish my goals in life. Their presence and prayers made my graduate years an enjoyable experience.

TABLE OF CONTENTS

LIST OF FIGURES

LIST OF TABLES

ABBREVIATIONS

^{1}H-NMR	Proton nuclear magnetic resonance
ACN	Acetonitrile
ACS	American Chemical Society
ADMA	1-(9-Anthryl)-3-(4-dimethylaniline) propane
atm	Atmosphere
au	Arbitrary unit
$CDCl_3$	Deuterated chloroform
CT	Charge transfer
DMA	*N*,*N*-dimethylaniline
DMSO	Dimethyl sulfoxide
EA	Ethyl acetate
fs	Femtosecond
FTIR	Fourier transform infrared spectroscopy
HEX	Hexane
HPLC	High performance liquid chromatography
J	Joules
λ_{ex}	Excitation Wavelength
MEM	Maximum entropy method

MHF	Multi-harmonic Fourier transform
ns	Nanosecond
PAH	Polycyclic aromatic hydrocarbon
PBA	Pyrene butyric acid
Pd/C	Palladium on carbon
PgC_n	*C*-alkylpyrogallol capsule
PMT	Photomultiplier tube
Py	Pyrene
sec	Second
THF	Tetrahydrofuran
wt	Weight

PROBING SUPRAMOLECULAR ASSEMBLIES *VIA* FLUORESCENCE REPORTER MOLECULES

Daniel B. Bassil

Dr. Sheryl A. Tucker, Dissertation Supervisor

ABSTRACT

Supramolecular, self-assembled nanocapsules have shown the capability to encapsulate organic guests. Since most of the work was done previously in the solid state, the novelty of this research was its focus on probing hydrogen-bonded *C*-alkylpyrogallol[4]arenes, PgC_6, nanocapsules in the solution. Nanocontainers of PgC_6 were self-assembled from six Pg building blocks, enclosing over 1200 $Å^3$ of space. Steady-state and dynamic fluorescence spectroscopic techniques were used to interrogate the organization of the capsule interior when fluorescent reporter molecules, (1-(9-anthryl)-3-(4-dimethylaniline) propane) and pyrene butyric acid, became entrapped. Solution state spectroscopic data, in agreement with solid state single crystal X-ray crystallographic results, determined the number of guests encapsulated, the nature of the

entrapment, and the robustness of the host-guest interaction. Additional work alluded to the goodness-of-fit criterion between guest and host for successful encapsulation of future entities. This work advanced the understanding of the unique nanopockets created by these PgC_6 assemblies.

Chapter 1: Introduction

I. Self-assembled nanocapsules:

According to the 1987 Nobel Laureate Jean-Marie Lehn, self-assembly is the "evolution towards spatial confinement through spontaneous connection of a few/many components, resulting in the formation of discrete/extended entities at either the molecular, covalent or the supramolecular, non-covalent level."[1] Lehn shared this honorable prize with Donald Cram and Charles Pedersen for their efforts in macromolecule recognition, particularly their synthesis of the cryptands.[2] Self-assembled nanocapsules form complex macromolecules from several building blocks connected together through different type of bonding: van der Waal's interaction, hydrogen bonds, metallic, and/or polar bonds.[3] Most important, the formation of the non-covalent, self-assembled capsules is not guided or dictated by any specific factor. The self-assembled capsules covered in this dissertation form through intermolecular interactions; a good example of the intramolecular self-assembly is the folding of proteins, which are not the subject of this work.

Nanocapsule is a general term for an entity that is capable, if the volume permits,[4,5] of hosting a guest in it is interior. In 1872, Adolf von Baeyer, was the first successful chemist to be able to create a nanocapsule – viscous brownish resins, with no characterization of its structure.

John Cornforth was the first to recognize that these capsules might house molecules.[6] Scientists have been greatly interested in the self-assembly phenomena, since these processes occur in biological systems, and research efforts in order to understand the theory behind the process are underway.[4,5] During the 1983 Nobel Lecture, Nobel Laureate Aaron Klug, highlighted the fact that many biological organisms are self-assembled, self-organized, and self-checking.[7] Klug's paper focused on the Tobacco Mosaic virus, which is the result of a self-assembly of the same protein around an embedded RNA. The virus consists of multiple layers of proteins and in every layer, 16⅓ units exist, leading to a cylindrical shaped species.[7] The same concept has been shown to be present in the formation of hemoglobin from polypeptide subunits.[8] Several other biological systems are also self-assembled species: spherical viruses (i.e. Human Wart virus[7] and Rhinovirus), helical rod-like species (i.e. Tobacco Mosaic virus[7], amphiphilic dendritic dipeptides[9] and others[10]) and virions (Cowpea chlorotic mottle virus). The Cowpea Chlorotic Mottle virus is the self-assembly of 180 identical units. This specific specie has a gating process allowing the release and entrapment of guests, depending on physiological changes.[11]

Supramolecular self-assembled nanocapsules are potentially useful models for complex biological processes.[12,13] For instance, the interior of these capsules resemble the hydrophobic pockets of enzymes.[14] The possibility of hosting a guest in a macromolecule has fascinated scientists for long time, especially given that nature has already created the cell with an enormous amount of particles inside a protective

environment. Self-assembling nanocapsules, tracking the changes of their interior, and investigating if any changes in the host-guest interaction occur or if the capsules communicate with each other would be a great start in replica of cell behavior. Understanding the host-guest relationship is currently a hot topic, since this might provide promising answers with regard to nanotechnologies involving drug delivery, receptors technology, clean chemical synthesis, assembly of novel materials, and separation science.[3,15] Details of these current issues are described below:

- In drug delivery technology,[16] physicians prefer to prescribe patients one pill a week or even a month versus daily pills.[17] A good example would be the drug for osteoporosis.[18] The slow release of the medicine from the capsule to the active site would make the pill active in the human body for a longer time. In addition, frequently swallowing pills might increase the chances of side effects, such as nausea and drowsiness.
- In the separation sciences, Sephadex® is a macromolecule with many hydrophobic pockets used in a column for separation of natural products like flavonoids. It packs smaller molecules first and eluting the larger ones first. Atwood *et al.* used the macromolecule techniques for clean fullerene separation.[19]
- In the assembly of novel materials, many are synthesized in today's industry, like the self-assembled "nano-ring" with several cobalt atoms self-assemble under a magnetic field. This ring was first introduced by a Purdue University research

group and was designed to speed computer memories and enhance the data storage capabilities.[20]

- In probing living cells, scientists are looking to interogate cells, while keeping them intact. Catherine Zandonella said back in 2003: "Can we probe the workings of cells without destroying them?" According to some U.S. researchers quoted in the same article, the answer is yes and "the answers rely in nanotechnology."[21]
- In food science, nanotechnology applications are numerous especially in the flavoring department where flavoring would be released or kept intact under extreme conditions such as freezing, cooking, heating etc.
- Applications of the nanocapsule technology also take place in the areas of pesticides and cosmetics.

Clearly, the fact that one/few guest(s) is/are surrounded by host blocks stabilized by non-covalent bonds are of great interest to today's chemical and biological challenges, where many questions could be answered.

II. Examples of several synthesized self-assembled nanocapsules:

One of the earliest capsules, carceplexe, was prepared by Cram *et al.* in 1989 and is held by covalent bonds.[22] Nearly a decade later Rebek *et al.* managed to synthesize a

non-covalent, self-assembled nanocapsule,[3] and in 1997 Atwood *et al.* synthesized a relatively larger capsule (1500 Å^3) held by 60 hydrogen bonds (Figure 1.1 and 1.2).[13] This Atwood macromolecule is the result of the self-assembly of six building blocks that are tetramers with resorcinol as a subunit. The resulting complex has a shape of a snub cube,[13] which is one of the 13 Archimedean solids.[23]

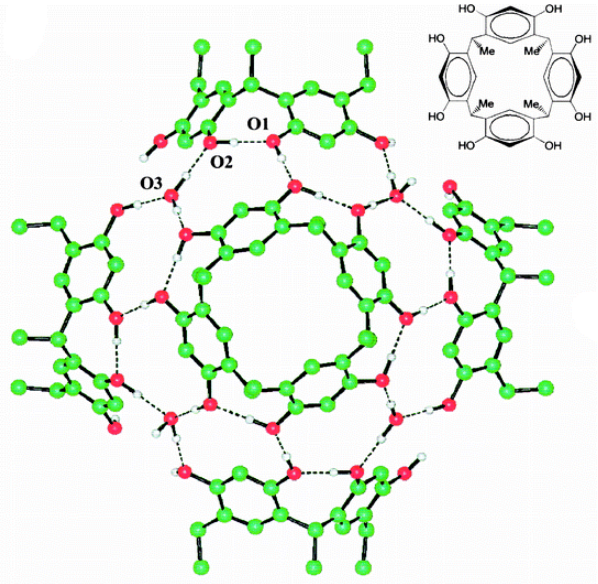

Figure 1.1 A view of the chiral spherical molecular assembly formed by *C*-methylcalix[4]resorcinarenes with water molecules (the dashed lines represents the hydrogen bonds).[13] The molecular structure of resorcinol is shown in the upper right side of the figure. (This structure is used with permission from Leonard R. MacGillivray, Assistant Professor; Department of Chemistry, The University of Iowa.[24])

The green volume shown in Figure 1.2 is the interior volume of the capsule that has a potential to be occupied by a guest; solvent is always encapsulated. In 1999, Mattay *et al.,* worked on a similar molecule held together by hydrogen bonds, but instead

of having resorcinol as a subunit, they used pyrogallol (Figure 1.3).[25] The latter has three *ortho*-hydroxyl groups versus two *meta*-hydroxyl groups for the resorcinol. That extra hydroxyl gave the capsule more strength to stay together, since there are a total of 72 hydrogen bonds versus 60. This capsule showed stability even in polar solvents, and the tails, which are pointing out of the molecular structure, can vary in length from two up to eleven carbons, increasing the hydrophobicity. The grey volume shown in Figure 1.3 is occupied by the solvent used for the crystallization or can be occupied by an organic molecule that has a smaller volume (e.g. pyrene butyric acid[5] or 1-(9-anthryl)-3-(4-dimethylaniline) propane[4]).

The self-assembly of this particular capsule occurs in a solvent that promotes hydrogen bonding, like acetonitrile (ACN) or ethyl acetate (EA). Most of the research reported in this dissertation utilized ACN; EA was used occasionally in order to avoid the use of a highly polar solvent that affects the spectroscopic analysis. For example, in ACN, the fluorescence emission charge-transfer is quenched and red shifted.[5,26] The building blocks are not able to form a capsule in presence of solvents that compete with hydrogen bonding like acetone or ethanol. In this solvent scenario, the resulting crystal produced is a wave-like polymer.

The main issues that a scientist encounters in using nanocapsules for guest encapsulation is making sure that the tetramers are available, checking if the stability of the capsule is affected by the solvent to be used, selecting guest molecules that are smaller than the host, and examining the organization of the interior. To date the

majority of studies have focused on solid-state nanocapsules; however, most applications take place in the solution phase. Therefore, this is the challenge that this work focuses on. Due to its high sensitivity and selectivity fluorescence spectroscopy, with fluorescent probes is the primary approach used in these studies to retrieve solution information from these nanocapsules hosts.

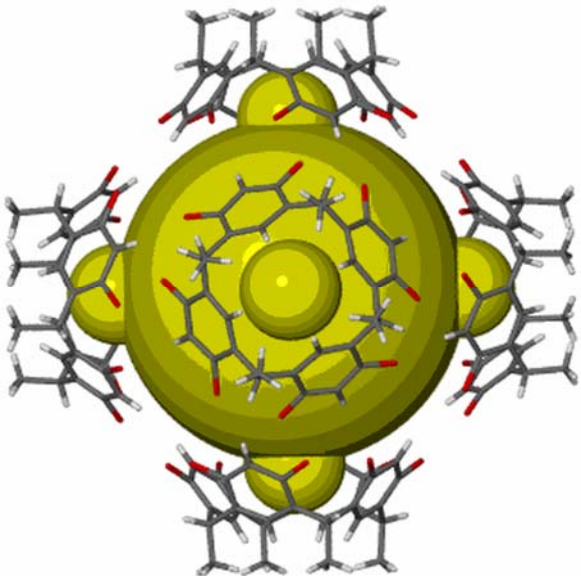

Figure 1.2 X-ray structure of *C*-methylcalix[4]resorcinarenes (hydrogen bonds are removes for clarity). The green color represents the interior volume of the capsule. (The structure was reproduced with permission from Robert M. McKinlay, PhD dissertation 2006; University of Missouri – Columbia.[27])

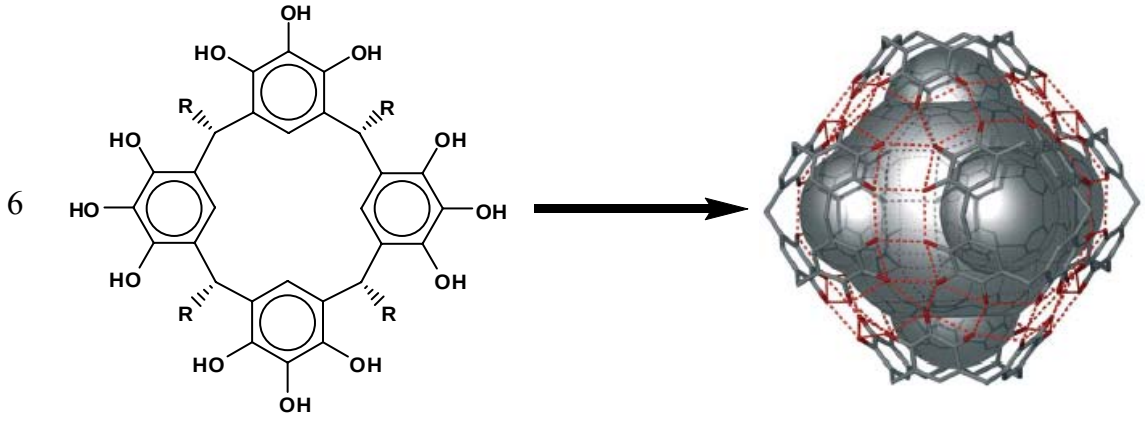

Figure 1.3 Spontaneous self-assembly of *C*-alkylpyrogallol[4]arenes from six tetramers of pyrogallol. Hydrogen bonds are shown as red dots, and the tails R = from C_2 to C_{10}, are removed for clarity reasons. This modified scheme is reproduced from Dalgarno *et al.* 2006.[4,12,25]

III. The fluorescence spectroscopy approach:

Fluorescence spectroscopic techniques are a stable for study complex systems due to minimal sample perturbation, selectivity and sensitivity, where traces amount of probes (10^{-9} mol L^{-1}) can be sensed. Fluorescent reporter molecules (i.e. polycyclic aromatic hydrocarbons) are widely used in both chemical and biological systems.[28-33] Fluorescent reporters respond to the surrounding microenvironment, in variety of ways shown in Figure 1.4, resulting in fluorescence emission intensity increases or decreases, spectral shifts, the appearance or disappearance of specific band(s), shortening or lengthening of the fluorescence lifetime, or even by the appearance of new lifetime decay(s).[34] Once a probe is successfully sequestered in a system information, such as

probe location, microenvironmental polarity, area openness and structural rigidity, may be retrieved. As seen in Figure 1.4, it may be advantageous to use several probes to fully understand a complex system.

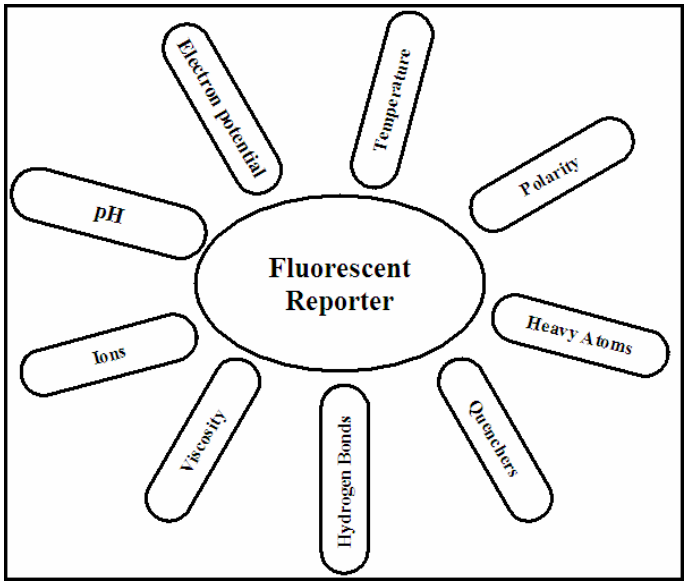

Figure 1.4 Diagram showing the different factors in the surrounding media that affect fluorescent reporters. (Diagram reproduced from Bernard Valeur 1993)[35]

IV. Probing nanocapsule via polycyclic aromatic hydrocarbons:

The self-assembling nanocapsules study here are complex systems, and very little is known about their behavior in solutions. As with traditional types of organized media, such as micelles, dendrimers and cyclodextrins, polycyclic aromatic hydrocarbons

(PAHs) are useful probes of these structures. In this work, several PAHs with a variety of properties were used to study the unique interior aspect of the spheroids: pyrene (solvent polarity probe); pyrene butyric acid (solvent polarity probe that posses a tail to assist with docking); 1-(9-anthryl)-3-(4-dimethylaniline) propane (ADMA; intramolecular charge-transfer complex former); perylene (anisotropy probe); benzo[a]pyrene (large π-surface); anthraquinone (additional chemical functionality incorporated into its base structure); and pentacene (very insoluble, planar, linear molecule).

Since the encapsulation does not affect the ground state, usually the absorbance spectrum of an encapsulated probe will not change compared to its free form in the same solvent. However, fluorescence emission is generally affected by association with other species. For example, if probe is protected from the solvent-solute collisions, non-radiative decay is minimized and its emission intensity is enhanced. In addition, the fluorescent lifetime generally becomes longer once the reporter is encapsulated, since it is protected for normal collisional deactivation.

The capsules are in dynamic systems where the pyrogallol tetramers may open, giving self-assemblies a chance to release their cargo; therefore, dynamic fluorescence techniques were also included in this study. Characterization of these nanocapsules in solution is discussed across this dissertation, where efforts focused on the success and the period of entrapment.

V. References:

(1) Lehn, J. M. *Supramolecular Chemistry: Concepts and Perspectives*, 1995.

(2) Dietrich, B.; Lehn, J. M.; Sauvage, J. P. *Tet. Lett.* **1969**, 2885-8.

(3) Conn, M. M.; Rebek, J., Jr. *Chem. Rev.* **1997**, *97*, 1647-1668.

(4) Dalgarno, S. J.; Bassil, D. B.; Tucker, S. A.; Atwood, J. L. *Angew. Chem., Int. Ed. Engl.* **2006**, *45*, 7019-7022.

(5) Dalgarno, S. J.; Tucker, S. A.; Bassil, D. B.; Atwood, J. L. *Science* **2005**, *309*, 2037-2039.

(6) Cornforth, J. W.; Hart, P. D.; Nicholls, G. A.; Rees, R. J.; Stock, J. A. *Br. J. Pharmacol. Chemother.* **1955**, *10*, 73-88.

(7) Klug, A. *Angew. Chem.* **1983**, *95*, 579-96.

(8) Ackers, G. K. *Biophys. J.* **1980**, *32*, 331-46.

(9) Percec, V.; Dulcey, A. E.; Balagurusamy, V. S. K.; Miura, Y.; Smidrkal, J.; Peterca, M.; Nummelin, S.; Edlund, U.; Hudson, S. D.; Heiney, P. A.; Duan, H.; Magonov, S. N.; Vinogradov, S. A. *Nature* **2004**, *430*, 764-768.

(10) Engelkamp, H.; Middelbeek, S.; Nolte, R. J. M. *Science* **1999**, *284*, 785-788.

(11) Douglas, T.; Young, M. *Nature* **1998**, *393*, 152-155.

(12) Cave, G. W. V.; Antesberger, J.; Barbour, L. J.; McKinlay, R. M.; Atwood, J. L. *Angew. Chem. Int. Ed.* **2004**, *43*, 5263-5266.

(13) MacGillivray, L. R.; Atwood, J. L. *Nature* **1997**, *389*, 469-472.

(14) Rudkevich, D. M. *Bull. Chem. Soc. Jpn.* **2002**, *75*, 393-413.

(15) Cave, G. W. V.; Antesberger, J.; Barbour, L. J.; McKinlay, R. M.; Atwood, J. L. *Angew. Chem., Int. Ed.* **2004**, *43*, 5263-5266.

(16) Shi, X.; Wang, S.; Chen, X.; Meshinchi, S.; Baker, J. R., Jr. *Mol. Pharm.* **2006**, *3*, 144-151.

(17) Chen, B. H.; Lee, D. J. *J. Pharm. Sci.* **2001**, *90*, 1478-1496.

(18) *Harvard women's health watch* **2005**, *12*, 3.

(19) Atwood, J. L.; Koutsantonis, G. A.; Raston, C. L. *Nature* **1994**, *368*, 229-31.

(20) Tripp, S. L.; Dunin-Borkowski, R. E.; Wei, A. *Angew. Chem., Int. Ed.* **2003**, *42*, 5591-5593.

(21) Zandonella, C. *Nature* **2003**, *423*, 10-2.

(22) Sherman, J. C.; Cram, D. J. *J. Am. Chem. Soc.* **1989**, *111*, 4527-8.

(23) MacGillivray, L. R.; Atwood, J. L. *Angew. Chem., Int. Ed.* **1999**, *38*, 1018-1033.

(24) MacGillivray, L. R., The University of Iowa, Iowa City, IA. Personal communication, **2006**.

(25) Gerkensmeier, T.; Iwanek, W.; Agena, C.; Frohlich, R.; Kotila, S.; Nather, C.; Mattay, J. *Eur. J. Org. Chem.* **1999**, 2257-2262.

(26) Lakowicz, J. R. *Principles of Fluorescence Spectroscopy*; 2nd ed.; Kluwer Academic/Plenum Publishers: New York, 1999.

(27) McKinlay, R. M. Ph.D. Dissertation, University of Missouri - Columbia, **2006**.

(28) Katusin-Razem, B.; Wong, M.; Thomas, J. K. *J. Am. Chem. Soc.* **1978**, *100*, 1679-86.

(29) Reichardt, C. *Chem. Rev.* **1994**, *94*, 2319-2358.

(30) Ribou, A.-C.; Vigo, J.; Salmon, J.-M. *Photochem. Photobio.* **2004**, *80*, 274-280.

(31) Richter-Egger, D. L.; Landry, J. C.; Tesfai, A.; Tucker, S. A. *J. Phys. Chem. A* **2001**, *105*, 6826-6833.

(32) Richter-Egger, D. L.; Tesfai, A.; Tucker, S. A. *Anal. Chem.* **2001**, *73*, 5743-5751.

(33) Sortino, S.; Giuffrida, S.; Fazio, S.; Monti, S. *New J. Chem.* **2001**, *25*, 707-713.

(34) Lakowicz, J. R. *Principles of Fluorescence Spectroscopy*; Plenum Press: New York, 1983.

(35) Valeur, B. *Molecular Luminescence Spectroscopy* **1993**, *77*, 25 - 84.

Chapter 2: Theory

The research project described in this dissertation involves probing nanocapsules with fluorescent reporter molecules and understanding complex systems; the main technique used for this purpose is molecular fluorescence, which is performed in an analytical photochemistry laboratory. Primary techniques used include UV-Vis absorbance and fluorescence emission and lifetime, and occasionally anisotropy. These experiments were carried out in conjunction with solid state experiments using proton nuclear magnetic resonance (^{1}H-NMR) and X-ray single crystal diffraction methods, contributions from the Atwood Group.

I. Absorption spectroscopy:

Absorption measurements are the very first experiment that a spectroscopist performs on the system of interest. This measurement gives critical information about where the analyte absorbs and what the concentration is. The absorbance and spectra values obtained also serve as a baseline for monitoring potential ground-state interactions, etc.

It is worth clarifying that *absorbance* is a numerical quantity unlike *absorption* which is the physical process of absorbing the light. Usually the absorbance spectrum is obtained by scanning across a specified wavelength region, where the result is a spectrum

of absorbance intensities in absorbance units (AU) versus wavelength (usually in nanometers). The absorbance law was first discovered by August Beer in 1852, Johann Heinrich Lambert in 1760), and Pierre Bouguer in 1729; it is known as Beer-Lambert-Bouguer law or more commonly Beer's Law (Equation 2.1 and 2.2):

$$A = \varepsilon bc \qquad \textbf{Equation 2.1}$$

$$A = -\log T = \frac{I}{I_0} \qquad \textbf{Equation 2.2}$$

where 'A' is the absorbance, 'ε' is the molar absorptivity in L mol^{-1} cm^{-1}, which is the amount of light absorbed by one molar of the species present and can be determined by measuring the absorbance of a known concentration, 'T' is the transmittance, 'b' represents the pathlength or the sample container size in cm, (typically 1 cm) and 'c' is the concentration of the molecule in mol L^{-1}. Molar absorptivities are larger than 10,000 for highly absorbing molecules and much smaller for weak absorbing molecules. Transmittance, commonly given as percent transmittance %T, is a quantity that reflects the amount of light passing through the solution compared to the reference signal (I/I_0). The higher the percent transmittance the less the solution is absorbing and vise versa. In my research, the pathlength was constant; therefore, the absorbance was directly proportional to the concentration of the solution, which allowed for an easy quantitative technique. For quantitative measurements the absorbance should be below 0.1 AU.

When the signal is above 1 AU, the absorbance versus concentration proportionality is no longer linear. This linear relation can be affected by several other factors as well that are well documented.[1,2]

II. Fluorescence spectroscopy general theory:

Figure 2.1 represents a modified Jablonski energy diagram showing the fluorescence emission path of one molecule after its absorption of light the appropriate energy. Ground (S_0) and excited (S_1 or S_2) electronic states, vibrational levels (ν_n), absorption (A), fluorescence emission (B), vibrational relaxation (C), intersystem crossing (D), and internal and external conversion (E) are noted. The energy difference (Equation 2.3) between S_1 and S_0 is proportional to the frequency (υ) of light or inversely proportional to the wavelength (Equation 2.4).[1,2]

$$E = h\nu \qquad \textbf{Equation 2.3}$$

$$E = \frac{hc}{\lambda} \qquad \textbf{Equation 2.4}$$

where h is the plank's constant (6.626×10^{-34} J.s), c is the speed of light (2.998×10^{8} $m.s^{-1}$), λ is the wavelength in meters and υ is the frequency in Hertz (s^{-1}).

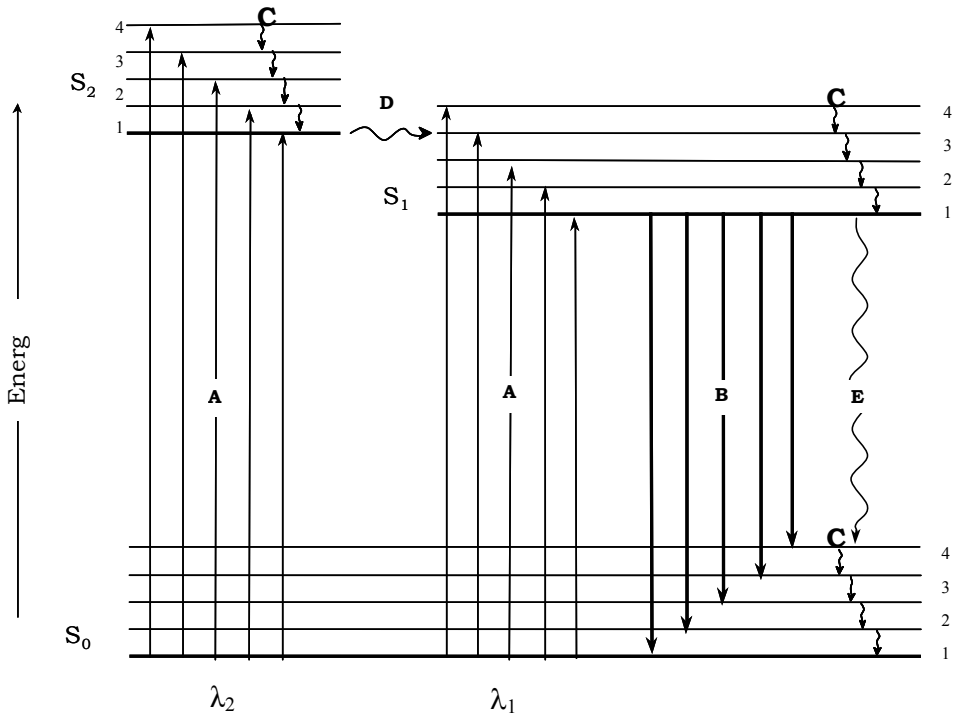

Figure 2.1 Modified Jablonski diagram showing the fluorescence path of one molecule straight after excitation following fluorescence. Ground (S_0) and excited (S_1 or S_2) electronic states, (ν_n) vibrational levels, absorption (A), fluorescence emission (B), vibrational relaxation (C), intersystem crossing (D), and internal and external conversion (E). Solid lines are indicative of radiative processes and wavy lines represent non-radiative pathways. (Redrawn from *the Principles of Fluorescence Spectroscopy*[3]).

After the absorption (~10^{-15} s) takes place[1], vibrational relaxation occurs permitting the relaxation of electrons to the lowest vibrational level in the excited level. The average vibrational relaxation time is on the order of 10^{-12} seconds.[1]

Fluorescence spectroscopy is the main technique used in the research presented in this dissertation, where reliable, and consist results can be obtained at low solution concentrations (*ca.* 10^{-10} mol L^{-1}) versus ^{1}H-NMR, which require significantly higher

concentrations. Fluorescence is one of several radiative phenomena that comprise the concept of luminescence, where light is emitted from any species without heat being involved. If heat is involved, the phenomenon is referred to as incandescence.

As the rate of fluorescence emission (k_{fl}) is measured as an excited state molecule in the lowest vibrational level of the first excited state (S_1) (Figure 2.1) returns to the ground state (S_0). Fluorescence emission competes with three other mechanisms listed below:

- Intersystem crossing (k_i; 10^{-12} – 10^{-4} seconds) which may result in phosphorescence (10^{-12} - 10^{2} seconds)
- Internal conversion (k_{ic}; 10^{-12} seconds)
- External conversion (k_{ec})

All of the above mechanisms are radiationless (aside from phosphorescence). Fluorescence emission may exist from 10^{-9} to 10^{-6} seconds, where molecules minimize the amount of time they spend in the excited state.[1,2,4]

The fluorescence emission spectrum (emission wavelength is plotted against the relative fluorescence intensity) is normally independent from the excitation wavelength. Excitation and absorbance spectra for fluorescent species in a solution may be the same if and only if all molecules that absorb also emit. The amount of fluorescence emission can be quantitated and expressed as quantum yield (Φ_{fl}, Equation 2.5):

$$\Phi_{fl} = \frac{k_{fl}}{(k_{fl} + k_i + k_{ic} + k_{ec})} \qquad \textbf{Equation 2.5}$$

The quantum yield is the ratio of the radiative relaxation rate over the total radiative and non-radiative rates.

In a more general over view is:

$$k_{nr} = k_{fl} + k_i + k_{ic} + k_{ec} + k_{rxn} + k_q \qquad \textbf{Equation 2.6}$$

where k_{nr} is the rate of the non-radiative relaxation, k_{rxn} is the rate calculated from an intramolecular reaction and k_q is the rate due to the fluorescence quenching such as from oxygen present in solution. The intensity of the fluorescence (I_{fl}) is proportional to the quantum yield and the number of absorbed photons (Equation 2.7):

$$I_{fl} = k(\Phi_{fl})P_0(1\text{-}10^{-\varepsilon bc}) \qquad \textbf{Equation 2.7}$$

where at low concentration ($\varepsilon bc << 0.05$ mol L^{-1} most preferably when absorbance is ~0.01). The fluorescence intensity is proportional to the absorbance (Equation 2.8):

$$I_{fl} = k(\Phi_{fl})P_0\varepsilon bc \qquad \textbf{Equation 2.8}$$

where *k* is the instrument constant, P_0 is the excitation intensity. At low concentrations fluorescence is a more selective and more sensitive technique than absorbance, since the relationship between the fluorescence emission intensity is linear with the concentration versus absorbance and the concentration have an exponential relation (Equation 2.9):

$$I = I_0 e^{-\varepsilon bc} \qquad \textbf{Equation 2.9}$$

Fluorescence emission and excitation scanning techniques are used regularly by fluorescence spectroscopists. With fluorescence emission scans, the excitation wavelength is fixed and the emission monochromator is scanned, resulting in an emission spectrum. The later technique is the opposite, where the emission wavelength is set and the excitation monochromator is scanned. When both of the emission and excitation wavelength are scanned sequentially, the technique is called excitation-emission matrix (EEM), where the output is a three dimensional fingerprint, giving more in-depth idea of the different species emitting present in solution.

III. Dynamic fluorescence spectroscopy:

a) Fluorescence lifetime:

Fluorescence lifetimes are the average times that a fluorescent molecule stays in the excited state before it decays to the ground state. Lifetime values result in an absolute unit, unlike the fluorescence emission intensity which is an arbitrary unit. Fluorescent reporters may have different lifetimes, depending on the media they are in. Temperature, pH, polarity, viscosity, and oxygen presence may also affect the lifetime. Lifetime techniques are sensitive and can provide additional information regarding the behavior of the probe in solution or even solid state. For example, once the molecule is in a protected environment or in an environment limiting its mobility, the lifetime gets longer. Micelles, dendrimers, or even viscous solvents are examples of protected environments.[1] Lifetime measurements reveal true time complexity of the sample under investigation.

Fluorescence lifetimes in this study were measured in the frequency domain, which uses a sinusoidally modulated light source, typically a continuous wave (CW) laser, to excite the fluorophore. The resulting emission is accordingly sinusoidally and modulated at the same circular frequency (ω). The circular frequency is equal to $2\pi f$, where f is the applied linear frequency. The fluorescence emission that has the same frequency will be delayed with a phase shift and the signal will be reduced (demodulated) as shown in Figure 2.2.[1,3,5]

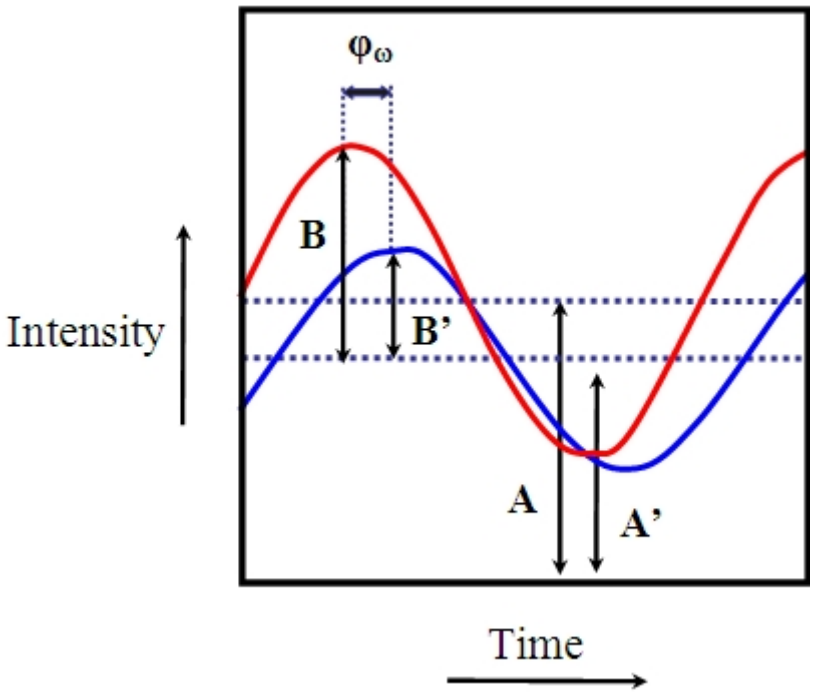

Figure 2.2 Modified phase and modulation diagram for the excitation of a reporter with the modulated light source, where φ_ω is the phase shift between the excitation (red) and the emission (blue) signals.[1] The dynamic to steady state intensity for the excitation and emission are respectively the ratios of B/A and B'/A', where A and A' represent the steady-state intensity, B and B' represent the dynamic-state intensity.

The phase (τ_p; Equation 2.10) and the modulation (τ_m; Equation 2.11) lifetimes are calculated respectively from the phase shift (φ_ω) and the demodulation factor (m_ω):[1,3,5,6]

$$\tau_p = \frac{(\tan\varphi_\omega)}{\omega} \qquad \textbf{Equation 2.10}$$

$$\tau_m = \frac{[\frac{1}{(m_\omega)^2} - 1]^{1/2}}{\omega}$$ **Equation 2.11**

The demodulation factor can be thought of as a ratio of the dynamic-state intensity (B or B') to steady-state intensity (A or A') for both excitation and emission signals (Equation 2.12):[7]

$$m_\omega = \frac{\text{Emission Intensity}}{\text{Excitation Intensity}} = \frac{A \times B'}{A' \times B}$$ **Equation 2.12**

In this technique, the fluorescence lifetime is inversely proportional to the linear applied frequency according to both Equations 2.10 and 2.11. For a single exponential decay, both the phase and modulation can be used to determine the actual lifetime of the fluorophore. For instance, a modulation frequency of 50 MHz and a lifetime of 8 ns, the phase angle calculated from Equation 2.10 would be 68.3°, and the modulation factor calculated from Equation 2.11 would be 0.37, where ω is 2π x 50 MHz. For a multi-exponential decay non-interaction, $\tau_p < \tau_m$ and with external interaction $\tau_p > \tau_m$. The lifetime and the demodulation factor have an inverse relationship, but the lifetime and the phase angle have a linear relationship.

The frequency-domain fluorescence lifetime instrument used in the course of this research utilizes a multiharmonic frequency (multi-harmonic Fourier transform)

modulator, where a synthesizer provides a base frequency and 60 harmonics are generated by a harmonic modulator. This technique allows for the simultaneous collection of both φ_ω and m_ω values across a range of frequencies that correspond to typical fluorophore lifetime values. The multi-harmonic Fourier transform, MHF, technique is advantageous over others, since it provides a wide range of generated frequencies to cover a "lifetime window".[8,9] Frequency-domain methods that do not utilize MHF technology consist of taking individual measurements over several frequencies to determine the correct lifetime of the species present in solution.[1] For complex chemical systems, MHF works better since the several lifetimes that may present in the sample are accounted for by the windowing. The process is fairly fast since the measurement of φ_ω and m_ω are taken simultaneously at all frequencies, a data set of sample and reference pairs can be collected in about 7 seconds with 50 internal averages. Before sample measurements are collected, a scatter solution is used as a calibration marker to accurately determine the lifetime of the reference used. The scatter used in this study was Kaolin where $\varphi_\omega = 0$ and $m_\omega = 1$.

b) Lifetime data analysis:

Lifetime data was analyzed by a self-modeling Maximum Entropy Method (MEM) commercial software package (Phase5, Maximum Entropy Data Consultants, Cambridge, UK),[8-10] and standard nonlinear least squares (NLLS) software program

(Globals Unlimited, Laboratory for Fluorescence Dynamics, Urbana-Champaign, IL). The minimization of goodness-of-fit parameter (χ^2; Equation 2.13) is used by NLLS analysis to determine whether the model is appropriate for the data. Non-linear least square analysis is widely applied for monoexponential species (Equation 2.14) and for multiexponential (Equation 2.15), where F_0 is the initial intensity, α_i the pre-exponential factor, and τ represents the decay of the fluorophore.

$$\chi^2 = \sum_{\omega} \left(\frac{(\varphi_{\omega,calc} - \varphi_{\omega,obs})^2}{\sigma_{\omega,\varphi 2}} + \frac{(m_{\omega,calc} - m_{\omega,obs})^2}{\sigma_{\omega,m2}} \right) / (N - M - 1) \quad \textbf{Equation 2.13}$$

$$F(t) = F_0 e^{-t/\tau} \quad \textbf{Equation 2.14}$$

$$F(t) = \sum_i \alpha_i F_0 e^{-t/\tau} \quad \textbf{Equation 2.15}$$

By using NLLS analysis (Equation 2.13), lifetimes and fractional intensities are resolved. Where $(\omega, calc)$ and (ω, obs) correspond to the calculated and observed values of the circular frequency (ω), respectively. The standard deviation between the calculated and observed ($\sigma_{\omega,\varphi}$ and $\sigma_{\omega,m}$) for the phase and the modulation are determined at a specific frequency, respectively. The total number of data, N, is twice the number of frequencies since both (φ) and (m) are measured at each frequency. The number of unknown lifetimes and fractional intensities is represented by the variable M. The χ^2 is considered statistically valid if its value is between one and two.[11,12] Non-linear least

square, NLLS, method is desirable when working with a well-behaved sample, simple such as the fluorescent components signatures are known.[8]

As suggested in the literature,[13] both NLLS and MEM lifetime analyses are performed for better data interpretation. One of the advantages of MEM over NLLS analysis is that it does not pre-require modeling – it is a "self-modeling" method.[8] The MEM analysis divides designated lifetime window (Figure 2.3) into equal increments, and the algorithm shifts fractional contributions of each lifetime increments resulting in a minimum χ^2 and simultaneously maximizing a statistical entropy (Shannon-Jaynes, Equation 2.16) function. The result is a unique unbiased solution (Figure 2.3) of fractional intensity and the defined lifetimes.[10,14]

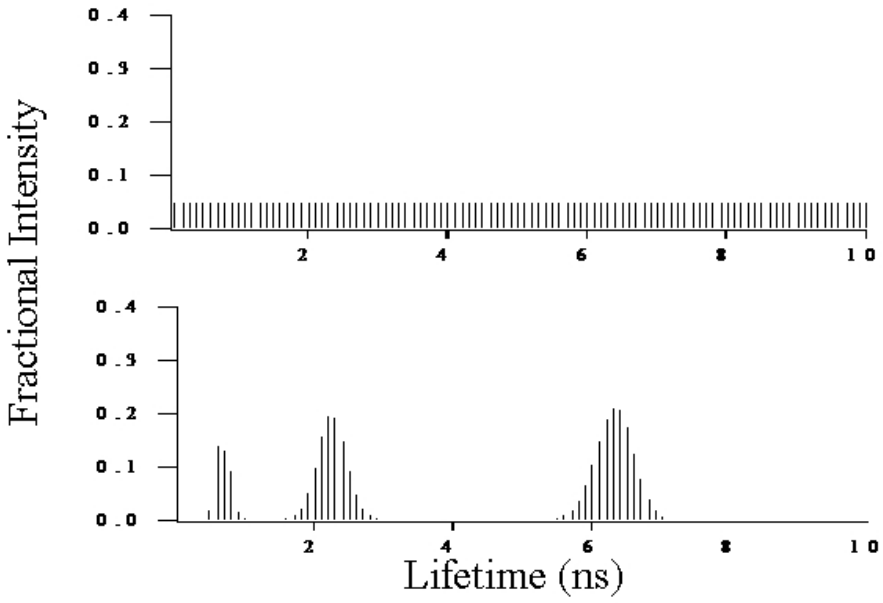

Figure 2.3 MEM's initial guess (top graph) and the final solution of MEM (bottom graph).

$$S = \sum_i p_i \log p_i \qquad \textbf{Equation 2.16}$$

In this work, lifetimes recovered from both methods were found to be in agreement within error. Total lifetime distribution analysis[13] (TLDA), that collects all the sample emission by using a broad filter window was also performed. In addition, broad (80 or 40 nm) and narrow (10 nm) band-pass filters that were centered at the spectral features of interest were included in the studies.

c) Fluorescence anisotropy:

Fluorescence anisotropy is widely used in photochemical laboratories especially, in the biochemical field.[15] Fluorescent probes respond to the polarization of the incident light, excitation source, accordingly, and depending on their rotational freedom during the excited state, their emission is partially polarized. Only those molecules whose transition moments are reoriented similarly to the excitation source polarization are excited – a process knows as photoselection.[1] In anisotropy measurements, the excitation source is vertically polarized to excite the sample, and horizontal (I_{11}), and vertical emissions, ($I_{\perp}$), may be collected sequentially or simultaneously. With these two intensities the fluorescence anisotropy value (r) can be determined (Equation 2.17):

$$r = \frac{I_{11} - I_{\perp}}{I_{11} - 2I_{\perp}} \qquad \textbf{Equation 2.17}$$

where I_{11} and $I_{\perp}$ represents the intensity of the horizontal emission and the vertical emission.[1] The 'r' value is directly proportional to the lifetime, according to the Perrin Equation, and it depends on the solvent viscosity and on the surrounding environment of the reporter. A tightly held fluorophore leads to higher anisotropic values (r = 0.4) versus smaller values (r = 0.0) in a nonviscous solvents.[1]

IV. Fluorescence quenching:

Fluorescence quenching was a critical technique used to reveal information about the encapsulation of the molecule. Fluorescence quenching has been shown to be successful at elucidating system information from several complex systems: Tucker *et al*. used selective quenching agents for polycyclic aromatic hydrocarbons, PAHs, in polyamido amine dendrimers;[16-18] other research groups[19-21] used aliphatic amines as selective quenchers of PAHs;[22] and quenching was used to detect nitrated explosives.[23] In most of our experiments, intermolecular quenching was used with the physical addition of a well-known quencher species containing an amine group, such as *N,N*-dimethylaniline (DMA), dimethylamine, trimethylanaline, nitromethane, diazabicyclo[2.2.2]octane, dibutylamine. Increments of the quencher are added until the

fluorescence emission is totally diminished. Typically, when the probe is encapsulated, the quencher has limited access to the interior of the spheroid, and this leads to less or no effective reduction of the emission intensity by the quencher.[24]

Quenching is a concept with a unique dynamic, consisting of decreasing the fluorescence emission of a species through collision deactivation in the excited state (Equation 2.18).

$$Ar^* + Q \xrightarrow{k_q} [Ar^* \cdot Q] \qquad \textbf{Equation 2.18}$$

where Ar represents the fluorophore (in our case Ar is a PAH), Q represents the quencher and k_q is the quenching rate constant. The quenching is known to be an adiabatic diffusion process. In the absence (Equation 2.19) or presence of the quencher (Equation 2.20), the change of the excited state species concentration is governed by the following equations:

$$\frac{d[Ar^*]}{dt} = k_a[Ar] - k_{fl}[Ar^*] - k_{ic}[Ar^*] - k_{nr}[Ar^*] \qquad \textbf{Equation 2.19}$$

$$\frac{d[Ar^*]}{dt} = k_a[Ar] - k_{fl}[Ar^*] - k_{ic}[Ar^*] - k_{nr}[Ar^*] - k_q[Q][Ar^*] \qquad \textbf{Equation 2.20}$$

where k_a, k_{fl}, k_{ic}, and k_{nr} correspond respectively to the rate constants of the absorbance, fluorescence, internal conversion, and non-radiative relaxation, and k_q is known as the Stern-Volmer quenching constant. [Ar*] and [Q] are the fluorophore and the quencher concentration, respectively. Under steady-state conditions $\frac{d[Ar^*]}{dt} = 0$, where [Ar*] can be solved from Equation 2.19 and 2.20, as shown in Equation 2.21 and 2.22:

$$[Ar^*] = \frac{k_a[Ar]}{(k_{fl} + k_{ic} + k_{nr})} = F_0 \qquad \textbf{Equation 2.21}$$

$$[Ar^*] = \frac{k_a[Ar]}{(k_{fl} + k_{ic} + k_{nr} + k_q[Q])} = F \qquad \textbf{Equation 2.22}$$

Equation 2.19 represents [Ar*] when [Q] is not present, this quantity is directly proportional to the original fluorescence intensity, F_0, (Equation 2.7) before the addition of a quencher, and F is the fluorescence intensity in presence of the quencher. Combining both Equations 2.21 and 2.22 to give the Stern-Volmer equation:

$$\frac{F_0}{F} = 1 + k_q[Q] \qquad \textbf{Equation 2.23}$$

The Stern-Volmer quenching constant, k_q, is the product of the true quenching constant and the excited state lifetime. This constant is determined from the slope of the line,

which can be extrapolated from the Stern-Volmer plot when absorbance corrected fluorescence intensity ratio versus the quencher concentration is plotted. This entity can be determined by a series of experiments involving a well-known concentration of the quencher and recording the fluorescence emission of the quenched fluorophore simultaneously. In general, quenching is the deactivation of a fluorescent species from the excited to the ground state. This quenching is known as dynamic quenching, and when the quencher affects the population of the excited state, it is known by static quenching.

The most common dynamic quenching mechanisms are either inter- or intramolecular charge transfer and quenching can be due to normal collisional deactivation from solvent molecules. Intermolecular charge transfer shown in Scheme 2.1, where an electron is donated from the quencher to the excited aromatic moiety forming an ionic complex, in few cases this complex is emissive:

$$Ar^* + Q \Leftrightarrow Ar^* \ldots Q \rightarrow (Ar^{-}Q^{+})^*$$

Scheme 2.1 Intermolecular charge transfer from the quenching agent to the acceptor, the aromatic species.

Energy transfer is also possible when both acceptor and donor are in the excited state. This phenomenon is known as charge pooling, where the fluorescence emission is delayed since the collision is usually between two species in their triplet state.

It is easy to differentiate between a dynamic and a static quenching (Scheme 2.2) although both result in a linear Stern-Volmer plot. Temperature plays a major role, higher temperature results in lower viscosity, promoting increased collisions, and the result is higher quenching efficiency in the dynamic quenching versus in the static quenching, where higher temperatures decrease the stability of the complex resulting in lower quenching rates. The fluorescence lifetime in the static mechanism is also unaltered. In the case of static quenching, perturbations also occur in the absorbance spectra since it is a ground state process versus for the dynamic process, where absorbance is not affected since it is an excited state mechanism.[1,3,4,19]

$$Ar + Q \rightarrow Ar - Q$$

Scheme 2.2 Showing the static quenching mechanism and the formation of a non-radiative complex in the ground state.

Equations in 2.24 show that the ratio of $\frac{F_0}{F}$ in the Stern-Volmer depends on the concentration of the quencher, where the concentration affects the ratio in the dynamic

quenching mechanism, where $k_{Ar...Q}$ is the association constant of the formation of the complex (Ar-Q).

$$k_{Ar...Q} = \frac{[Ar-Q]}{[Ar][Q]}$$

$$[Ar]_{total} = [Ar]_{free} + [Ar...Q]$$

$$k_{Ar...Q} = \frac{[Ar]_{total} - [Ar]_{free}}{[Ar]_{free}[Q]}$$

$$k_{Ar...Q} = \frac{[Ar]_{total}}{[Ar]_{free}[Q]} - \frac{[Ar]_{free}}{[Ar]_{free}[Q]}$$

$$k_{Ar...Q}[Q] = \frac{[Ar]_{total}}{[Ar]_{free}} - 1$$

$$1 + k_{Ar...Q}[Q] = \frac{[Ar]_{total}}{[Ar]_{free}} = \frac{F_0}{F}$$

$$\frac{F_0}{F} = 1 + k_{Ar...Q}[Q] \qquad \textbf{Equations 2.24}$$

Intramolecular charge transfer was studied as well in this dissertation, where an in-house synthesized probe 1-(9-anthryl)-3-(4-dimethylaniline) propane (ADMA) (Figure 2.4) was used as a fluorescent reporter to probe the interior of the nanocapsule. The ADMA molecule has two moieties: one acceptor connected *via* propyl carbon chain to a donor. This is an example of an Ar – D system, where Ar represents the fluorescent

moiety and D represents the donor entity. When Ar – D moieties are covalently connected by less then 8 Å an intramolecular exciplex is formed upon excitation. This phenomenon is a diffusion controlled process is therefore affected by the viscosity and polarity of the solvent. It is limited by geometrical constraints of the surrounding media as well.[24-30]

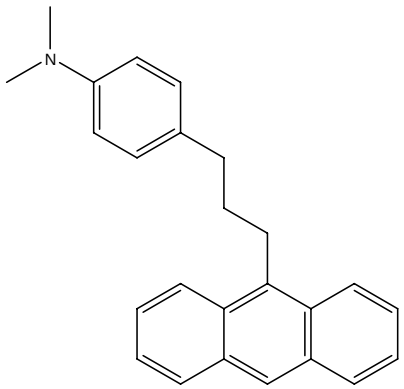

Figure 2.4 Molecular structure of (ADMA).

Figure 2.5 shows the free energy of electron transfer in Ar – D systems. Marcus Theory predicts that stabilization of product results in reduction of the activation barrier. A more detailed aspect of the ADMA photochemistry is discussed in Chapter 6.

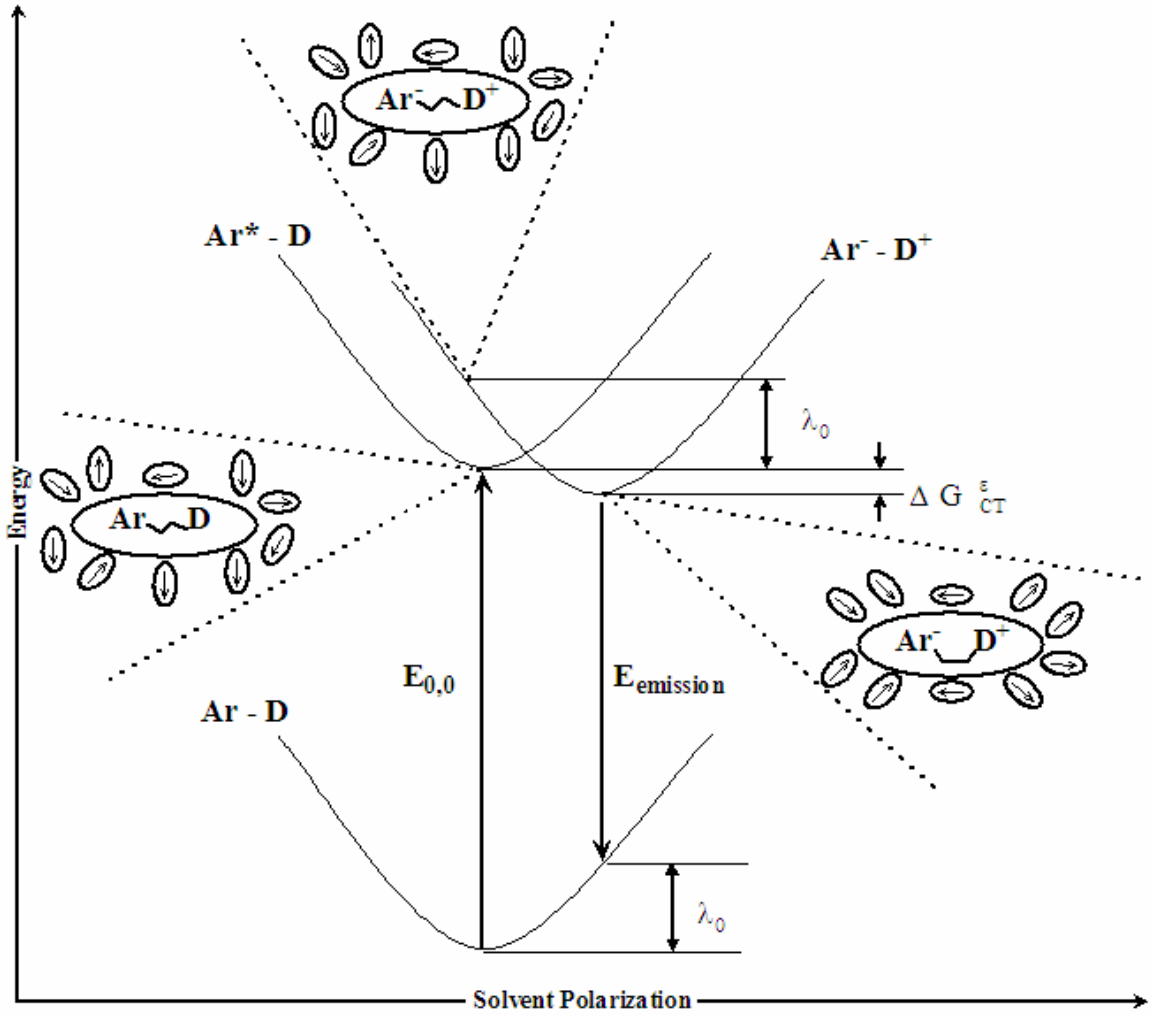

Figure 2.5 Solvent reorganization in charge transfer in Ar – D systems; modified energy diagram of the charge transfer, redrawn from Kauffman *et al.* [37]

V. Solvatochromism:

Solvatochromism comes from the two words: solvate and chroma where the latter is based on the Greek word for color. Solvatochromism means the system changes color with respect to the solvent system used. Spectroscopically, this means there is a shift of the wavelength maxima in the absorbance and/or emission spectra. A positive wavelength shift is called bathochromic or red shift, a negative wavelength shift is called hypsochromic or blue shift. This phenomenon is widely used to study the polarity of complex systems using dyes, that systematically respond to polarity, such as pyrene or several of the Reichardt's dyes.[31] Solvatochromism is well described in Figure 2.6, where it is shown how the ground and excited energy states change and correspond according to the polarity of the solvent.

Non-radiative relaxation allows the solvent dipole moments to reorient and realign with the solute's excited-state dipole moment. Fluorescence emission from the solute occurs, allowing the reorientation of the solute prior to that of the solvent. Higher polar solvents promote higher relaxation rates, since they have larger dipole moment that will further stabilize the electronic state.

Solvatochromism is used to characterize and identify natural products, especially flavonoids where hydroxyl group substitution on the phenol rings effects the absorbance spectrum. Pyrene, pyrene butyric acid, and other reporter molecules are commonly used to investigate organized media[32,33] and were used here to probe the nanocapsules. One of

the objectives in this research is to determine the nature of the microenvironment afforded by the interior of the capsule. Pyrene is a great candidate because its fine spectral structure changes with the polarity of the surrounding solvent. The ratio of the first versus the third vibronic band in the fluorescence emission indicates how polar the solvent is. For example, for nonpolar hexane the ratio of I/III bands is 0.59, and it is 1.95 for very polar dimethyl sulfoxide.[34-36]

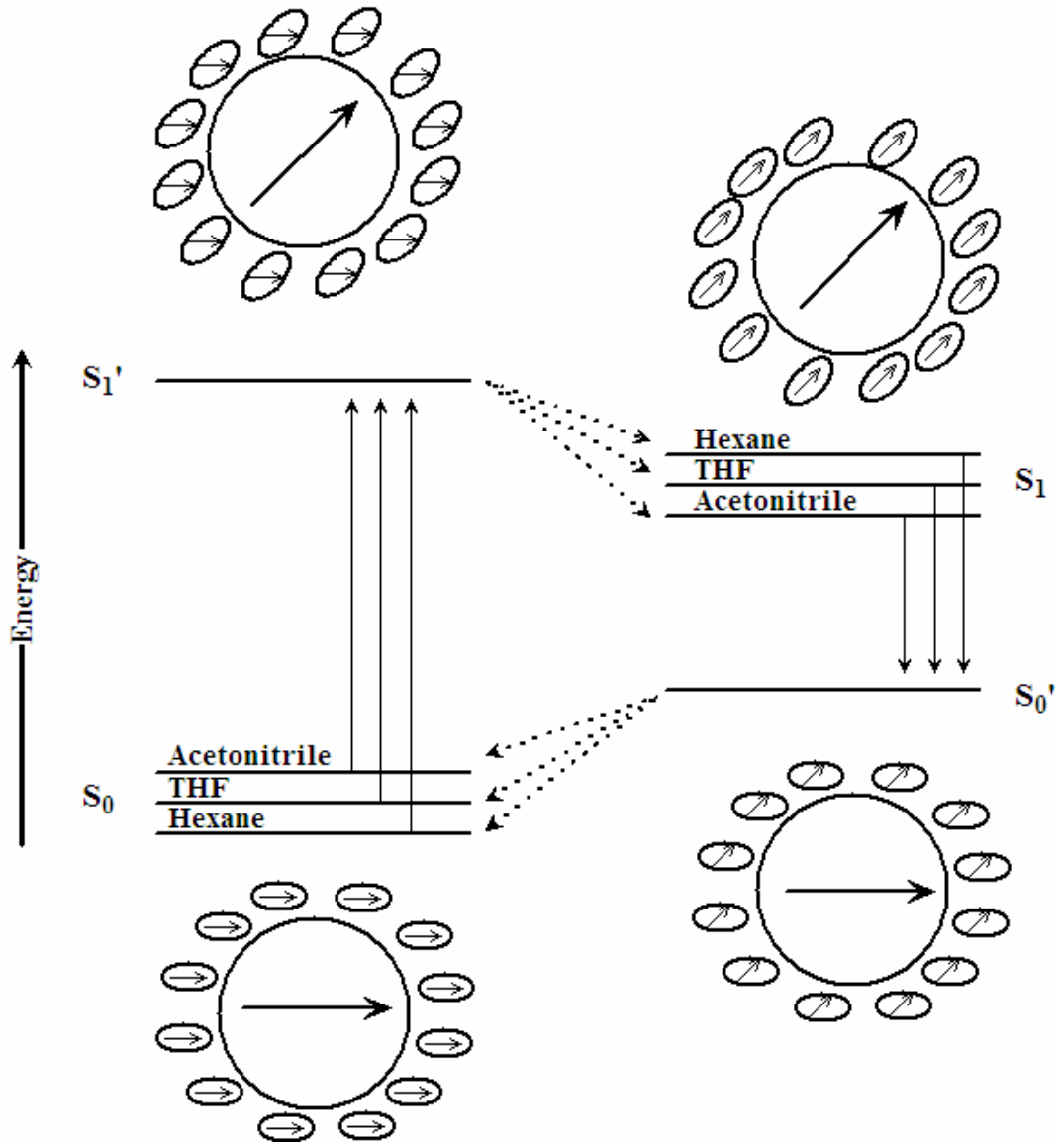

Figure 2.6 Modified Jablonski diagram showing the relaxation process: dashed lines correspond to the non-radiative relaxation, solid lines represent the absorbance and the emission. S_0 represents the electronic ground state. (Redrawn from *Rutan et al.*)[38]

VI. References:

(1) Lakowicz, J. R. *Principles of Fluorescence Spectroscopy*; Plenum Press: New York, 1983.

(2) Skoog, D. A.; Leary, J. A. *Principles of Instrumental Analysis*; 4 ed.; Saunders College Publishing: Fort Worth, 1992.

(3) Lakowicz, J. R. *Principles of Fluorescence Spectroscopy*; 2nd ed.; Kluwer Academic/Plenum Publishers: New York, 1999.

(4) Tucker, S. A. Ph.D. Dissertation, University of North Texas, **1994**.

(5) Smalley, M. B.; Shaver, J. M.; McGown, L. B. *Anal. Chem.* **1993**, *65*, 3466-72.

(6) Watkins, A. N.; Ingersoll, C. M.; Baker, G. A.; Bright, F. V. *Anal. Chem.* **1998**, *70*, 3384-3396.

(7) Gratton, E.; Jameson, D. M.; Hall, R. D. *Annu. Rev. Biophys. Bioeng.* **1984**, *13*, 105-24.

(8) Shaver, J. M.; McGown, L. B. *Anal. Chem.* **1996**, *68*, 611-20.

(9) Shaver, J. M.; McGown, L. B. *Anal. Chem.* **1996**, *68*, 9-17.

(10) Brochon, J. C.; Livesey, A. K.; Pouget, J.; Valeur, B. *Chem. Phys. Lett.* **1990**, *174*, 517-22.

(11) Geng, L.; McGown, L. B. In *SPIE Proceedings*; Lakowicz, J. R., Ed. Bellingham, WA, 1992; Vol. 1640.

(12) Shaver, J. M. Ph.D. Dissertation, Duke University, 1995.

(13) McGown, L. B.; Hemmingsen, S. L.; Shaver, J. M.; Geng, L. *Appl. Spectrosc.* **1995**, *49*, 60-6.

(14) Livesey, A. K.; Skilling, J. *Acta Crystallogr., Sect. A: Found. Crystallogr.* **1985**, *A41*, 113-22.

(15) Foster, T. H.; Pearson, B. D.; Mitra, S.; Bigelow, C. E. *Photochem. Photobio.* **2005**, *81*, 1544-1547.

(16) Wade, D. A. Ph.D. Dissertation, University of Missouri - Columbia, **2000**.

(17) Wade, D. A.; Torres, P. A.; Tucker, S. A. *Anal. Chim. Acta* **1999**, *397*, 17-31.

(18) Wade, D. A.; Tucker, S. A. *Talanta* **2000**, *53*, 571-578.

(19) Richter-Egger, D. L. PhD. Dissertation, University of Missouri~Columbia, 2001.

(20) Richter-Egger, D. L.; Landry, J. C.; Tesfai, A.; Tucker, S. A. *J. Phys. Chem. A* **2001**, *105*, 6826-6833.

(21) Richter-Egger, D. L.; Tesfai, A.; Tucker, S. A. *Anal. Chem.* **2001**, *73*, 5743-5751.

(22) Goodpaster, J. V.; McGuffin, V. L. *Anal. Chem.* **2000**, *72*, 1072-1077.

(23) Goodpaster, J. V.; McGuffin, V. L. *Anal. Chem.* **2001**, *73*, 2004-2011.

(24) Dalgarno, S. J.; Bassil, D. B.; Tucker, S. A.; Atwood, J. L. *Angew. Chem., Int. Ed. Engl.* **2006**, *45*, 7019-7022.

(25) Chuang, T. J.; Cox, R. J.; Eisenthal, K. B. *J. Am. Chem. Soc.* **1974**, *96*, 6828-31.

(26) Crawford, M. K.; Wang, Y.; Eisenthal, K. B. *Chem. Phys. Lett.* **1981**, *79*, 529-533.

(27) Gusten, H.; Meinsner, R.; Schoof, S. *J. Photochem.* **1980**, *14*, 77.

(28) Okada, T.; Fujita, T.; Kubota, M.; Masaki, S.; Mataga, N.; Ide, R.; Sakata, Y.; Misumi, S. *Chem. Phys. Lett.* **1972**, *14*, 563.

(29) Wang, Y.; Crawford, M. C.; Eisenthal, K. B. *J. Am. Chem. Soc.* **1982**, *104*, 5874-5878.

(30) Wang, Y.; Crawford, M. K.; Eisenthal, K. B. *J. Phys. Chem.* **1980**, *84*, 2696-2698.

(31) Reichardt, C. *Chem. Rev.* **1994**, *94*, 2319-2358.

(32) Dumas, D.; Muller, S.; Gouin, F.; Baros, F.; Viriot, M.-L.; Stoltz, J.-F. *Arch. Biochem. Biophys.* **1997**, *341*, 34-39.

(33) Ribou, A.-C.; Vigo, J.; Salmon, J.-M. *Photochem. Photobio.* **2004**, *80*, 274-280.

(34) Acree, W. E., Jr.; Tucker, S. A.; Fetzer, J. C. *Poly. Arom. Compd.* **1991**, *2*, 75-105.

(35) Dong, D. C.; Winnik, M. A. *Photochem. Photobio.* **1982**, *35*, 17-21.

(36) Dong, D. C.; Winnik, M. A. *Can. J. Chem.* **1984**, *62*, 2560-5.

(37) Kauffman, J. F.; Khajehpour, M.; Saleh, N. i. *J. Phys. Chem. A* **2004**, *108*, 3675-3687.

(38) Cecil, T. L.; Rutan, S. C. *Anal. Chem.* **1990**, *62*, 1998-2004.

Chapter 3: Materials and Methods

I. Materials:

Neat solvents and chemicals were obtained in the purest commercially available form, used as received, and are as follows: 9-acetylanthracene (99% pure), cyclohexane (99% A.C.S. spectrophotometric grade), anthracene (95%), *N,N*-dimethylaniline, DMA, (99.7% redistilled), *N,N*-dimethylamino benzaldehyde, (99.5% redistilled), palladium on carbon, Pd/C, (5% and 10%), POPOP (1,4-bis[5-phenyl-2-oxazolyl]benzene), pyrene (98%), pyrene butyric acid, PBA, (97%), pyrogallol, Pg, (99% A.C.S. reagent), and super hydride (1.0 M lithium triethylborohydride in tetrahydrofuran) from Sigma-Aldrich, Saint Louis, MO; acetonitrile, ACN, (HPLC grade), ethyl acetate, EA, (optima grade), hexane, HEX (optima grade), hydrogen peroxide, H_2O_2, (certified A.C.S. grade), ethanol (A.C.S. grade), light mineral oil (μ = 0.02310 Pa·s), magnesium sulfate, $MgSO_4$, (certified anhydrous), methylene chloride (HPLC, stabilized), methanol (HPLC grade), sodium hydroxide (certified A.C.S. grade), and tetrahydrofuran, THF, (certified grade) from Fisher-Scientific, Fair Lawn, NJ; and microscope immersion oil (high viscosity, 1250 CS) from Stephens-Scientific, Riverdale, NJ. *C*-alkylpyrogallol[4]arenes[1,2] (PgC_n) and 1-(9-anthryl)-3-(4dimethylaniline) propane, ADMA,[3] were synthesized according to literature procedures.[1-3]

The general experimental methodology is presented here with details specific to each guest further delineated within the respective chapters.

Figure 3.1 illustrates the synthesis of the tetramers or building blocks, where six of the latter self-assemble to form *C*-hexylpyrogallol[4]arenes nanocapsules. The synthesis of the building blocks were performed as follows: Ten grams (0.0725 mol) of pyrogallol (MW: 126.11 g/mol) and 1107 mL of heptaldehyde (density 0.82, MW: 114 g/mol) were dissolved in the minimum amount of ethanol, and the reflux process was started. Just before the solution boiled, the heat was removed, and 5 mL of the acid (1 mL of concentrated chloric acid per 2 g of pyrogallol) were added. The heat was returned, and the reaction was then refluxed for few hours.

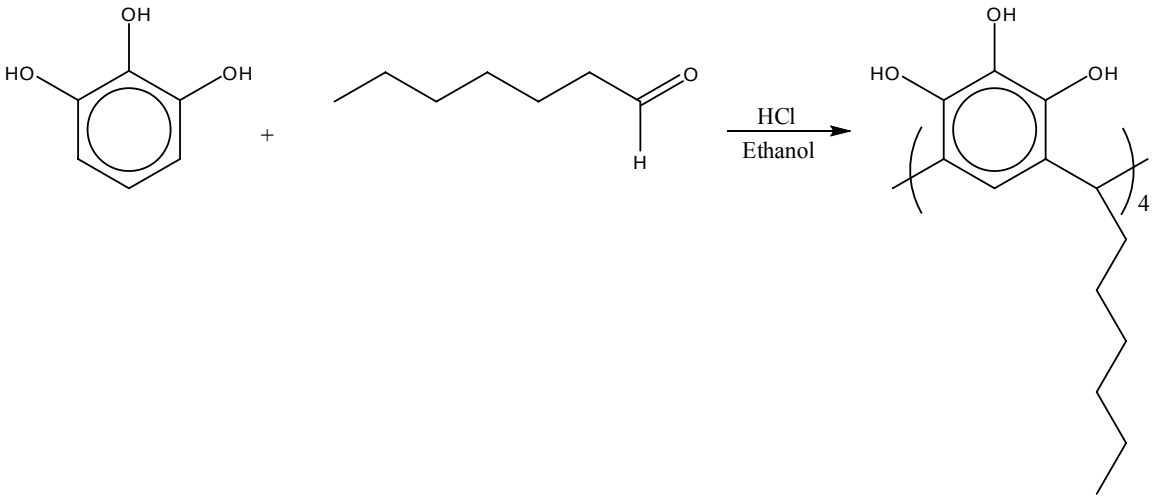

Figure 3.1 PgC_6 building block's synthesis from Pg and heptaldehyde.

The self-assembly of the supramolecular complexes and encapsulation of a guest was facilitated by sonication of saturated solution of *C*-alkylpyrogallol[4]arenes (PgC_n) and the guest in either ACN or EA as follows:[4] sixty mg of PgC_n were added to 6 mL of saturated guest solution in ACN in a 20 mL screw top scintillation vial; and the mixture was heated with a heat gun (below the boiling stage) until the powder totally dissolved. The solution was then diluted with ~20 mL of ACN and sonicated for about 15 minutes, allowing the encapsulating process to start.

The contents were allowed to sit for two days, while the color and possible crystal formation was monitored. If in two days, no crystals appeared, a slow evaporation technique was performed, were the cap of the vial was kept half open in order to evaporate the solvent slowly. As previously reported, crystals were characterized by single crystal X-ray diffraction and proton nuclear magnetic resonance (^{1}H-NMR) spectroscopy.[4]

Stock solutions (~10^{-3} M) of the free fluorophore and the encapsulated complex were prepared by dissolving the dye or a single crystal of the latter in the appropriate solvent. To confirm probe occupation within the nanocapsules, crystals were irradiated at the appropriate wavelength (e.g. 369 nm for ADMA) with a UV lamp to observe the fluorescence. Diluted samples were prepared by quantitatively transferring known aliquots of the stock solutions into volumetric flasks and diluting to volume. The final concentration of the fluorophore in any solvent system was optically dilute (~10^{-6} M). Samples were examined immediately upon mixing with the exception of the time-lapse

studies that were stored in the dark in sealed vials, and were interrogated at room temperature (20-25 °C).

The samples were allowed to age after dissolving the crystal; the process took place in a dark place at ambient temperature. The purpose of the aging process is to study the robustness of the capsule.

II. Instrumental measurements:

All spectra were collected in 1 cm^2 Suprasil quartz cuvettes, and absorption spectra were recorded on a Hitachi U-3000 double-beam spectrophotometer (Danbury, CT) with a scan rate of 120 nm/min and a slit width of 1 nm. Spectra were blank corrected for the possible absorption of solvent and nanocapsules in solution.

Fluorescence spectra were measured with a Varian Cary Eclipse Fluorometer (Palo Alto, CA). The excitation source was a 15 W Xenon arc lamp, pulsed at 80 Hz. Samples were excited at the optimal absorbance wavelength, (see Table 3.1), and the emission was collected from a window, denoted as the excitation wavelength plus 5 nm till 600/700 nm, in most cases, with 2 nm steps and with a slit width of 5 nm (or 2.5 nm for better fine structure resolution) in both the excitation and the emission compartments. The scan rate was 120 nm/min, and averaging time was 0.5 seconds (averaging 40 samples readings per point). All emission spectra are blank, absorbance corrected, and corrected from the inner-filter effect as well (Equation 3.1)[5].

Fluorescent Probe	Excitation λ (nm)	Emission λ (nm)
1-(9-Anthryl)-3-(4-dimethylganiline) propane	369	394, 396, 415, 540
Anthracene	357	376, 398, 422, 448
Anthraquinone	270	290, 350
Benzo[a]pyrene	383	402, 460, 453
Pentacene	235, 300, 400	333
Perylene	434	463, 495
Pyrene	342	372, 378, 383, 388, 393
Pyrene butyric acid	342	374, 380, 386, 394

Table 3.1 Fluorescence excitation and the major emission wavelengths of the fluorescent reporter molecules used through out this research.

$$F_{cor} = F_{obs}\left[\frac{2.303A_{exc}(0.55-0.45)}{10^{-A_{exc}0.45}-10^{-A_{exc}0.55}}\right] \qquad \textbf{Equation 3.1}$$

where F_{cor} and F_{obs}, represent the corrected and the observed fluorescence intensity respectively, A_{exc} is the optimal absorbance wavelength used for the excitation of the sample. The number 0.55 and 0.45 are the typical cell geometry values that are illustrated from Figure 3.1, where X=U=0.45 cm and Y=V=0.55 cm.[6] The correction factor, $F_{prim} \approx 10^{0.5Aexc}$, is equal the ratio of F_{cor} and F_{obs} (Equation 3.2):

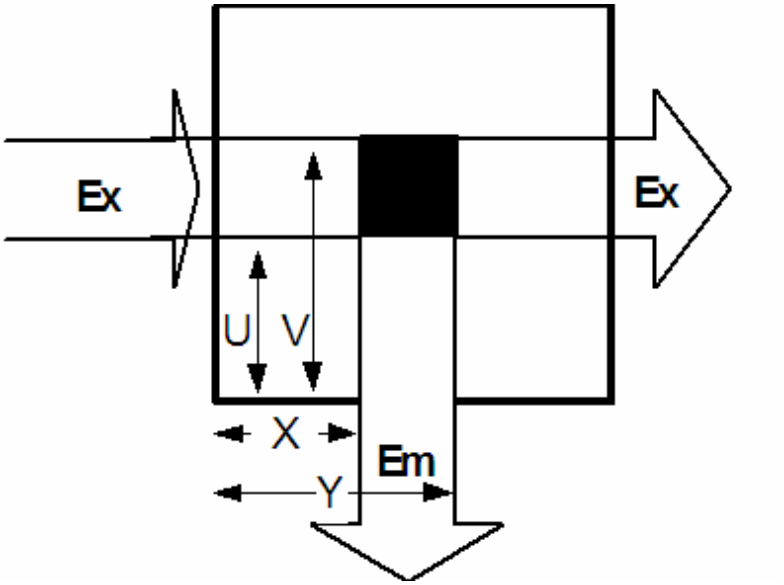

Figure 3.2 Reproduced representation of the effect of sample geometry, and the dimensions used for the inner-filter correction.[7]

$$F_{prim} = \frac{F_{cor}}{F_{obs}}$$ **Equation 3.2**

For solution measurements a 90º excitation-emission geometry is used, as the signal to noise ratio is maximized. A primary inner-filtering is a self-quenching mechanism, and secondary inner-filter that may occur also is a self-absorption mechanism.[5,6,8-10] Inaccurate conclusion can be drawn and quantitative concentration comparison would be impossible upon failure to correct the emission spectra,.

III. Quenching studies:

To further assess the nature of and extent to which the fluorescent guests remain encapsulated in solution, we added a known fluorescence quenchers. In neat solvents, fluorophores form an excited-state charge-transfer complex (or exciplex), with quenchers, leading to a new broad emission band.[11]

Quenching studies were performed as follows: five μL of the quencher were initially added to the sample already in the cuvettes, and then increments of 5 μL were added until the fluorescence emission signal was totally quenched. The sample volume was initially 2500 μL leaving room for 500 μL of quencher, if necessary (3000 μL total cuvette volume).[12] The solution was then vigorously mixed after each addition and allowed to stand for less then a minute to re-equilibrate.

IV. Fluorescence lifetime measurements:

Lifetimes were collected in the frequency domain,[13,14] on a SLM 48000 DSCF/MHF spectrofluorometer, with multiharmonic, Fourier transform (MHF) phase-modulation capabilities. The excitation source was a Coherent Innova 307C argon ion laser (Santa Clara, CA) operated at 351 nm and 250 mW. In MHF mode, however, only a small fraction of the excitation power interrogates the sample. A base frequency of 4.0 MHz and a cross-correlation frequency of 7.000 Hz were used, ten pairs of sample-

reference measurements were collected in triplicate for each sample, and each measurement contained 50 internal averages. The lifetime reference (τ_{ref} = 1.34 ns) was POPOP in ethanol. The following filters were employed for ADMA emission collection: a 370 long-pass (KV-370 Schott Glass Technologies, Duryea, PA)/610 short-pass (03 SWP 610 Melles Griot, Irvine, CA) filter combination, a 400 nm (80 nm band pass: 03 FIB 002 Melles Griot), a 550 nm (40 nm band pass: 03 FIV 044 Melles Griot), a 420 nm (10 nm band pass: P10-420-F-Q920 Corion CVI Laser Corporation, Albuquerque, NM), and a 540 nm (10 nm band pass: P10-540-F-986P Corion CVI). Lifetime data were analyzed by a self-modeling maximum entropy method (MEM) commercial software package (Phase5, Maximum Entropy Data Consultants, Cambridge, UK),[15-17] and results were compared to those obtained from a standard nonlinear least squares (NLLS) software program (Globals Unlimited, Laboratory for Fluorescence Dynamics, Urbana-Champaign, IL). Three replicates for each sample were analyzed with Phase5, as both individual and combined files, using a lifetime window containing 500 discrete, equally spaced cells from 0.01 ns to 50 ns. The three individual replicates and a linked file were also analyzed with Globals.

V. Fluorescence anisotropy:

Steady-state anisotropy measurements were collected in 'L' format[6] using Glan Thompson polarizers and 370 long-pass (KV-370 Schott Glass Technologies, Duryea,

PA)/610 short-pass (03 SWP 610 Melles Griot, Irvine, CA) filter combination. For this purpose, the excitation source was a Coherent Innova 307C argon ion laser (Santa Clara, CA) operated at 351 nm and 250 mW. Four polarizer orientations (0º – 0º, 0º – 90º, 90º – 0º, 90º – 90º) and an internal average of five signal sampling were used.

VI. High performance liquid chromatography:

For ADMA characterization, high performance liquid chromatography (HPLC) chromatograms were collected on a Shimadzu LC-6A (Kyoto, Japan) dual pump system with flow rate of 0.08 mL/min and a Shimadzu SPD - 6A D_2 lamp detector (Kyoto, Japan) set at 245 nm. All experiments were run on Econosil Silica Column 250 x 4.6 mm 10 um (Alltech; Columbia, MD), with a mobile phase composition of: ACN:Water (75:25) and a 10 μL sample loop. The column was regenerated with 100% ACN, and pre-equilibrated with ACN:Water (75:25) at a 0.01 mL/min flow rate for 12 hours prior the separation.

VII. References:

(1) Cave, G. W. V.; Antesberger, J.; Barbour, L. J.; McKinlay, R. M.; Atwood, J. L. *Angew. Chem., Int. Ed.* **2004**, *43*, 5263-5266.

(2) Gerkensmeier, T.; Iwanek, W.; Agena, C.; Frohlich, R.; Kotila, S.; Nather, C.; Mattay, J. *Eur. J. Org. Chem.* **1999**, 2257-2262.

(3) Syage, J. A.; Felker, P. M.; Zewail, A. H. *J. Chem. Phys.* **1984**, *81*, 2233-56.

(4) Dalgarno, S. J.; Bassil, D. B.; Tucker, S. A.; Atwood, J. L. *Angew. Chem., Int. Ed. Engl.* **2006**, *45*, 7019-7022.

(5) Tucker, S. A. Ph.D. Dissertation, University of North Texas, **1994**.

(6) Lakowicz, J. R. *Principles of Fluorescence Spectroscopy*; Plenum Press: New York, 1983.

(7) Wade, D. A. Ph.D. Dissertation, University of Missouri - Columbia, **2000**.

(8) Holland, J. F.; Teets, R. E.; Kelly, P. M.; Timnick, A. *Anal. Chem.* **1977**, *49*, 706.

(9) Parker, C. A.; Barnes, W. J. *Analyst* **1957**, *82*, 606.

(10) Yappert, M. C.; Ingle, J. D. *Appl. Spectrosc.* **1989**, *43*, 759.

(11) Gupta, D.; Basu, S. *J. Photochem.* **1975**, *4*, 307-8.

(12) Dalgarno, S. J.; Tucker, S. A.; Bassil, D. B.; Atwood, J. L. *Science* **2005**, *309*, 2037-2039.

(13) Mitchell, G.; Swift, K. *Dep. Astron. St. Mar. U.* **1990**, 270-274.

(14) Spencer, R. D. Ph.D. Dissertation, University of Illinois, Urbana, IL, **1970**.

(15) Brochon, J. C.; Livesey, A. K.; Pouget, J.; Valeur, B. *Chem. Phys. Lett.* **1990**, *174*, 517-22.

(16) Shaver, J. M.; McGown, L. B. *Anal. Chem.* **1996**, *68*, 611-20.

(17) Shaver, J. M.; McGown, L. B. *Anal. Chem.* **1996**, *68*, 9-17.

Chapter 4: The Encapsulation of Pyrene

I. Pyrene monomer fluorescence in homogeneous solvents:

Macromolecular chemists have used pyrene (Py, Figure 4.1) in order to probe specific complex systems, such as micelles[1] and several other cavities.[2] Pyrene is widely used to report microenvironmental polarity.[3] It is a condensed aromatic hydrocarbon that shows significant fine structure in its solution phase monomer fluorescence emission spectrum.[1] For example, in Figure 4.2, the vibronic fine structure of the Py emission spectrum is depicted as shows five well-resolved peaks between 370 nm and 400 nm.[4] As mentioned in Chapter 2, the emission intensities of the various vibronic bands of Py were found to show a strong dependence on the solvent environment[5] a concept first published by Nakajima.[6] Empirically, the intensity ratio of the first and the third vibronic band (I/III) of the Py emission has been found to vary with the microenvironmental polarity. For example, the ratio has been found to be 0.58 in aliphatic hydrocarbons (*i.e.* hexane, HEX) and 1.87 in water.[2]

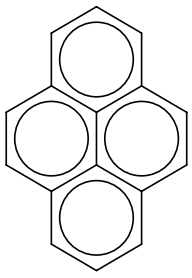

Figure 4.1 Molecular structure of Py.

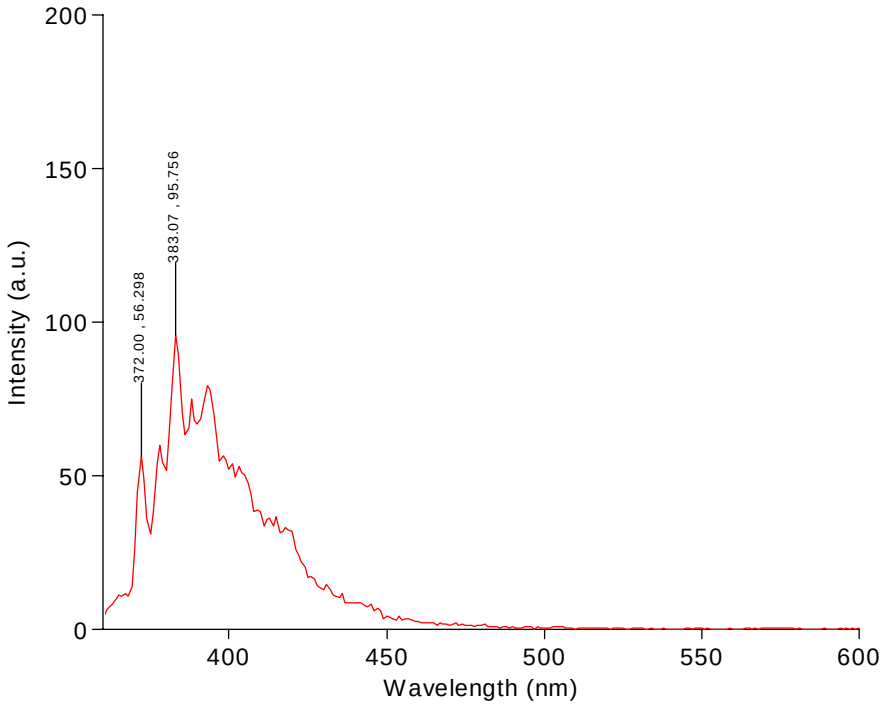

Figure 4.2 Fluorescence spectrum of Py in HEX, showing the wavelength of the peak I and III (emission and excitation bandpasses are 2.5 nm).

i) Reproduction of the pyrene scale:

Because of instrumental variations from laboratory to laboratory, it is necessary to produce an in-house solvent polarity ruler. Table 4.1 summarizes the relative peak intensities for I and III vibronic bands of the Py monomer measured here for 12 different solvents, ordered by increasing polarity. Fluorescence emission spectra were obtained using an excitation wavelength of 340 nm. Measured I/III values are reproducible to ± 0.02, well within the experimental error, agreeing with those found in the literature for

these solvents.

	This work	Literature Values		
Solvent	I/III	I/III[7]	I/III[3]	I/III[4]
Hexane	0.59	0.58		0.58
Amyl alcohol	1.02		0.94	
Tetrahydrofuran	1.27	1.35		1.35
Toluene	1.02	1.04	1.11	1.04
Benzene	1.15	1.05	1.14	1.05
Ether	0.94	1.02	0.93	
Ethyl acetate	1.45	1.37	1.45	1.37
Methylene chloride	1.38	1.46	1.35	
Acetonitrile	1.78	1.79	1.75	1.79
Ethanol	1.23	1.18	1.10	
Xylene	1.06	1.01		0.95
Water	1.68	1.87	1.59	

Table 4.1 Solvent dependence of I/III band intensities in Py monomer fluorescence.

Use of the Py-scale will assist in determining where the probe is located. For example, *exo*- versus *endo*-capsule, the Py-scale value for EA is 1.45; therefore, we would know that Py is fully encapsulated with the EA crystallization solvent if the Py value is ~1.5. For these studies to be conclusive, it was necessary to dissolve the assembly in nonpolar media, such HEX. If Py is *exo*-capsule in the HEX, the value is ~ 0.6. Non-purified samples might have encapsulated Py (polar environment), and external Py molecules (nonpolar environment). The emission of the non-purified sample will expectantly provide a Py-scale value between 0.58 and 1.45. A value in this range will be an indication that a portion of Py remains unencapsulated in the nanocapsules.

ii) Pyrene photochemistry:

Pyrene was one of the very first probes that we attempted to encapsulate in *C*-hexylpyrogallol[4]arene, PgC_6, for the purpose of understanding of interiors of the nanocapsules in solution. Beyond the Py scale, Py also has several additional interesting photophysical properties, that make it an effective probe, notably the long lifetime of the monomer and the efficient formation of excimers and exciplexes (homogenous and heterogeneous excited-state complex, respectively).[1] Due to its long lifetime, the (diffusion-controlled) emissive charge transfer (CT) exciplex, resulting from excitation of Py in presence of a donor, can be monitored. "Diffusion controlled" reactions are those that do not have an activation barrier, the reaction occurs as soon as the two species come together. This mechanism involves a diffusive encounter of the excited singlet-state Py molecule (Py*) with a donor quencher, such as *N*,*N*-dimethylaniline (DMA, Figure 4.3), as shown in Scheme 4.1.

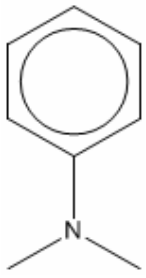

Figure 4.3 Molecular structure of *N*,*N*-dimethylaniline.

$$Py^* + DMA \underset{\text{Diffusion}}{\rightleftharpoons} Py^* \cdots DMA \longrightarrow \underset{\text{Emissive exciplex}}{(Py^-DMA^+)^*}$$

Scheme 4.1 Quenching scheme of Py by DMA, with the formation of the emissive exciplex.

Fluorescence emission of Py is quenched through photo-induced electron transfer from DMA (donor) to Py (acceptor).[8] Exciplex formation is due to the interaction of an excited Py and DMA, as detected by the presence of a broad featureless band in the 440 nm region (Figure 4.4). The exciplex is formed due to a diffusion of the donor to the acceptor.

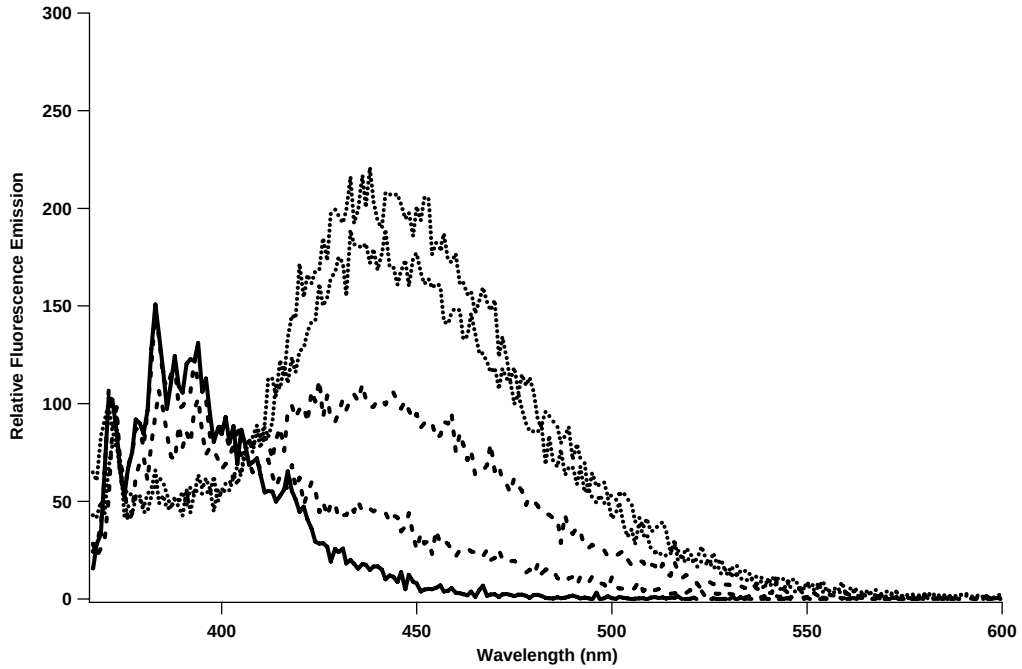

Figure 4.4 Fluorescence emission spectra of Py at various loading levels of DMA (excitation at λ=336 nm). The emission of Py in HEX (10^{-6} mol/L) is shown in solid, the black dashed spectra represents two different loads of 10% DMA, versus the black dotted represents loads from 100% DMA.

Figure 4.5 illustrates the increase of CT emission (440 nm), in presence of higher concentrations of DMA that promote Py-DMA* exciplex formation, and it also shows the reduction fluorescence emission intensity of the Py monomer, (350-450 nm) with increased DMA concentration. The fluorescence intensity is proportional to the concentration of the emitting species (Py-DMA* exciplex).[9] The I/III ratio of the Py fluorescence fine structure does not change with the addition of DMA.

II. Encapsulated pyrene:

The capability of the PgC_n nanocapsule (host) to encapsulated Py (guest) was investigated. In order to understand the interior environment of the nanocapsules; the emission of Py alone and in presence of the DMA (fluorescence quencher) is compared. By monitoring the fluorescence of the Py exciplex, with respect to the Py monomer, information such as probe location and the polarity, structural rigidity, and area openness of the capsule interior can be ascertained.

The PgC_6 nanocapsules were crystallized from neat solvents in presence of Py, and fluorescence emission spectra (Figure 4.4) were collected at various loading levels of the quencher. Results were compared with free Py, diluted in a solution of preformed 'empty' nanocapsules (Figure 4.5).

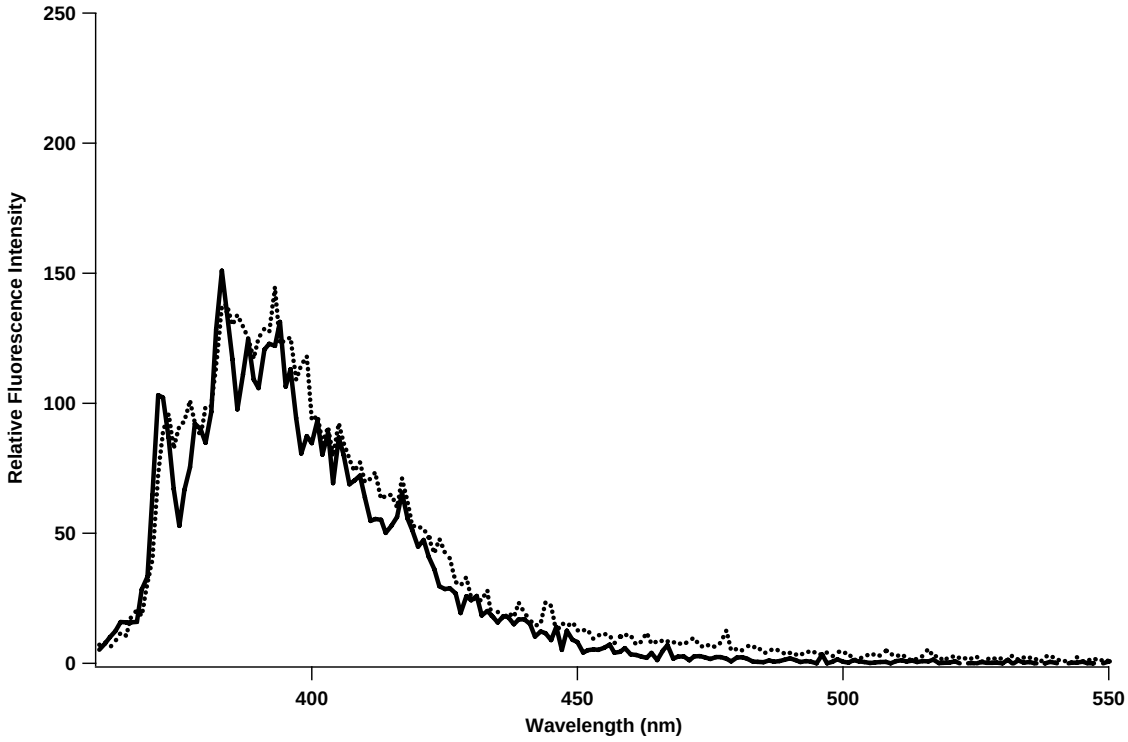

Figure 4.5 Fluorescence emission spectra of Py-PgC_6 in HEX (dotted), and of preformed capsules and Py in HEX (solid).

In Figure 4.6 the fluorescence emission of Py-PgC_6 in HEX versus Py in HEX presence of performed capsule is similar. No signal enhancement, due to entrapment, is noted. The Py value is I/III = 0.68 in HEX and 0.70 for Py-PgC_6. Figure 4.5 summarizes the investigation of the inner-cavity of the nanocapsules utilizing Py. In the first measurement, we do not see any CT emission in the 440 nm region, due to the absence of the DMA as quencher. Upon addition of DMA (Figure 4.6), we observe a CT emission intensity. When the concentration of the quencher increases (Figure 4.7 and 4.8), we noticed an increase in the difference between the Py-PgC_6 and the Py just added to

preformed nanocapsules. This limited observation indicates that Py may be entrapped with the crystallization acetonitrile (ACN), as it inhibits CT emission.

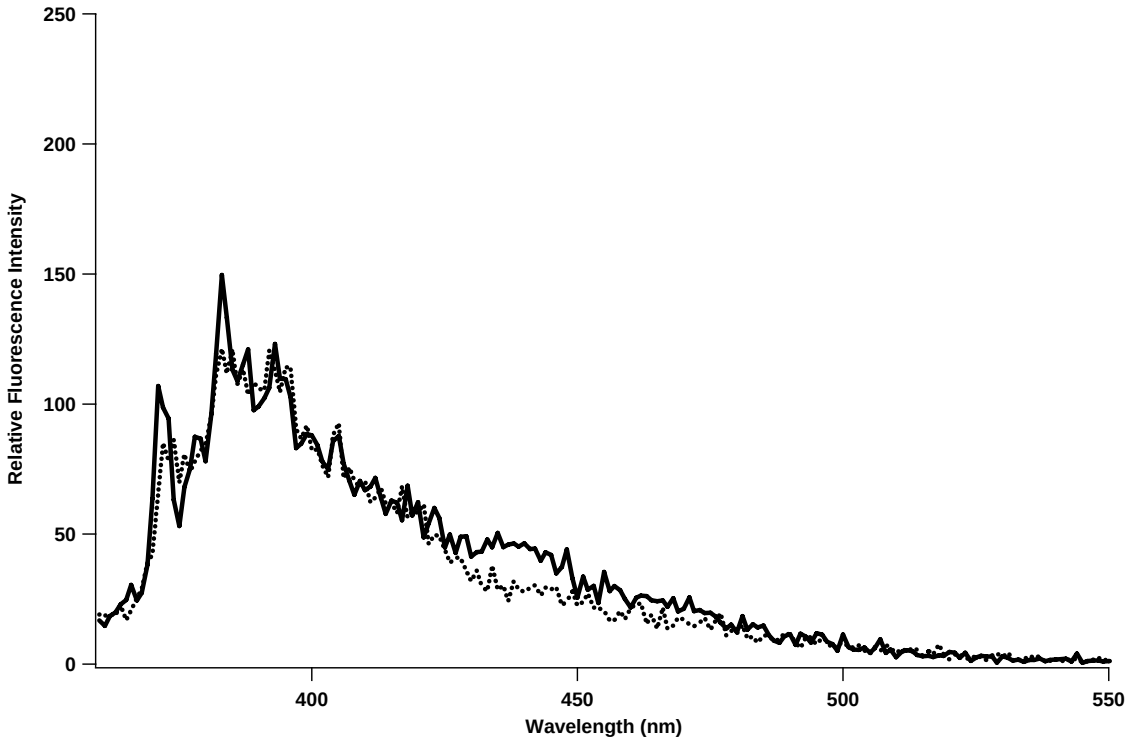

Figure 4.6 Fluorescence emission spectra of Py-PgC_6 in HEX (dotted) and of preformed capsules and Py (solid) plus one drop of 10% DMA.

This concept will be further studied in Chapter 5, where we confirmed that DMA is small enough to penetrate the hydrogen bonds seem, and will quench the fluorescence of the inside probe.[10]

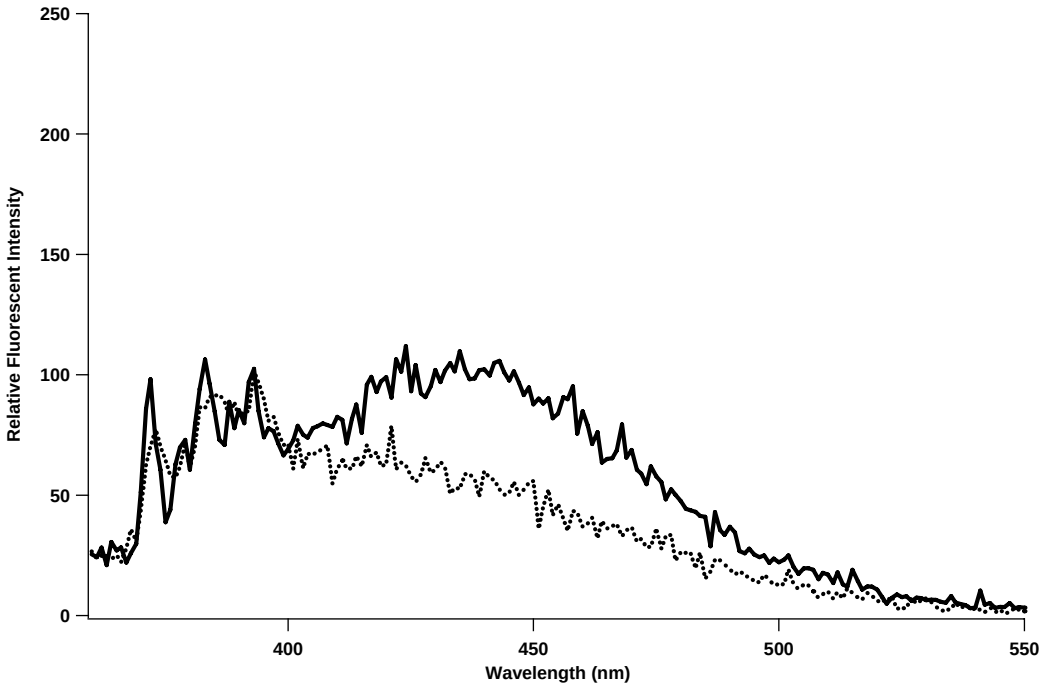

Figure 4.7 Fluorescence emission spectra of Py-PgC_6 in HEX (dotted) and of preformed capsules and Py (solid) plus two drops of 10% DMA.

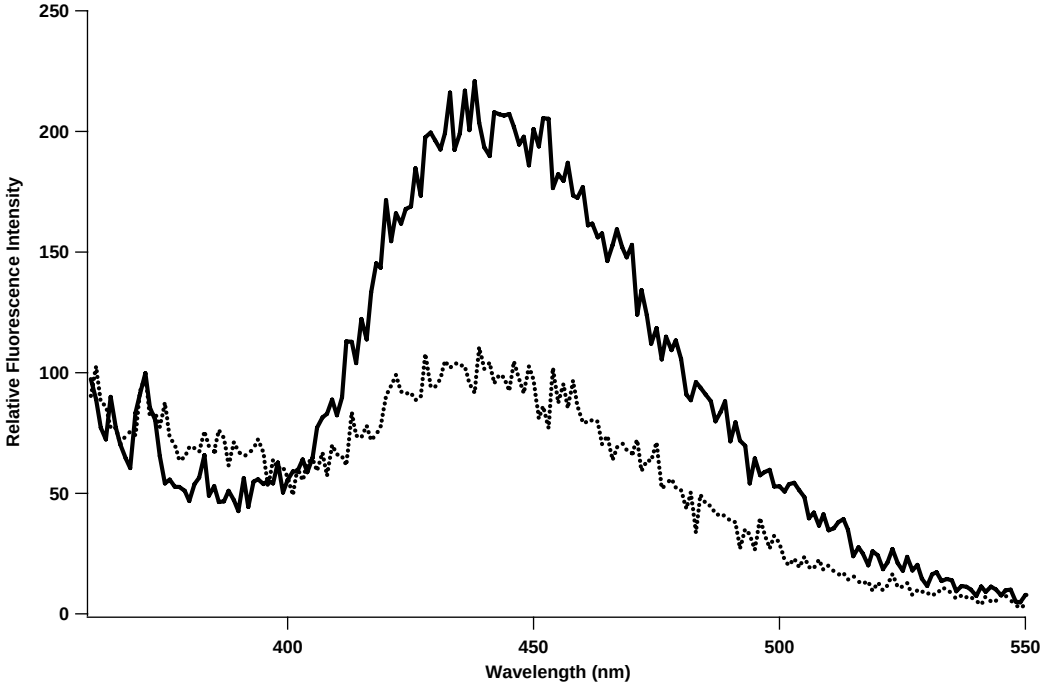

Figure 4.8 Fluorescence emission spectra of Py-PgC_6 in HEX (dotted) and of preformed capsules and Py (solid) plus two drops of 100% DMA.

If the Py was encapsulated (Py-PgC_6) in the nanocapsule, no CT band should exist. Unfortunately, Figure 4.6 – 4.8 still shows the presence of CT emission. It is thought that this emission comes from external Py (non-encapsulated), but entrapped between capsule aggregates. Remarkably, functionalizing the outer shell of the nanocapsule with different alkyl chains leads to a highly specific solid-state packing arrangement.[11] In other words, the pyrogallol nanocapsules tend to pack and form aggregates among themselves in solution, and the nanocapsules are then separated by their lipophilic tails. Notably, the alkyl chains of neighboring capsules only partially interpenetrate, as they form lipophilic membranes between the nanocapsules. When the lipophilic tail is six carbon atoms in length, the nanocapsules are not forced away from one another, but rather congregate to form hydrogen-bonded nanorods,[11] which is the case in our study. When the crystals are formed, many Py molecules, due to the excess of the latter, get trapped between the capsules, and that is where the intensity - attenuated CT is thought to come from in the study.

This work was done with the PgC_6, and additional studies were carried out in a similar fashion with PgC_n nanocapsules. For example, we examined different tail length (C_n), and tails with various functionalities, such as [-(CH_2)-Br]. The results were consistent with *C*-hexylpyrogallol[4]arenes, and the sequestered Py had same fluorescence emission in all these different capsules. These measurements do no appear to be sensitive to any tail affect that may cause organization between capsules, as seen in the solid state.

III. Conclusion:

These Py experiments were insufficient to fully understand the host-guest properties of PgC_n in solution. It appears that, PgC_6 was not able to keep Py ensnared in solution, which about whether the host or guest controls encapsulation. Given these results, we decided to work with a Py molecule that has a tail that might assist the probe in docking in the nanocapsule. This concept is still been used in biological laboratories, where they use carboxylic acids to anchor probes in the cell membranes.[12] However, work with this probe allowed for experimental protocols to be defined and refined to ultimately have a sensitive method to probe nano-cavities using molecular spectroscopy as a tool.

IV. References:

(1) Kalyanasundaram, K.; Thomas, J. K. *J. Am. Chem. Soc.* **1977**, *99*, 2039-44.

(2) Pratim Parui, P.; Narayan Nath, D.; Chowdhury, M. *Chem. Phys. Lett.* **2004**, *396*, 329-334.

(3) Dong, D. C.; Winnik, M. A. *Photochem. Photobio.* **1982**, *35*, 17-21.

(4) Acree, W. E., Jr.; Tucker, S. A.; Fetzer, J. C. *Poly. Arom. Compd.* **1991**, *2*, 75-105.

(5) Ndou, T. T.; Von Wandruszka, R. *J. Luminesc.* **1990**, *46*, 33-8.

(6) Nakajima, A. *Bull. Chem. Soc. Jpn.* **1971**, *44*, 3272-7.

(7) Dong, D. C.; Winnik, M. A. *Can. J. Chem.* **1984**, *62*, 2560-5.

(8) Steiner, U. E.; Ulrich, T. *Chem. Rev.* **1989**, *89*, 51-147.

(9) Khajehpour, M.; Kauffman, J. F. *Chem. Phys. Lett.* **1998**, *297*, 141-146.

(10) Dalgarno, S. J.; Tucker, S. A.; Bassil, D. B.; Atwood, J. L. *Science* **2005**, *309*, 2037-2039.

(11) Cave, G. W. V.; Antesberger, J.; Barbour, L. J.; McKinlay, R. M.; Atwood, J. L. *Angew. Chem. Int. Ed.* **2004**, *43*, 5263-5266.

(12) Dumas, D.; Muller, S.; Gouin, F.; Baros, F.; Viriot, M.-L.; Stoltz, J.-F. *Arch. Biochem. Biophys.* **1997**, *341*, 34-39.

Chapter 5: The Encapsulation of Pyrene Butyric Acid

I. Introduction:

Given that it was possible that pyrene (Py) leached from the *C*-hexylpyrogallol[4]arene, PgC_6, capsules after dissolving the crystal into a neat solvent or that it did not encapsulate very well, pyrene butyric acid (PBA, Figure 5.1) was examined in hope that the additional appendage might facilitate its entrapment. It is also solubility probe[1-3] with similar photochemical properties to Py; however, PBA has a carboxylic acid tail that might introduce additional bonding with the capsule interior.[4] This concept was used by Dumas *et al.*, to anchor Py, with a carboxylic acid moiety (butyric acid) near the phospholipidic region of the erythrocyte membrane.[5] Pyrene butyric acid is also well known as an oxygen sensor for biological systems. For instance, it is used to monitoring the oxygen level in living cells, proteins and micelles.[6,7] The fluorescence lifetime of PBA molecules increases about ten-fold in absence of oxygen versus in presence of it (200 versus 8 ns).[7,8] In this study, we successfully entrapped two PBA in one capsule.[4]

Capsule-bound PBA, PBA-PgC_6 (**1** Figure 5.1), was prepared by the assembly process shown schematically in Figure 5.1. Pyrene butyric acid, PBA, has a volume[9] of 260 $Å^3$; therefore, sequestering this probe is possible since the interior volume of PgC_6 is ~1250 $Å^3$.

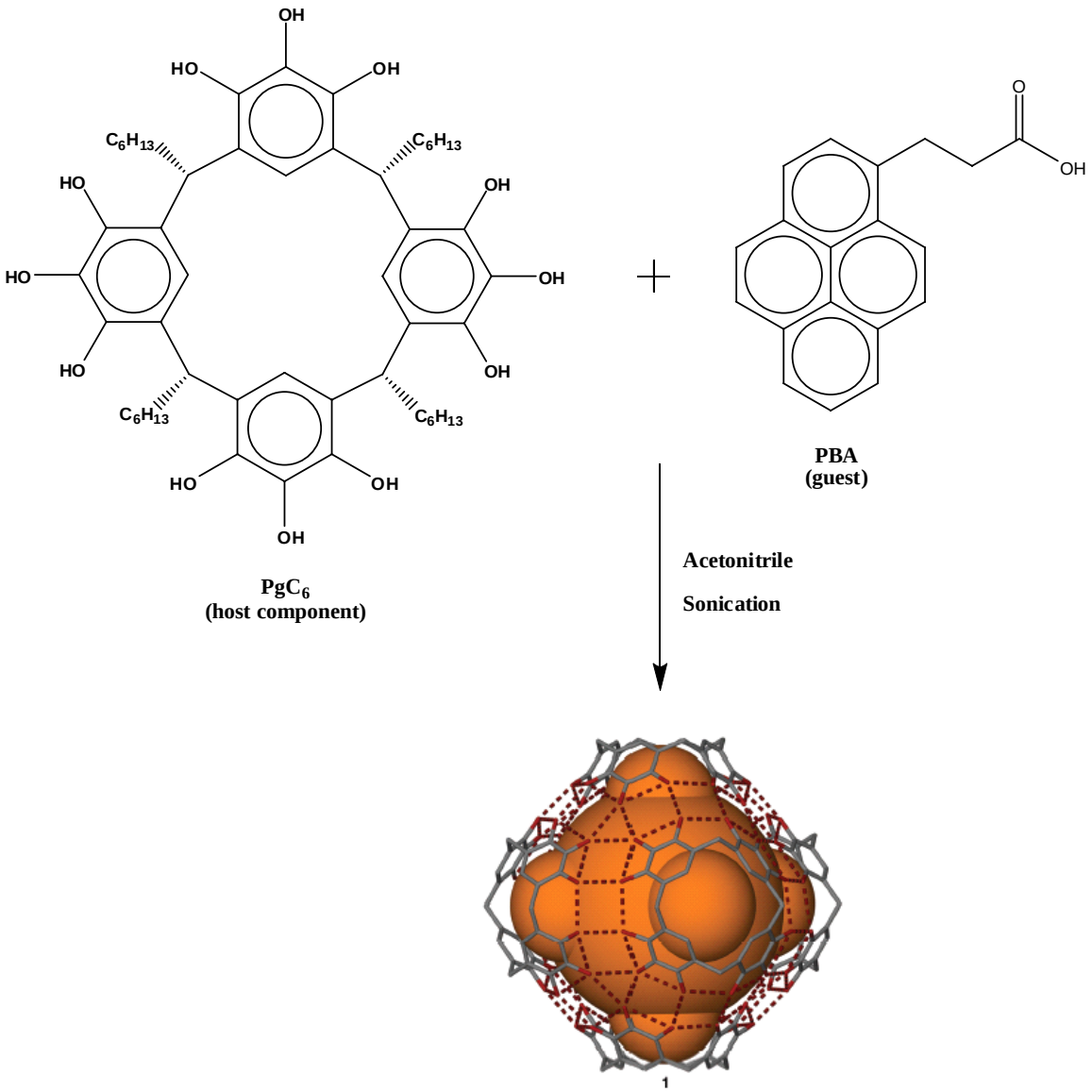

Figure 5.1 Schematic for the formation of hexameric assembly **1 (**PgC_6) containing the fluorophore PBA. The encapsulated space, occupied by PBA and ACN, is depicted in orange.

Single crystal X-ray diffraction studies show not only that the PBA molecules interact with the capsule walls in the solid state, but also that the π-surfaces of the PBA guest molecules are well separated from one another within the capsule (Figure 5.2).[10] The distance between the pyrene planes in a doubly occupied capsule is sufficient for one or more acetonitrile (ACN) molecules, but it was not possible to model the diffuse electron density in this position as such. From the crystal structure, it is clear that there is guest-to-wall binding, attributable to π-stacking and CH…π interactions between PBA and PgC_6. Three crystallographically unique interactions were evident: two CH…π interactions, with CH…aromatic centroid distances of 2.832 and 2.930 Å; and one π stacking interaction with an aromatic centroid…centroid distance of 3.847 Å. Additional interactions may be present between the butyric acid functionality and the hydroxyl groups, but these could not be identified because of the extensive disorder present between the pyrene rings.

II. Results:

Proving that the contents of the capsules will remain ordered in solution is a fairly novel idea, and none too trivial. The crystals were dissolved, as described earlier, in several solvents, including nonpolar (ε = 1.89 for HEX) to very polar solvents (ε = 37.5 for ACN).[11-14] After several measurements, it was clear that HEX was the most favorable solvent for the studies, although cyclohexane gave us consistent results as well.

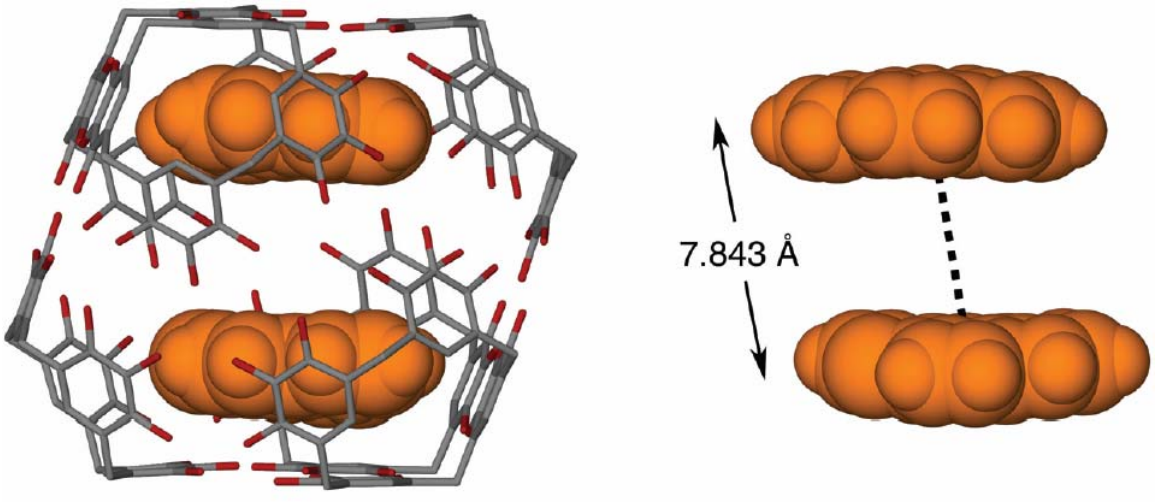

Figure 5.2 Diagram of the crystal structure of the encapsulated PBA in PgC_6. The distance between the centroids of the polyaromatic guests is 7.843 Å. The remaining void space is occupied by the carboxylic side of the probe (not shown) and by solvent ACN molecules.

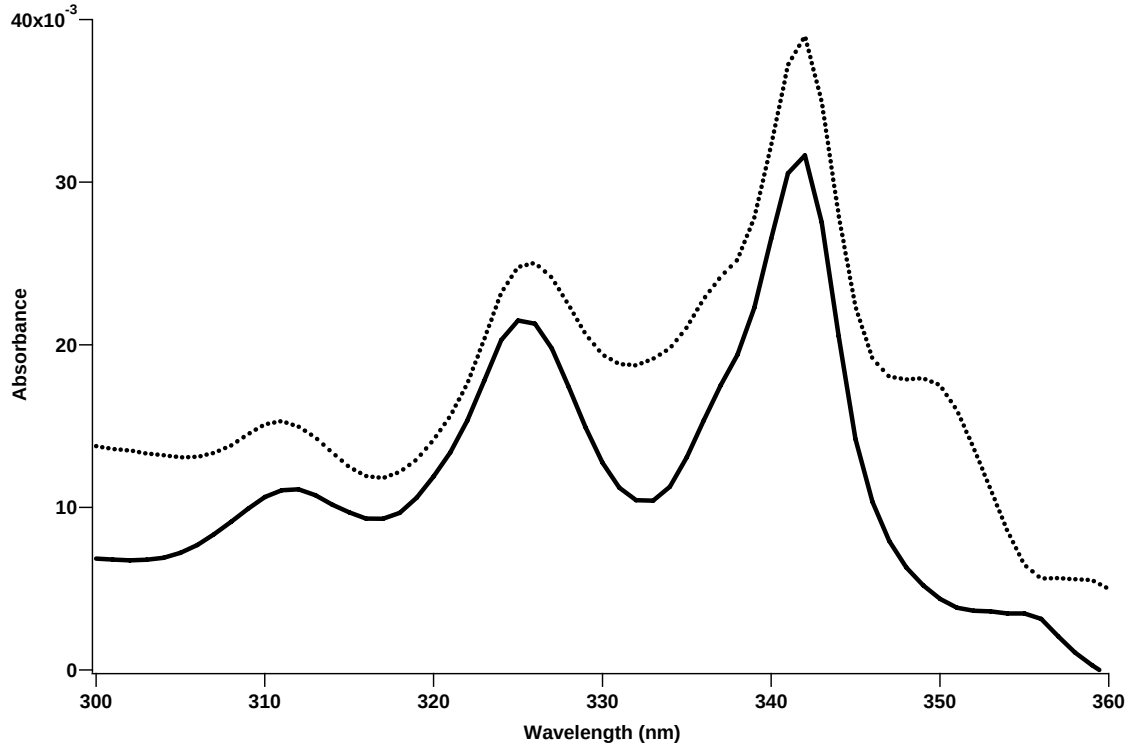

Figure 5.3 Absorbance spectra of free PBA (solid) and PBA-PgC_6 (dotted) in HEX.

Evidence of this guest-to-wall binding is also present in solution. The formation of a ground state complex between PBA and the capsule wall results in expected spectral perturbations (Figure 5.3), compared to free PBA in HEX.[15,16] The absorbance spectra of PBA in both solutions (Figure 5.3), free probe and as an encapsulated probe (PBA-PgC_6) shows the same spectra profile with the exception that the PBA-PgC_6 shows an extra shoulder band around the 350 nm area. Given the solid-state data, this shoulder was attributed to the π-stacking, which was confirmed by the appearance of the shoulder in the absorbance of PBA in toluene, where PBA π-stacks with the aromatic ring. Similar changes were noticed with the fluorescence emission spectrum of PBA-PgC_6 (Figure 5.4), where the second vibronic band fine structure was lost in the encapsulated sample, as well as in toluene.

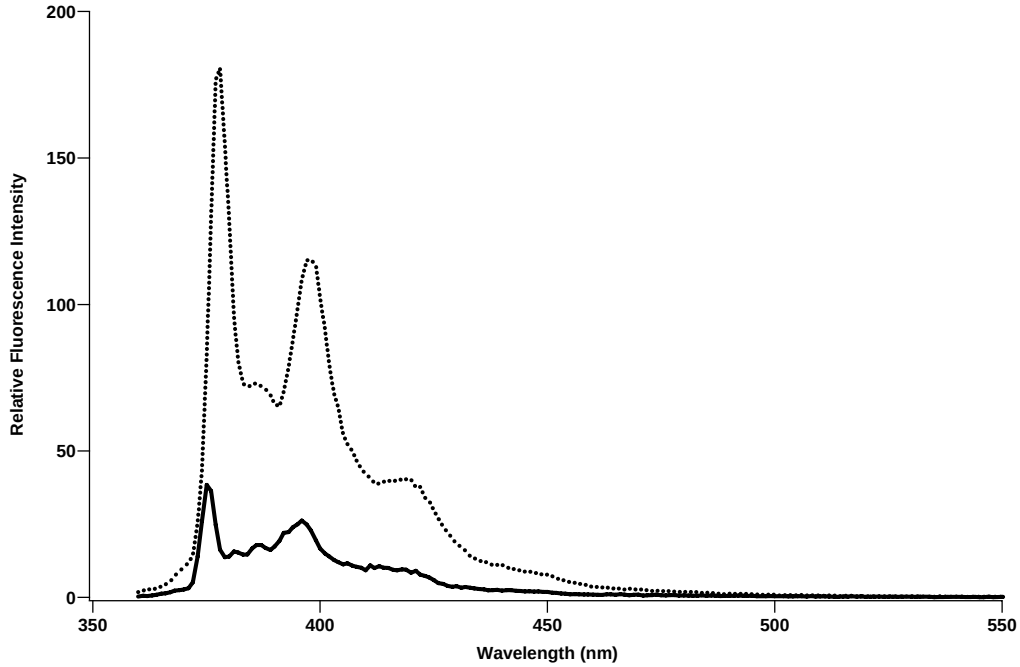

Figure 5.4 Fluorescence emission spectra of free PBA (solid) and PBA-PgC_6 (dotted)

In the solid-state the result from the X-ray and the ^{1}H-NMR also indicated that the population of the crystals collected was 150%; some of the capsules are doubly occupied, while others are monopopulated. However, communication between both entities in the solid sate does not exist because few ACN molecules are sandwiched in between (Figure 5.5).[4]

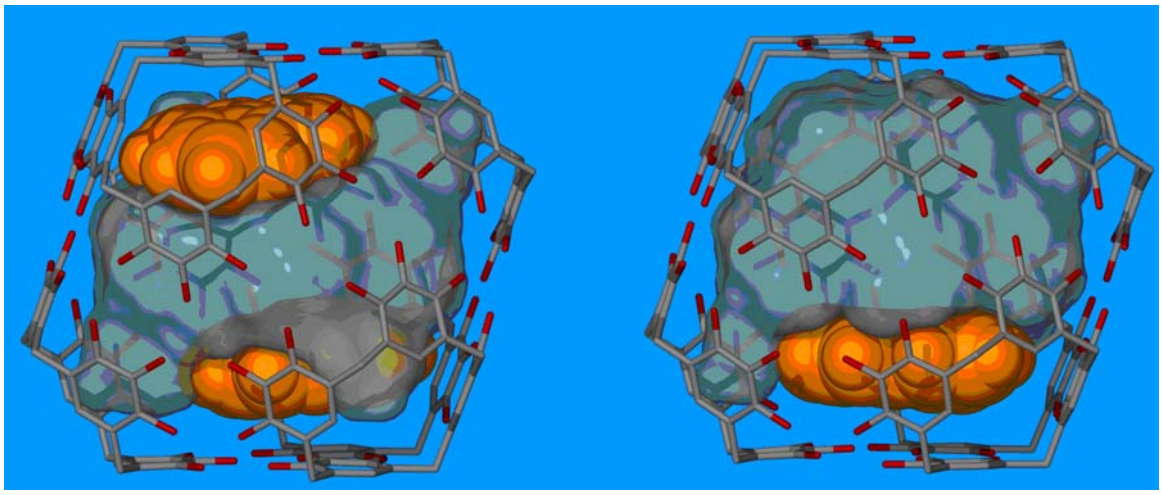

Figure 5.5 Diagram of the crystal structure of PBA-PgC_6, showing the area (green) where more than one molecule of ACN is present.

In solution, it is noted that the fluorescence emission intensity of the PBA-PgC_6 in HEX is four times more enhanced compared to the free PBA in HEX (Figure 5.4). This increased quantum yield appears to result from the structural constraints imposed by the host, which minimize radiationless excited-state decay pathways, such as collisional quenching by solvent molecules. Furthermore, there is no emission intensity seen in

Figure 5.4 at 470 nm, characteristic of an excimer, or excited-state PBA dimer.[16] This result confirms that in solution, as in the solid state, any capsules that contains two guests keeps them apart, suggesting the co-encapsulation of the crystallization solvent, ACN.

To further assess the nature of and extent to which PBA guests remain encapsulated in solution, we added a known fluorescence quencher, *N,N*-dimethylaniline (DMA) to the mixture. In HEX solution, free PBA forms an emissive excited-state, charge-transfer (CT) complex (exciplex) with DMA, leading to a new emission band at 440 nm (Figure 5.6). This exciplex was not observed in HEX solutions of PBA-ACN-PgC_6 with DMA added (Figure 5.1), suggesting that the PBA guests do not leave the capsule. The DMA molecules are small enough to penetrate the hydrogen bonds seams, and thereby, quench PBA fluorescence, as noted by the reduced emission intensity seen in Figure 5.7. The lack of exciplex emission confirms the presence of residual ACN within the capsules, because it is known that polar solvents inhibit emission from the exciplex.[17]

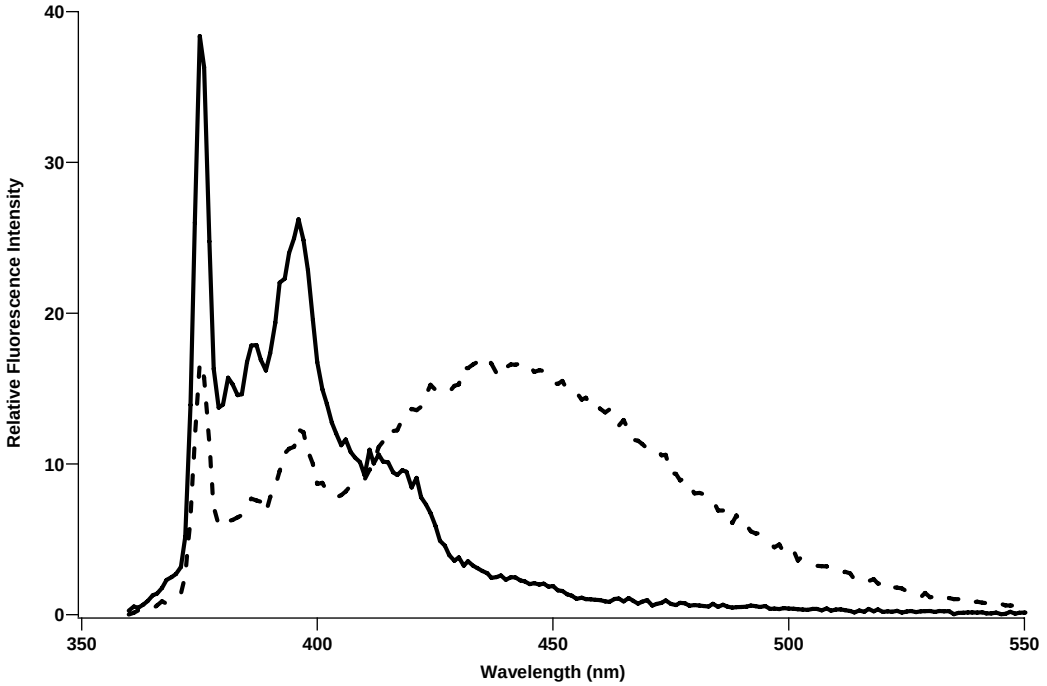

Figure 5.6 Fluorescence emission spectra of PBA in HEX (solid) with the addition of 10 μL of 100% DMA (dashed).

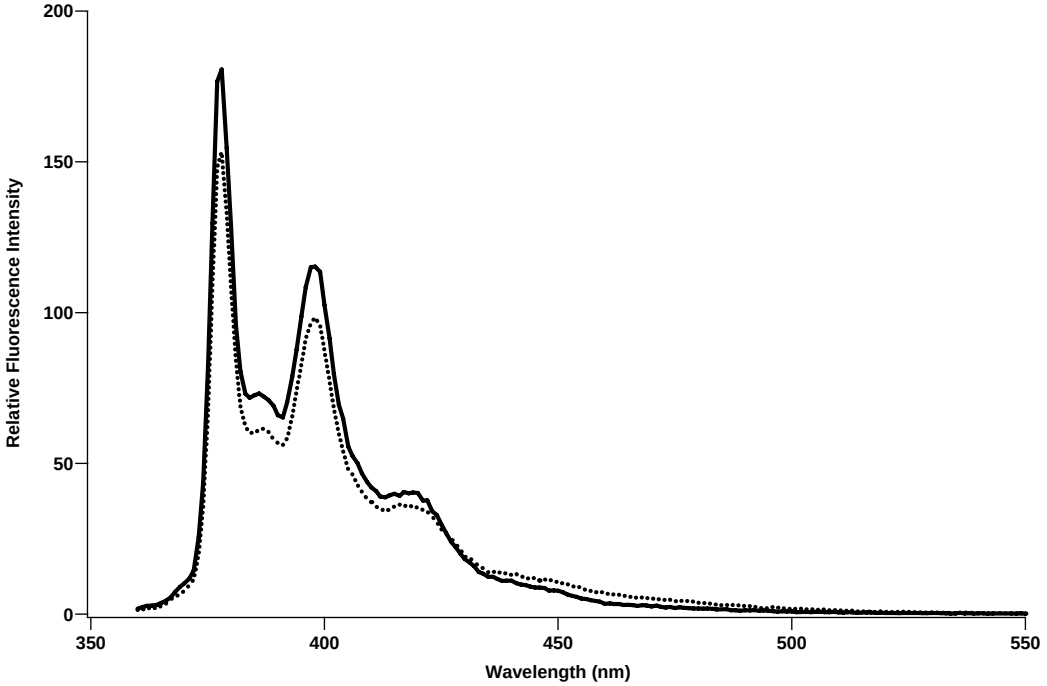

Figure 5.7 Fluorescence emission spectra of PBA-PgC_6 in HEX (solid) with the addition of 10 μL of DMA (dotted).

As a control study, we confirmed polar solvents inhibit exciplex emission in HEX solutions. As seen in Figure 5.8 the exciplex emission is indeed inhibited, with the increase in microenvironmental polarity with ACN the addition of ACN. Moreover, the maximum of CT-band is also red shifted, consistent with DMA-quenching literature (Figure 5.10).[4,13,17-19] Once the species is surrounded by highly polar solvent, the heteroexcimer complex switches from the higher excited state to a lower state, since the dielectric constant is increased and the complex would be stabilized.

As an another control, we added free PBA to the (Figure 5.9) PBA-ACN-PgC_6 in HEX with DMA already added, and the exciplex emission emerged as expected (Figure 5.11). It is, therefore, clear that, at least in nonpolar solvents, the PBA guests in PBA-ACN-PgC_6 remain tightly enclosed and do not exchange with external PBA.

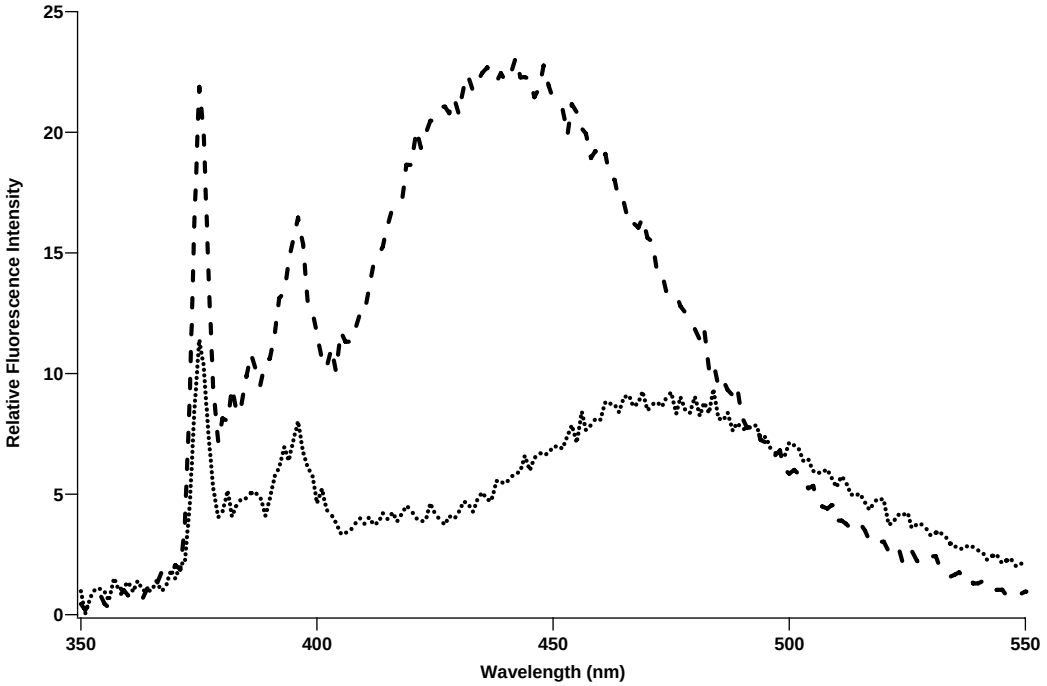

Figure 5.8 Fluorescence emission spectra of PBA in HEX with DMA (dashed) with the addition with the addition of 100 μL of ACN (dotted).

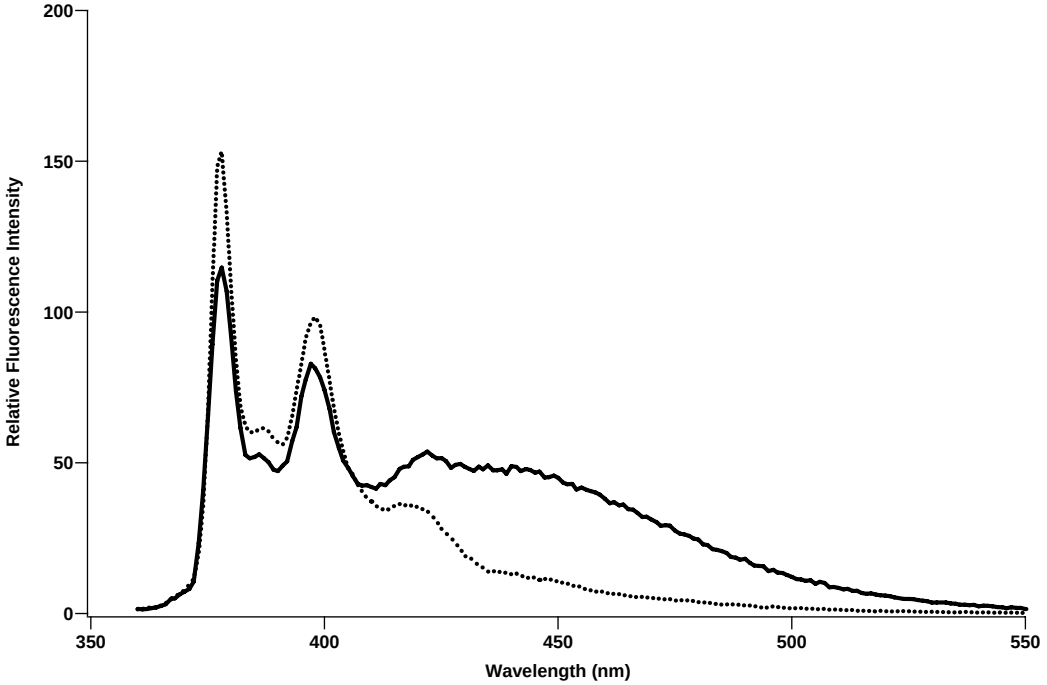

Figure 5.9 Fluorescence emission spectra of PBA-PgC_6 in HEX + 10 μL of 100% DMA (dotted) with the addition of *exo*-capsule PBA (solid).

The quenching mechanism for PBA by DMA is diffusion controlled as shown in Scheme 5.1:

$$PBA^* + DMA \underset{\text{Diffusion}}{\rightleftharpoons} PBA^* \cdots DMA \longrightarrow \underset{\text{Emissive exciplex}}{(PBA^-DMA^+)^*}$$

Scheme 5.1 Quenching scheme of PBA by DMA, and the formation of the emissive exciplex.

As mentioned in Chapter 2, quenching can occur by two separate mechanisms – static: that involves the formation of complexes in the excited state, and dynamic, that involves collisions with the solvent molecules. As seen in Figure 5.10, low quencher concentration (2%), the Stern-Volmer relationship for F_0/F versus [Q] is linear (Equation 2.22).

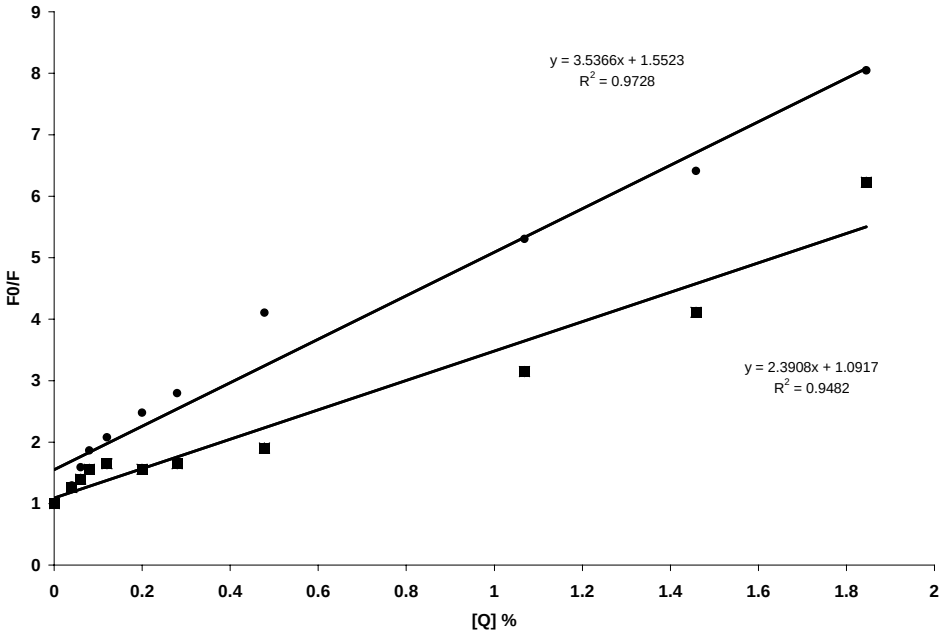

Figure 5.10 Stern-Volmer plot of quencher concentration versus fluorescence emission intensity change; free PBA (dots) and PBA-ACN-PgC_6 (square) in HEX.

Free PBA is quenched more efficiently than the encapsulated PBA since DMA has better access to the free probe than to the sequestered PBA ($k_{PBA} > k_{PBA\text{-}PgC_6}$), which is surrounded by ACN molecules in the self-assembled capsule.

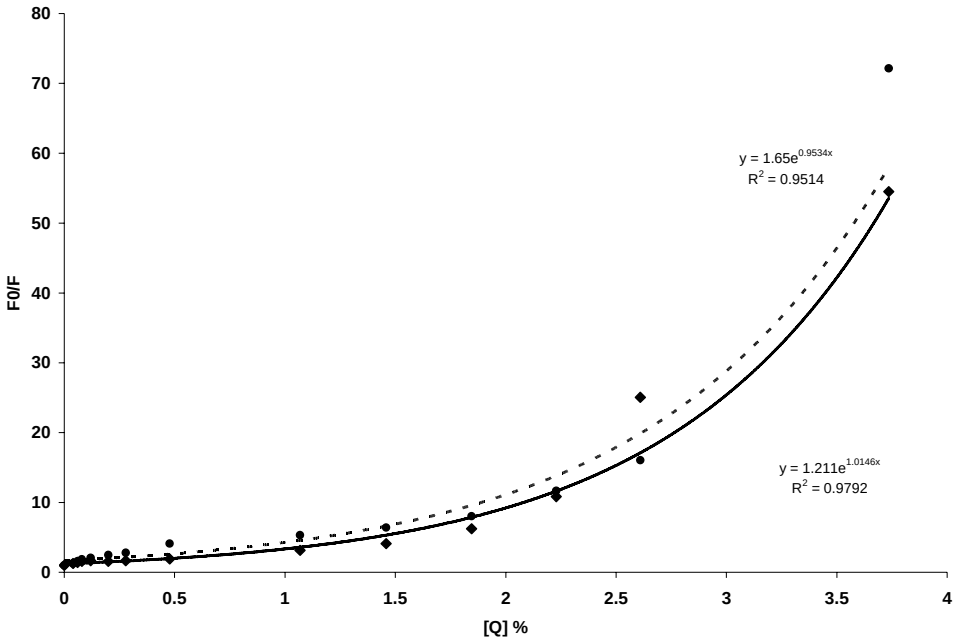

Figure 5.11 Stern-Volmer plot at high quencher concentration, free PBA (solid, dots) and PBA-PgC_6 (dashed line, diamonds) in HEX.

As seen in Figure 5.11, for higher quencher concentration, an upward curve starts to form leading to a conclusion that both static and dynamic quenching occur.[20] Since the relation (Equation 5.1) is mainly directed by $[Q]^2$ versus [Q] for the static alone, and the upward curvature is due to the square factor.

$$\frac{F_0}{F} = (1 + k_Q[Q])(1 + k_{Ar...Q}[Q]) \qquad \textbf{Equations 5.1}$$

Another common explanation of the nonlinearity of the Stern-Volmer plot is that the quencher does not have accessibility to the fluorophore.[15]

The supramolecular assembly was also found to be very robust in polar solutions. Acetonitrile stock solutions of PBA-ACN-PgC_6 were allowed to sit for 30 days and were then transferred to HEX. The amount of PBA that leached from the capsules, as measured by exciplex formation with DMA, was only ~10%.

From the data in Figures 5.12 and 5.13, we concluded that solvent exchange from the capsule to the surrounding media and vice versa does not occur, particularly given the fact that, HEX and ACN are not miscible. Therefore, the solvent encapsulated along with PBA does not change. The emission spectra from stocks solutions of PBA-ACN-PgC_6 in HEX and ACN have the same profile as free PBA in ACN (Figure 5.12 and 5.13).

Lifetime measurements were performed on PBA-ACN-PgC_6 and compared with free PBA (Figure 5.14) in the same solvent, and the results were consistent with the steady-state data. The lifetime of PBA in an environment affording protection from normal collisional deactivation is longer, and this is consistent with the fluorescence emission data where an increase of the quantum yield appears to result from the structural constraints imposed by the host. Using NLLS and MEM analysis, free PBA in HEX has

a recovered lifetime of 8.1 ns (Figure 5.14) and the PBA-ACN-PgC_6 a rather distributed lifetime of ~120 ns.

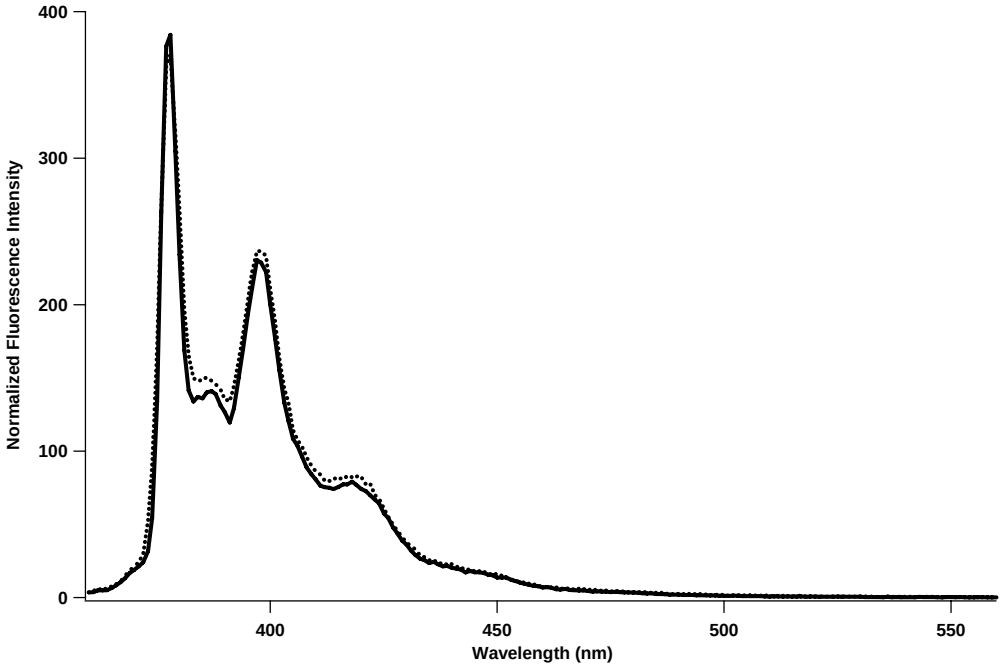

Figure 5.12 Fluorescence emission spectra of two samples of PBA-ACN-PgC_6 in HEX: First sample from an ACN stock solution (solid); second sample prepared from a HEX stock solution (dotted).

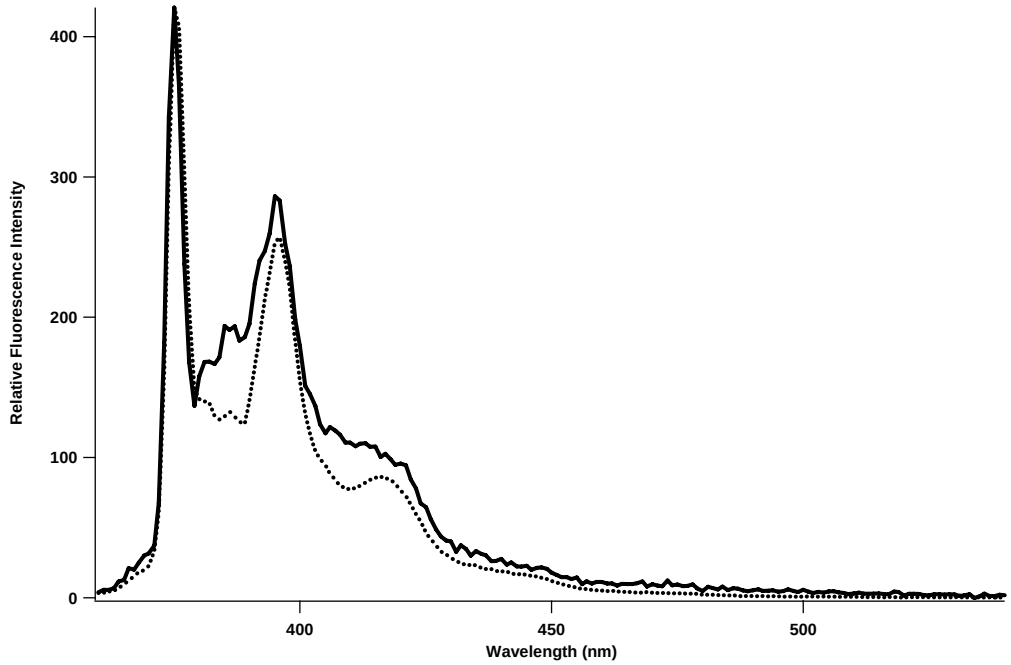

Figure 5.13 Fluorescence emission spectra of two samples of PBA in HEX (solid) and in ACN (dotted).

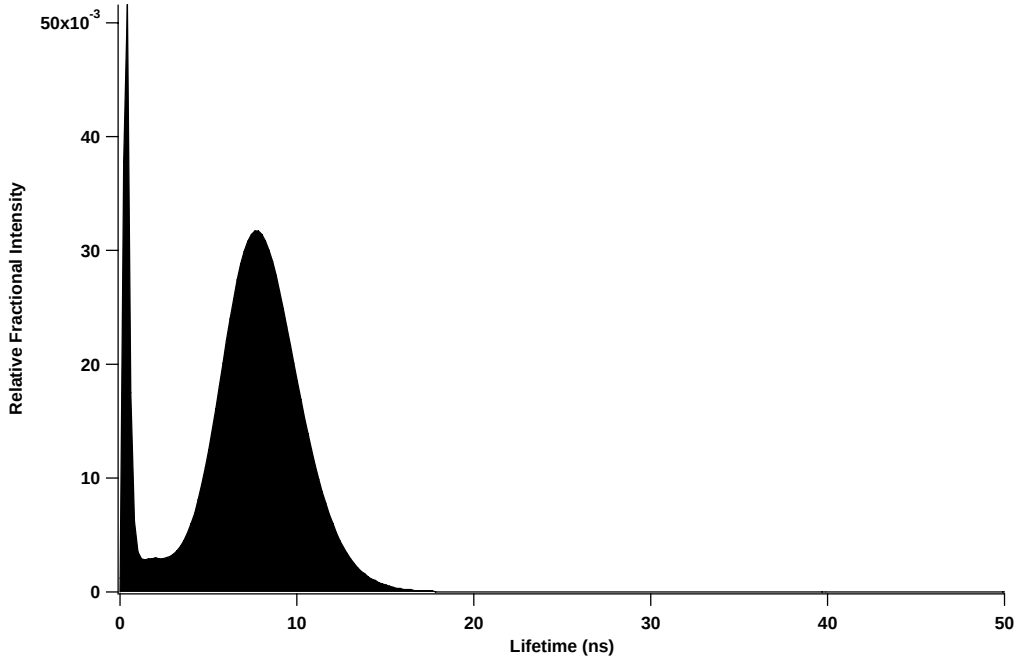

Figure 5.14 Representative MEM plot of the fluorescence lifetime distribution recovered for the PBA in HEX.

The lifetime results for PBA-ACN-PgC_6 are in the same range as free PBA in an oxygen free solvent (i.e. free of the collisional deactivation). This is consistent with the expected microenvironment of the constrained fluorophore.

III. Conclusion:

Despite recent strides in the synthesis of elaborate nanometer-scale molecular hosts, the internal structure of these self-assembled cages remains ill-characterized. Here we used PBA as guests in PgC_6 capsules to relay information about the chemical environment on the interior of the assemblies. Spectroscopic and single crystal X-ray crystallographic studies showed that, in both solution and the solid state, the host can encapsulate two PBA guests and keep them well separated through specific interactions with the capsule walls and the presence of crystallization solvent, ACN.

IV. References:

(1) Acree, W. E., Jr.; Tucker, S. A.; Fetzer, J. C. *Poly. Arom. Compd.* **1991**, *2*, 75-105.

(2) Hara, K.; Ware, W. R. *Chem. Phys.* **1980**, *51*, 61-8.

(3) Nakajima, A. *Bull. Chem. Soc. Jpn.* **1971**, *44*, 3272-7.

(4) Dalgarno, S. J.; Tucker, S. A.; Bassil, D. B.; Atwood, J. L. *Science* **2005**, *309*, 2037-2039.

(5) Dumas, D.; Muller, S.; Gouin, F.; Baros, F.; Viriot, M.-L.; Stoltz, J.-F. *Arch. Biochem. Biophys.* **1997**, *341*, 34-39.

(6) Mitnick, M. H.; Jobsis, F. F. *J. Appl. Physiol.* **1976**, *41*, 593-597.

(7) Ribou, A.-C.; Vigo, J.; Salmon, J.-M. *Photochem. Photobio.* **2004**, *80*, 274-280.

(8) Kalyanasundaram, K.; Thomas, J. K. *J. Am. Chem. Soc.* **1977**, *99*, 2039-44.

(9) *The molecular volume of PBA was calculated using Chem3D Ultra 10.0 (www.CambridgeSoft.com)*.

(10) *Crystal data for **3**: $C_{177.50}H_{237.75}N_{3.25}O_{37.50}$, M = 3016.96, triclinic, a = 19.567(3), b = 22.605(3), c = 23.309(3) Å, α = 69.819(3), β = 70.133(3), γ = 72.(2)°, U = 8887(2) Å^3, μ = 1.127 mm^{-1}, T = 173(2) K, space group P$^{\bar{}}$1, Z = 2, Mo-Kα radiation (λ = 0.71073 Å), Final GOF = 1.624, R_1 = 0.1810, 60406 reflections measured, 37293 unique (R_{int} = 0.0722) which were used in all calculations. The final ωR(F^2) was 0.4443 (all data). X-ray data was collected on a Bruker SMART 1000 CCD diffractometer. CCDC 276051 contains the supplementary crystallographic data for this paper. These data can be obtained free of charge at www.ccdc.cam.ac.uk/conts/retrieving.html [or from the Cambridge Crystallographic Data Centre, 12 Union Road, Cambridge CB2 1EZ, UK; fax: (internat.) +44-1223/336-033; Email: deposit@ccdc.cam.ac.uk*

(11) Crawford, M. K.; Wang, Y.; Eisenthal, K. B. *Chem. Phys. Lett.* **1981**, *79*, 529-533.

(12) Kauffman, J. F.; Khajehpour, M.; Saleh, N. i. *J. Phys. Chem. A* **2004**, *108*, 3675-3687.

(13) Okada, T.; Fujita, T.; Kubota, M.; Masaki, S.; Mataga, N.; Ide, R.; Sakata, Y.; Misumi, S. *Chem. Phys. Lett.* **1972**, *14*, 563.

(14) Okada, T.; Migita, M.; Mataga, N.; Sakata, Y.; Misumi, S. *J. Am. Chem. Soc.* **1981**, *103*, 4715-20.

(15) Lakowicz, J. R. *Principles of Fluorescence Spectroscopy*; Plenum Press: New York, 1983.

(16) Lakowicz, J. R. *Principles of Fluorescence Spectroscopy*; 2nd ed.; Kluwer Academic/Plenum Publishers: New York, 1999.

(17) Gupta, D.; Basu, S. *J. Photochem.* **1975**, *4*, 307-8.

(18) Dalgarno, S. J.; Bassil, D. B.; Tucker, S. A.; Atwood, J. L. *Angew. Chem., Int. Ed. Engl.* **2006**, *45*, 7019-7022.

(19) Khajehpour, M.; Kauffman, J. F. *J. Phys. Chem. A* **2000**, *104*, 9512-9517.

(20) Weber, G. *Trans. Farad. Soc.* **1948**, *44*, 185-9.

Chapter 6: The Encapsulation of 1-(9-Anthryl)-3-(4-Dimethylaniline) Propane

I. Introduction:

To date, 1-(9-anthryl)-3-(4-dimethylaniline) propane (ADMA, Figure 6.1) and its derivatives[1] have been used to study solvation and reactivity in complex media, such as supercritical fluids,[2,3] micelles,[4] and polymers.[1] Herein, the encapsulation of ADMA in both *C*-hexylpyrogallol (PgC_6) and *C*-decylpyrogallol (PgC_{10}) hexamers in the presence of either acetonitrile, ACN, (PgC_{10}) or ethyl acetate, EA, (PgC_6 and PgC_{10}) is reported.

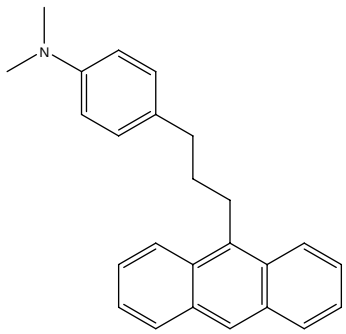

Figure 6.1 Molecular structure of ADMA.

This study differs markedly compared to the pyrene butyric acid, PBA, work, where the *N*,*N*-dimethylaniline, DMA, quencher had to be added to a solution containing

the host-guest assembly.[5] The ADMA molecule contains both a fluorescent moiety, anthracene (electron acceptor, A) and quenching unit, dimethylaniline (donor, D), which are connected by a propyl linker. Therefore, ADMA can undergo intramolecular charge transfer (CT), when irradiated by having the anthracene moiety accepting an electron from the DMA fragment. Moreover, the ADMA molecule can fold to form a sandwich-like arrangement with π-stacking between DMA and the anthracene moeity.[6]

The ADMA molecule is an example of a D-$(CH_2)_n$-A system. Charge transfer in such D-A systems is diffusion controlled. In the case of ADMA, diffusion can be restricted by many factors, including solvent viscosity or polarity, as well as steric constraints that keep the donor and acceptor apart.[2,7-9] Hence, ADMA has been extensively studied in solvents with a wide range of dielectric constants (ε), such as EA (ε = 6.02), tetrahydrofuran, (THF, ε = 8.05), and ACN (ε = 37.5).[3,9-14] Like PBA-DMA system, CT in ADMA results in intense exciplex emission (*ca.* 540 nm) in solvents such as EA and THF, but not ACN, due its high dielectric constant.[13]

In addition, the relatively large π-surface in ADMA may promote adhesion to the inner capsule walls, which is a desirable property believed to contribute to the robustness of the PBA-ACN-PgC_6 complex. The PgC_n host capsules can accommodate an ADMA guest molecule, with a molecular volume of ~347 $Å^3$,[15] calculated from the X-Seed software.[15] It is anticipated that ADMA will adjust its spatial conformation in response to the potential host-guest interactions with the hexameric assembly.

II. 1-(9-anthryl)-3-(4-dimethylaniline) propane synthesis:

The three-step ADMA synthesis (Figure 6.2, 6.4, 6.6) was performed in house by repeating the Syage *et al.* procedure with minor modifications as follows:[16]

Stage I (Figure 6.2): Nine g of 9-acetylanthracene were diluted in 300 mL of anhydrous ethanol and mixed with solution of 7 g of *N,N*-dimethylamino benzaldehyde, in 50 mL ethanol. After the solution was prepared, an addition of 25 mL of 3mol L^{-1} sodium hydroxide was made. The solution was stirred for 48 hours at room temperature (~23 ^{o}C), and a yellow precipitate started to form after couple hours of reaction. The solid was then filtered and recrystallized from methanol separated by high performance liquid chromatography, HPLC, and analyzed by proton nuclear magnetic resonance, ^{1}H-NMR, and Fourier transform infrared spectroscopy, FTIR (Figure 6.3).

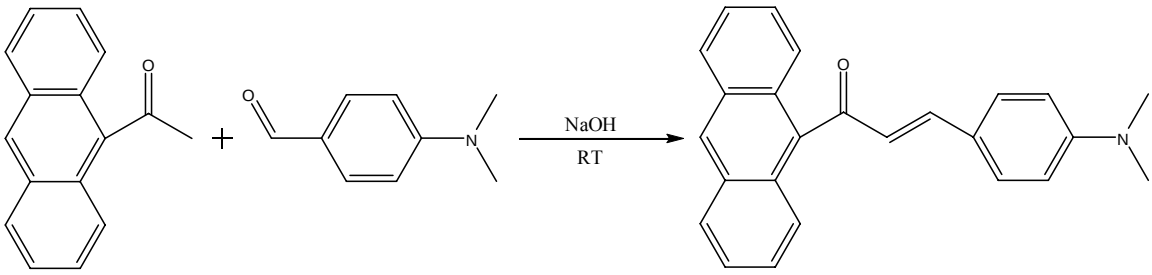

Figure 6.2 Stage I: Aldol condensation base catalyzed by sodium hydroxide.

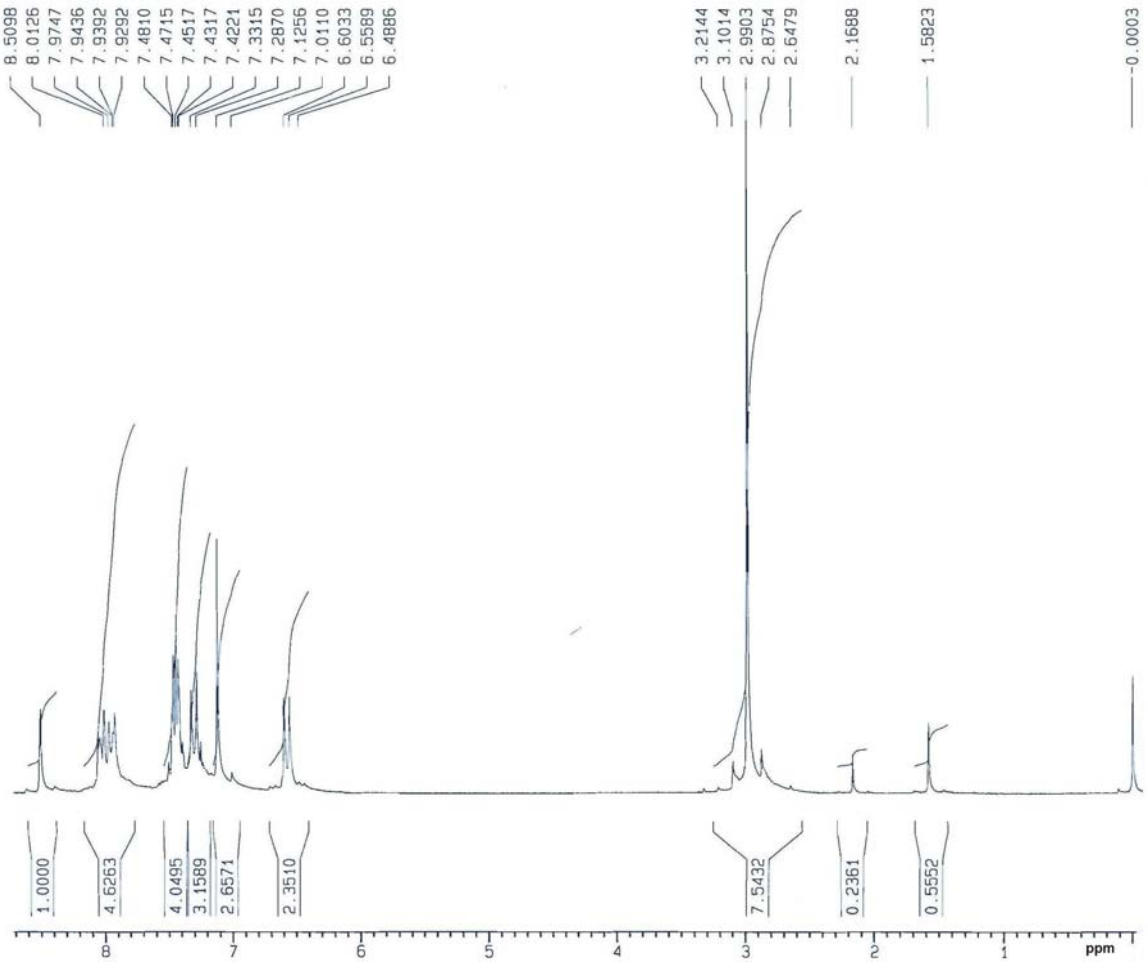

Figure 6.3 ^{1}H-NMR spectra of the Stage I product: Yield 94%, [NMR ($CDCl_3$) δ 2.99 (*s*,6), 6.56 (*d*,2), 7.01 (*s*,2), 7.28 (*d*,2), 7.45 (*d*,2), 7.94 (*m*,4), 8.51 (*s*,1)], [FTIR (CCl_4) 1585, 1600 cm^{-1}].

Stage II (Figure 6.4): Using 10% or 5% wt. palladium on carbon (Pd/C) hydrogenation of Stage I product (3g diluted in 200 mL of THF) was carried out at atmospheric pressure with hydrogen bubbled through the solution overnight. The catalyst was filtered from the solution, and then it was rotovapped until a dry thick gel was obtained. Recrystallization

of product from methanol was performed as well and it was also separated by HPLC and analyzed by ^{1}H-NMR and FTIR (Figure 6.5).

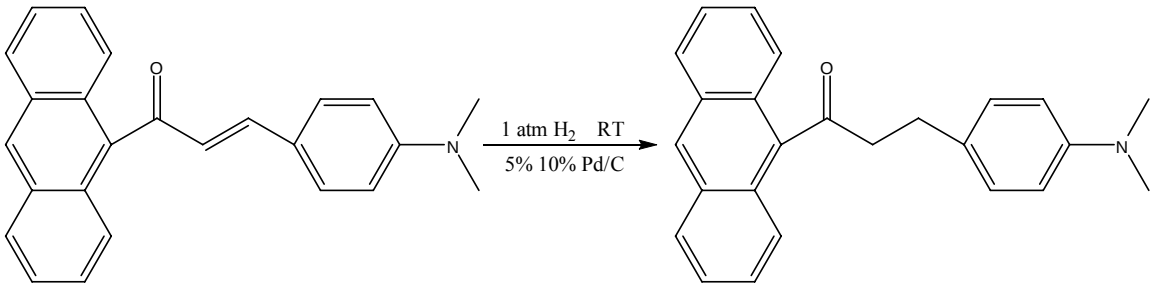

Figure 6.4 Stage II: Hydrogenation reaction of the Stage I product.

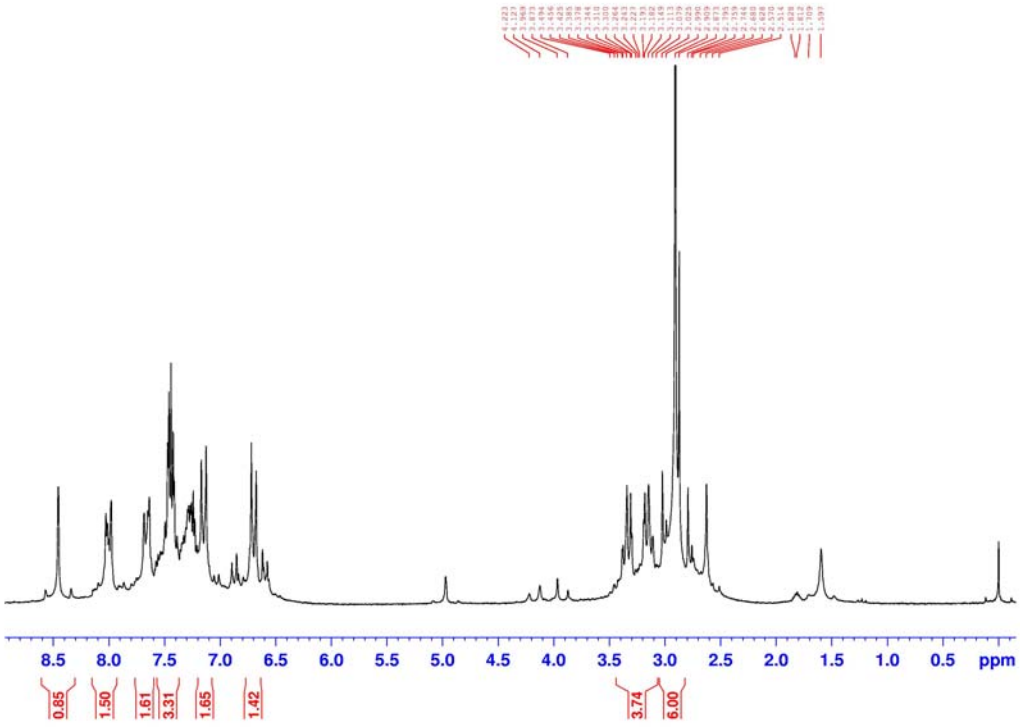

Figure 6.5 ^{1}H-NMR spectrum of the Stage II product: Mp 100 ^{o}C, Yield 90%, [NMR ($CDCl_3$) δ 2.99 (*s*,6), 3.20 (*q*,4), 6.68 (*d*,2), 7.17 (*d*,2), 7.26 (*d*,2), 7.46 (*m*,4), 7.98 (*m*,2), 8.46 (*s*,1)], [FTIR (CCl_4) 1600 cm^{-1}].

Stage III (Figure 6.6): The Stage II carbonyl product was deoxygenated by using super hydride under nitrogen to avoid the moisture from the surrounding environment, using a Schlenk line as follows: Three and one half g of dried Stage II product were dissolved in ~ 50 mL of super hydride and stirred at room temperature for 30 minutes in a dry flask. After 2 hours of refluxing (*ca.* 90 ^{o}C), 70 mL of 3 mol L^{-1} NaOH and 35 mL methanol were added. After 3 hours, ~8 mL of hydrogen peroxide (H_2O_2) was added, and after 12 hours of refluxing, 10 mL of H_2O_2 was added. With the solution cooled to room temperature, a liquid-liquid separation was performed. The aqueous phase was washed with ethyl ether, and the ether combined with the organic phase, which was dried with magnesium sulfate ($MgSO_4$), filtered, and rotovapped.

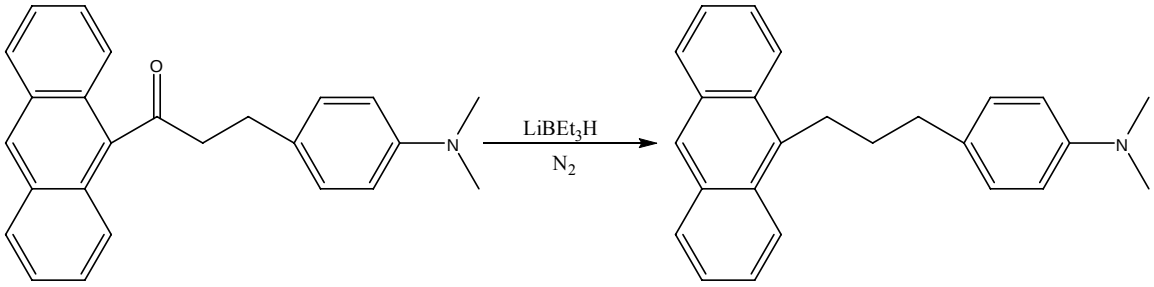

Figure 6.6 Stage III: Reduction of the carbonyl group on the Stage II.

All products were separated and purified via flash chromatography; every fraction was fully analyzed by means of ^{1}H-NMR (Figure 6.7), FTIR, and HPLC (Figure 6.8). Good fractions were selected and combined. Crystallization in ethanol resulted in white crystals of ADMA and were analyzed by single crystal X-ray diffraction (Figure 6.9).

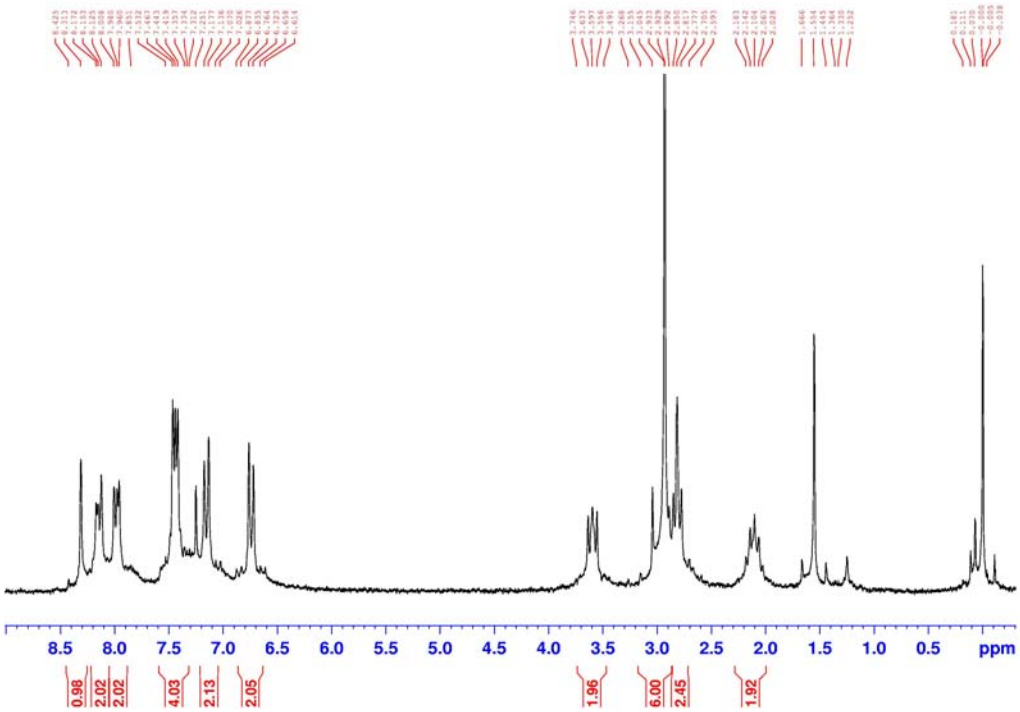

Figure 6.7 ^{1}H-NMR spectrum of ADMA: Mp 101 ^{o}C, Yield 50%, [NMR ($CDCl_3$) δ 2.99 (*s*,6), 3.20 (*q*,4), 6.74 (*d*,2), 7.18 (*d*,2), 7.44 (*m*,4), 7.98 (*m*,2), 8.15 (*m*,2), 8.31 (*s*,1).]

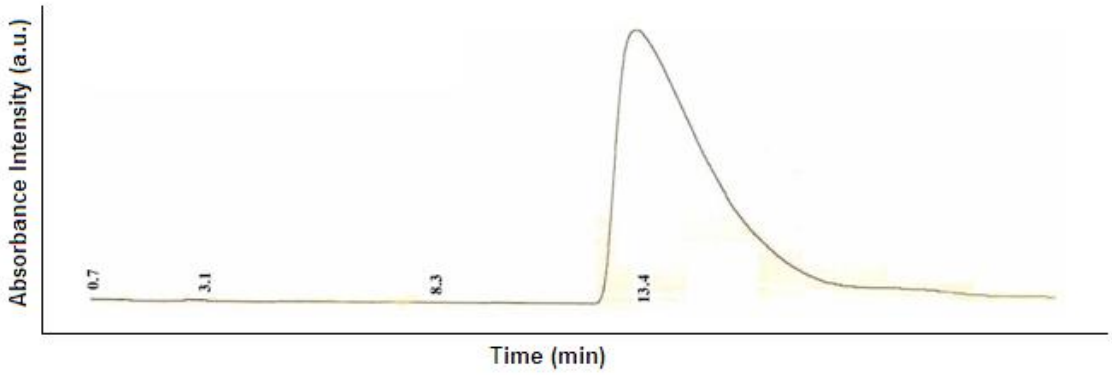

Figure 6.8 The chromatogram of ADMA from stage III after purification. The fluorescent probe elutes at 13.4 minutes.

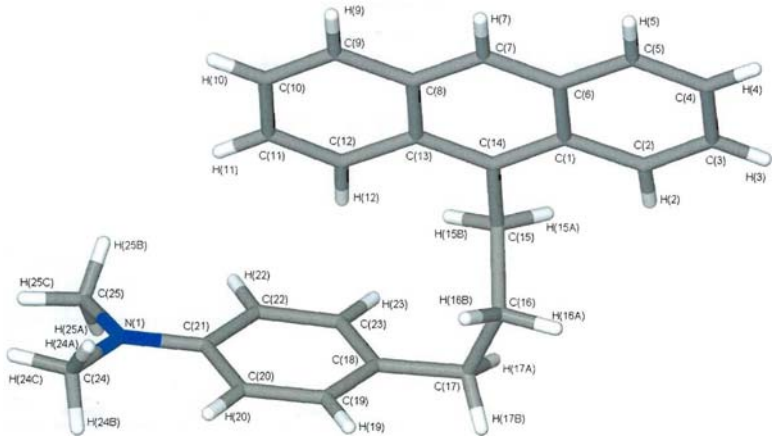

Figure 6.9 X-ray structure of the final ADMA product. Melting point: 101°C, crystallized from ethanol.[17]

III. 1-(9-anthryl)-3-(4-dimethylaniline) propane spectroscopic properties:

Nanocapsule crystals, containing ADMA and EA or ACN, were dissolved and studied in THF. Steady-state, fluorescence emission measurements determine the overall or average spectral properties of a sample. Whereas, dynamic fluorescence lifetime techniques are frequently used to enhance steady-state measurements, providing more detailed information through the additional discriminating factor.[18,19] Given the complex nature of the PgC_6 supramolecular assemblies, both fluorescence emission spectra and lifetimes were measured.

The absorbance profile of ADMA (Figure 6.10) looks the same in a variety of solvents and encapsulated in the nanocapsules. We do notice a minor shift (less than 3

nm) in the spectrum from a polar solvent (e.g. ACN) to a nonpolar solvent (e.g. HEX), but while consistent is within experimental error.

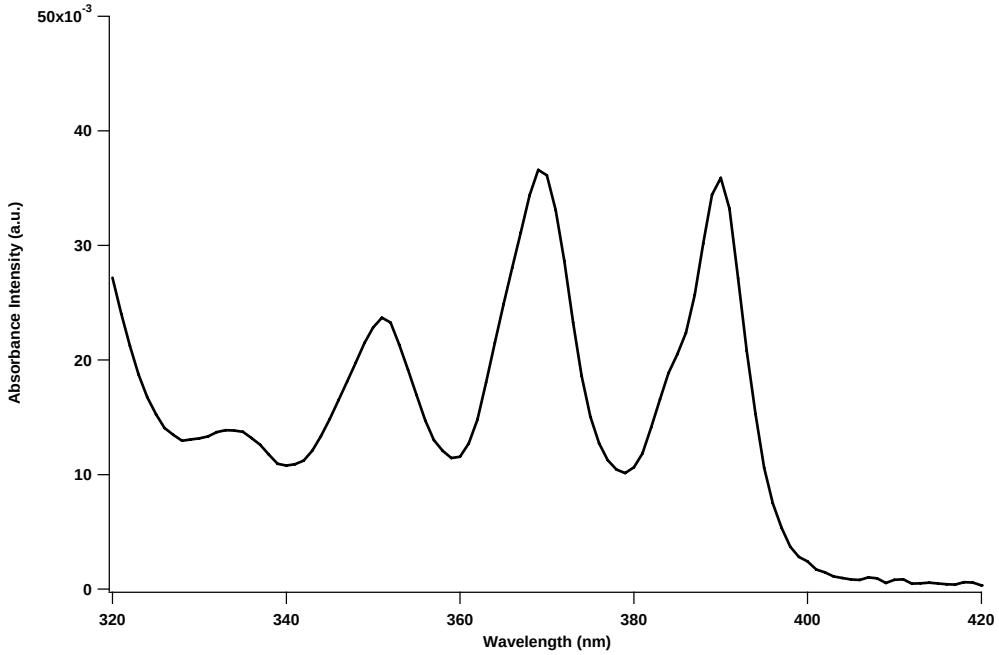

Figure 6.10 Absorbance spectra of ADMA in THF.

As seen in Figure 6.11, in the ground state, the unfolded conformation of ADMA is energetically more stable than the folded conformation. Following excitation (e.g. 369 nm), the ADMA molecule will undergo intramolecular CT following two different mechanism, depending on the surrounding media's polarity: (1) In nonpolar solvents, folding must precede CT; (2) In polar solvents, CT precedes folding, where the loose heteroexcimer takes place as an intermediate conformation before the molecule folds forming the emissive exciplex; and (3) In highly polar solvents, an extended form shows an energetically more stable conformation, where the CT is not emissive.[2,12] The ADMA photochemistry is comparable to free anthracene – DMA exciplex formation in solution,

where CT does occur in a diffusion controlled manner depending on the solvent polarity and viscosity.[2,7-9]

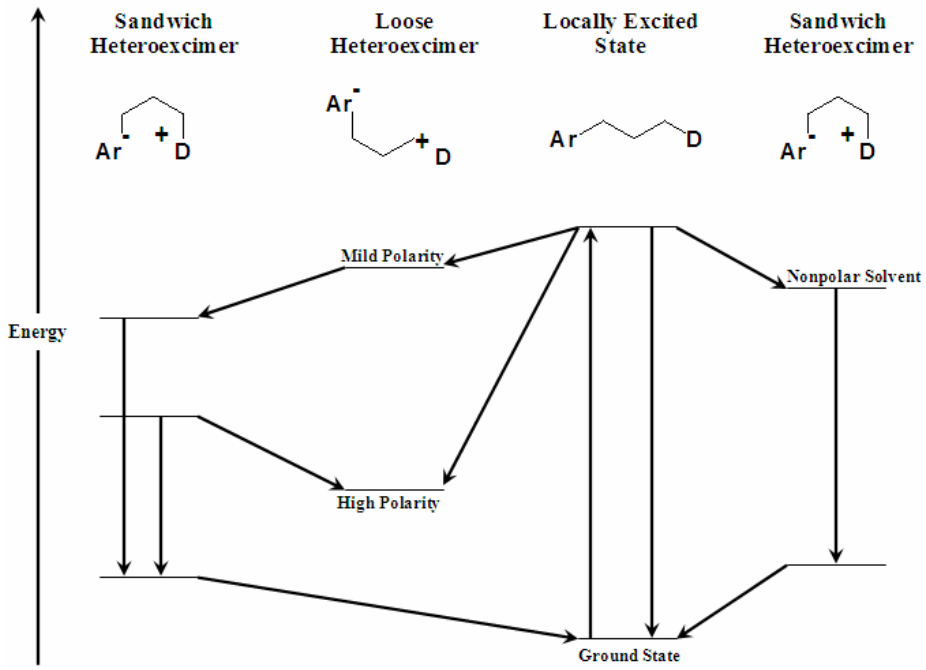

Figure 6.11 Kinetic scheme for photoinitiated (369 nm) charge transfer in ADMA (diagram reproduced from Kauffman *et al.*)[2,12]

Figure 6.12 shows the fluorescence emission spectra of free ADMA in neat solvents. Note that the 380-450 nm region of the spectrum is the contribution from the anthracene moiety of ADMA and is the same shape as the anthracene fluorophore alone in the same solvents. In agreement with the literature,[11,12] ADMA exciplex emission in THF and EA is distinct – a broad, featureless band at 540 nm. In ACN, exciplex emission is not easily discernable, but there is a very weak broad emission band centered around 580 nm. This observation is also consistent with the ADMA and DMA literature,

where exciplex emission, *if noted*, is red shifted (580 *vs.* 540 nm) due to an increase in the microenvironmental polarity of ACN, relative to THF or EA.[5,11,20,21]

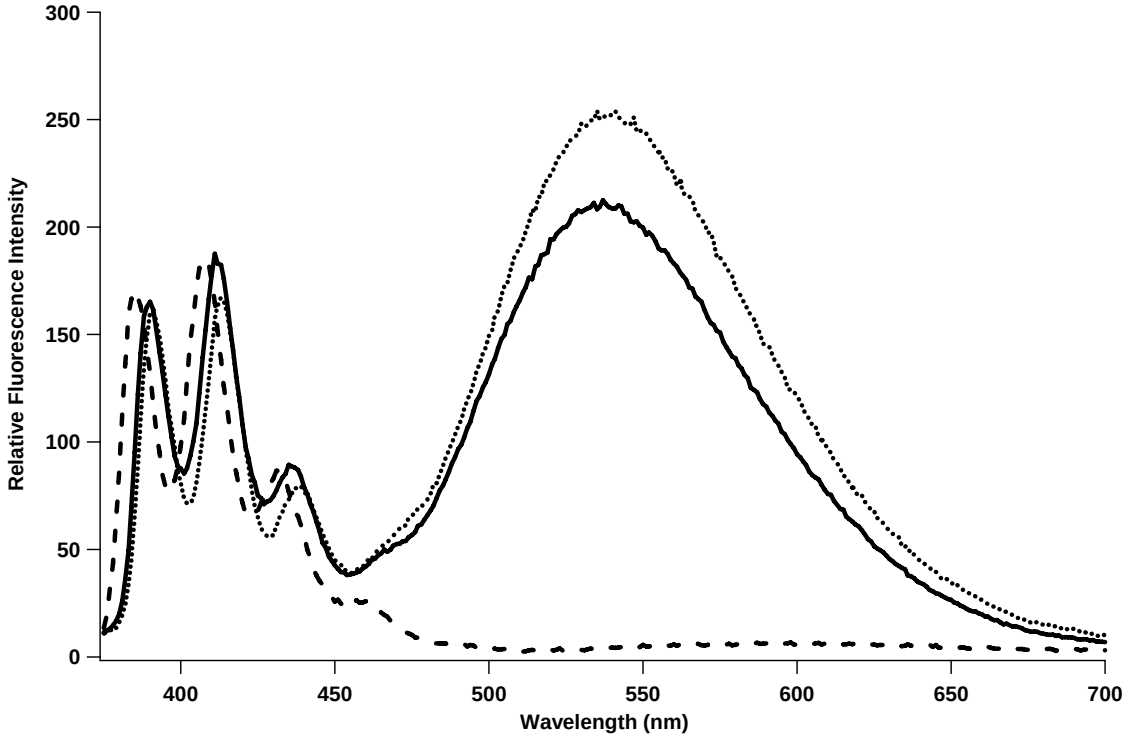

Figure 6.12 Fluorescence emission spectra of ADMA in THF (dotted) EA (solid) and ACN (dashed); spectra are blank and absorbance corrected.

The intensity profile of the ADMA in mineral oil (Figure 6.13) is enhanced due to the high viscosity of the surrounding environment which prevents the solvent collisions that quench the fluorescence signal, insulating ADMA in a protective environment. However, ADMA in oil at higher temperature (60º C), where the solvent viscosity decreases, CT increases because the molecule has more freedom to change its conformation.

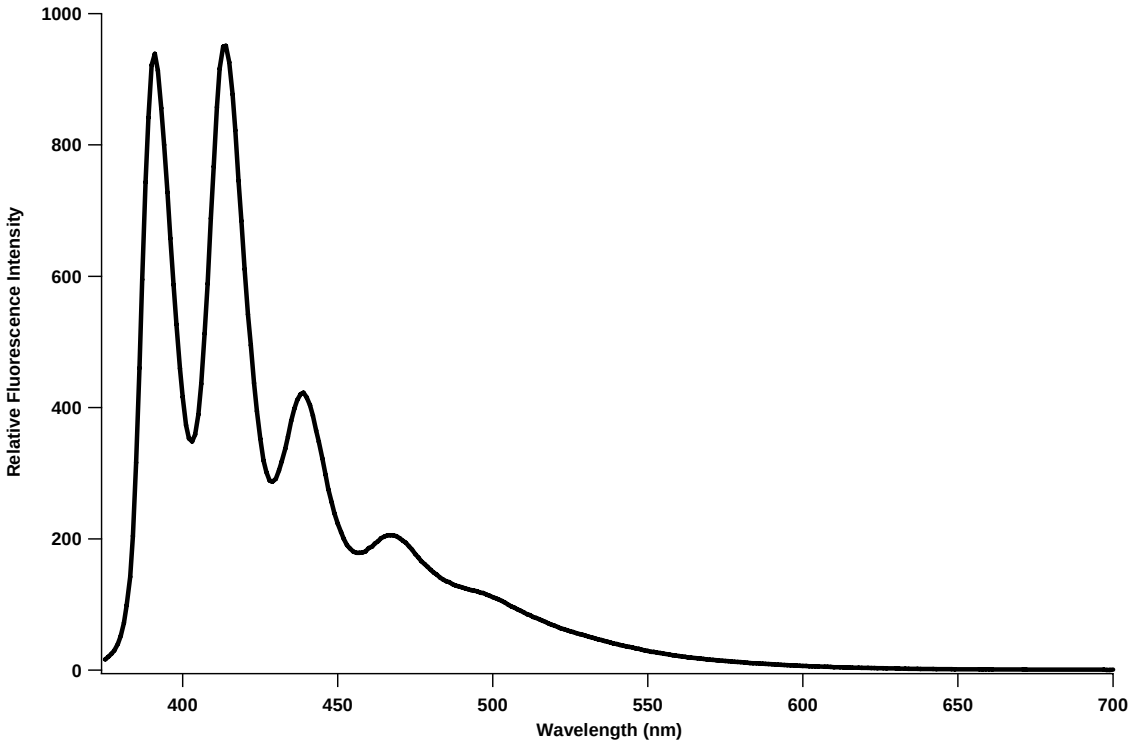

Figure 6.13 Fluorescence emission spectra of ADMA in mineral oil (μ = 0.02310 Pa·s) at room temperature.

Also consistent with published reports,[3,10,12,14,22,23] is the recovery of two definitive lifetime components (τ_2 and τ_3) in Table 6.1 that are attributable to ADMA. The τ_2 contribution (*ca.* 4 ns in THF and EA) is due to the decay of the anthracene moiety. A similar lifetime is recovered for ADMA in ACN, where only one lifetime is recovered (Figure 6.14).[11,13] Comparable lifetime results were observed in light mineral oil, where exciplex emission is minimized due to the high solvent viscosity (μ = 0.02310 Pa·s), which prevents ADMA from folding (Figure 6.15). In addition, the

lifetime of anthracene, the parent compound, was measured in THF and is 3.92 ns (Figure 6.16).

Sample	τ_1	(α_1)	τ_2	(α_2)	τ_3	(α_3)	χ^2
ADMA in ACN	0.00	(0.33)	6.48	(0.67)			1.4
ADMA in EA	0.08	(0.14)	4.31	(0.21)	13.32	(0.65)	2.3
ADMA in THF	0.00	(0.079)	4.33	(0.18)	16.96	(0.74)	3.9
ADMA-ACN-PgC_6 in THF	0.17	(0.033)	4.67	(0.76)	14.69	(0.21)	1.1

a Using the 370-610 nm filter combination.

Table 6.1 Representative fluorescence lifetimes (τ) and fractional intensities (α) of ADMA recovered using NLLS analysis.[a]

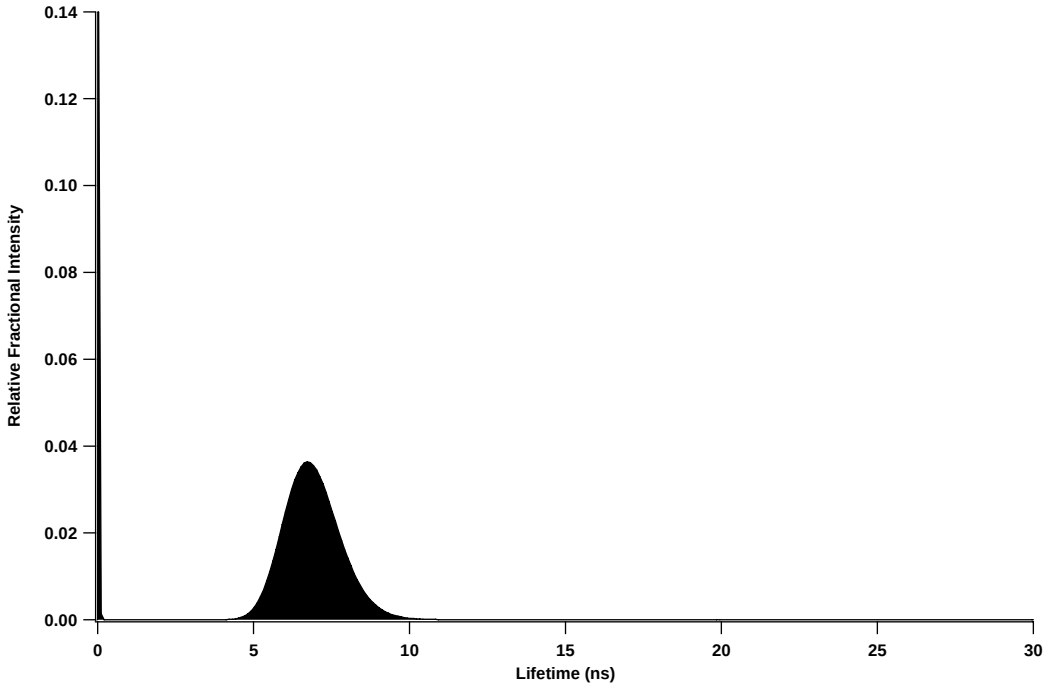

Figure 6.14 Representative MEM plot of the fluorescence lifetime distribution recovered for the ADMA in ACN.

These lifetime assignments were confirmed by isolating specific spectral regions with band-pass filters, as described previously. The τ_3 lifetime (*ca.* 15 ns) is attributed to the exciplex decay, also in agreement with literature.[3,10-12] Figure 6.15 summarizes the mechanism of the CT of ADMA in solvents. The resulting CT complex exhibits an emission spectrum, which is well separated from the anthracene spectrum. Kauffman *et al.* showed that the lifetime associated with k_3 ($\tau_{ct} = k_3^{-1}$), which is related to the CT, is long comparing with the other lifetimes ($\tau_d = (k_1 + k_2 + k_{nr})^{-1}$), which is related to the anthryl moiety.[3]

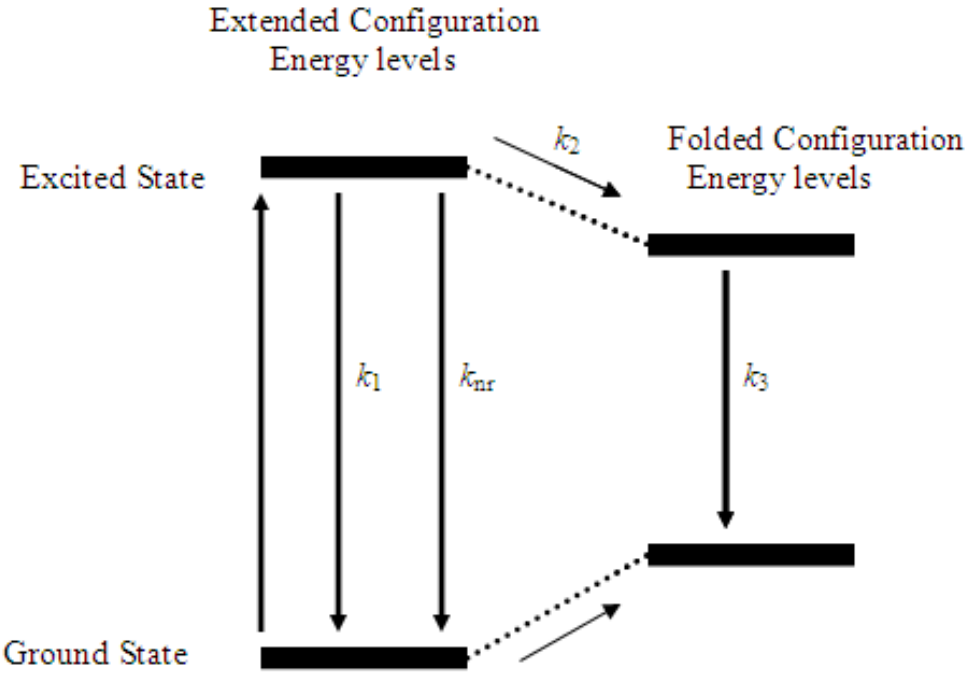

Figure 6.15 Mechanism for the photo excitation and subsequent relaxation of the ADMA molecule in nonpolar solvents, k_1 and k_{nr} are the radiative and non-radiative constants for the anthracene moiety, respectively; k_2 is the chain relaxation rate constant and k_3 is the radiative rate constant for exciplex emission.[3] (Scheme reproduced from[3]).

The shortest lifetime component, τ_1, is observed in both samples and blanks, is noted in previous studies,[24-26] and is attributed to scatter and instrumental artifact.[27,28] In addition, in polar solvents ($\varepsilon > 5.4$), ADMA is reported to have bi-exponential decay,[12,22] including a picosecond lifetime component. Given the frequency range of the instrument, this component is irresolvable and may contribute the larger fractional intensity ($\alpha \approx 0.3$) assigned to τ_1 of free ADMA in ACN.

In general, the fluorescence lifetime data and steady-state emission spectral profiles agree. In THF and EA, the exciplex emission of free ADMA is prominent in both the spectra (Figure 6.12) and the lifetime distribution ($\alpha \approx 0.7$ for τ_3, Table 6.1). Despite there being occasional evidence of very weak exciplex formation in the emission spectrum for ADMA in ACN,[7,13] no lifetime attributable to exciplex emission is recovered, consistent with the literature.[5,11,20,21 3,10,12,14,22,23]

IV. Encapsulated 1-(9-anthryl)-3-(4-dimethylaniline) propane:

The supramolecular assembly, in Figure 6.18, was formed by sonication of a hot saturated solution of ACN containing *C*-hexylpyrogallol[4]arene (PgC_6) and ADMA. Crystals were allowed to grow by after slow evaporation of the solvent. Single crystal X-ray diffraction along with ^{1}H-NMR spectra shows that 50% of the capsules are occupied by the probe ADMA. Originally, the encapsulation procedure was performed in a slightly different manner, where two equivalents of ADMA were added to six

equivalents of the *C*-alkyl-pyrogallol[4]arene, PgC_n, building block (i.e. a 2:1 ratio of ADMA to capsules), which are then crystallized from methanol. The ADMA-PgC_n complex was then recrystallized from ethyl acetate and washed with cold acetonitrile.[29] In order to maximize the chance of encapsulation Dalgarno *et al.* switched to a saturated probe solution in ACN, increasing the probability to entrap a guest by 100 folds.[5,30] The crystals of the nanocapsules containing the probe have a diamond-like geometry, identical to those of the pure ACN solvate, thus indicating successful probe encapsulation.[5,30]

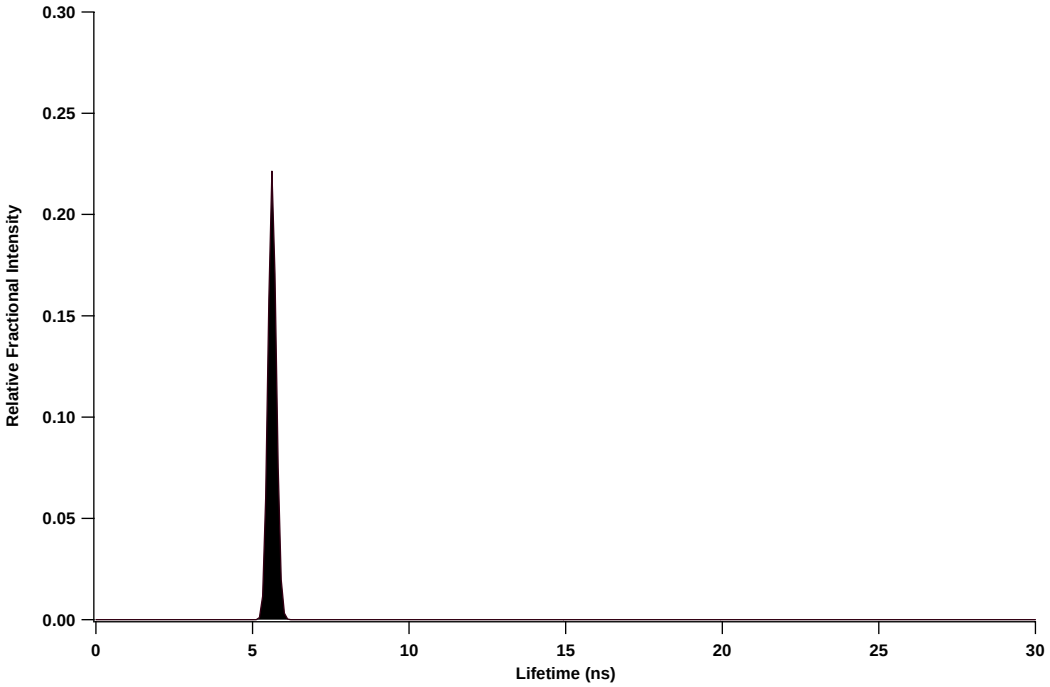

Figure 6.16 Representative MEM plot of the fluorescence lifetime distribution recovered for free ADMA in mineral oil.

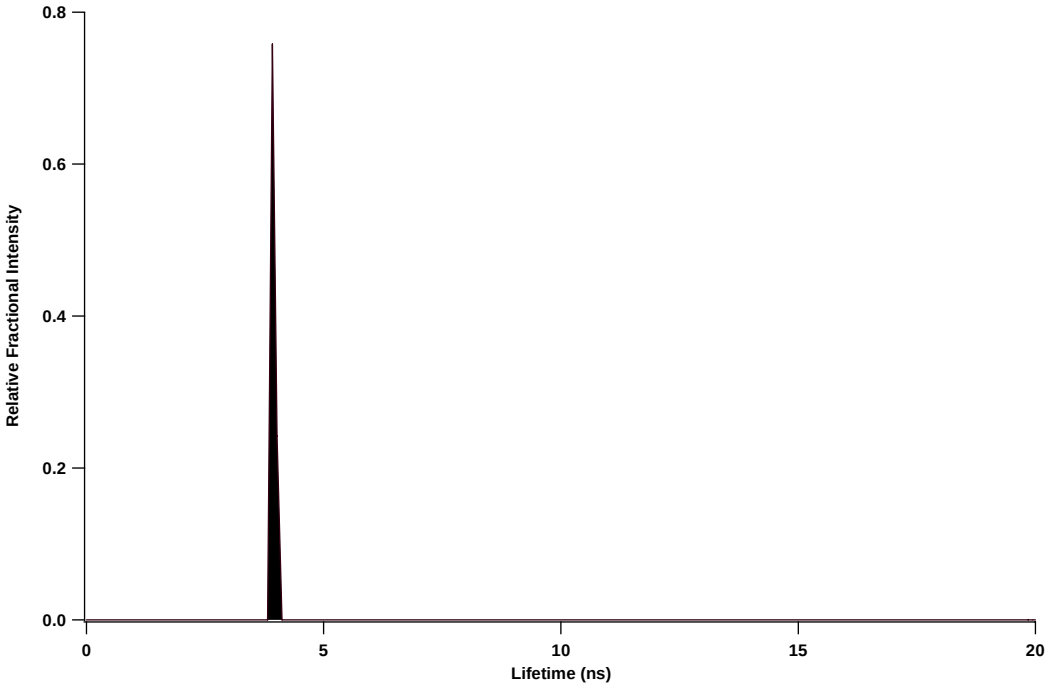

Figure 6.17 Representative MEM plot of the fluorescence lifetime distribution recovered for anthracene in THF.

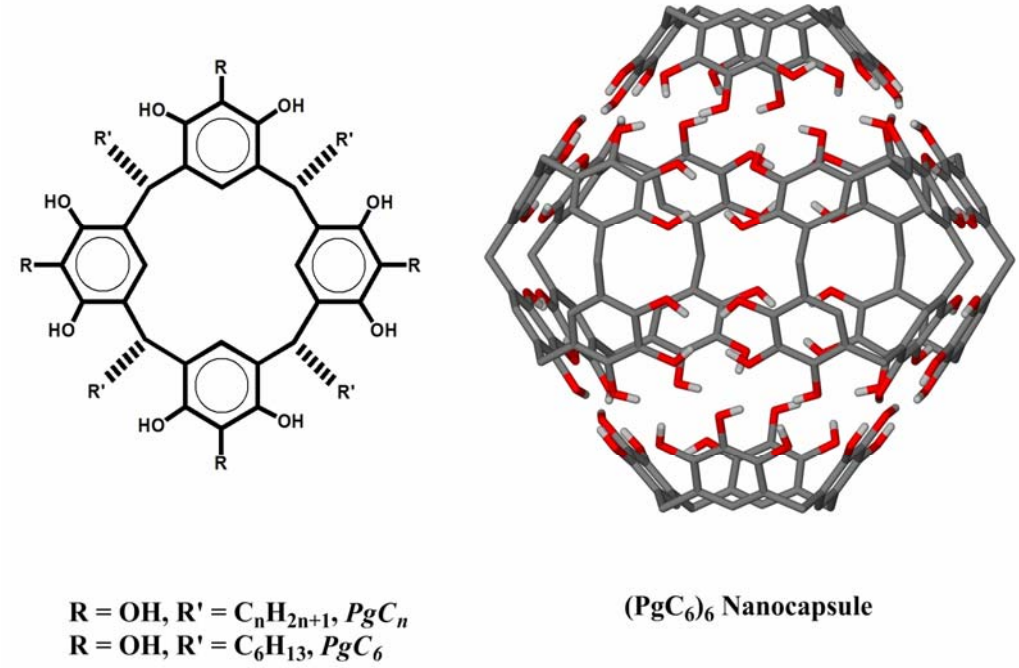

Figure 6.18 Chemdraw of CMRC, PgC*n*, PgC_6, and a diagram of the PgC_6 hexamer framework showing the possible space for molecular encapsulation.

Single-crystal X-ray diffraction and ^{1}H-NMR spectroscopy reveal PgC_6 nanocapsules that have an overall population rate of ~50%, and that are likely to be monopopulated.[30] This is substantially lower than the PBA occupancy rate (150%) and may be attributable to the conformational flexibility of ADMA. The crystal unit cell dimensions closely match those found for PBA-containing nanocapsules, with an interior volume of ~1250 Å^3.[5]

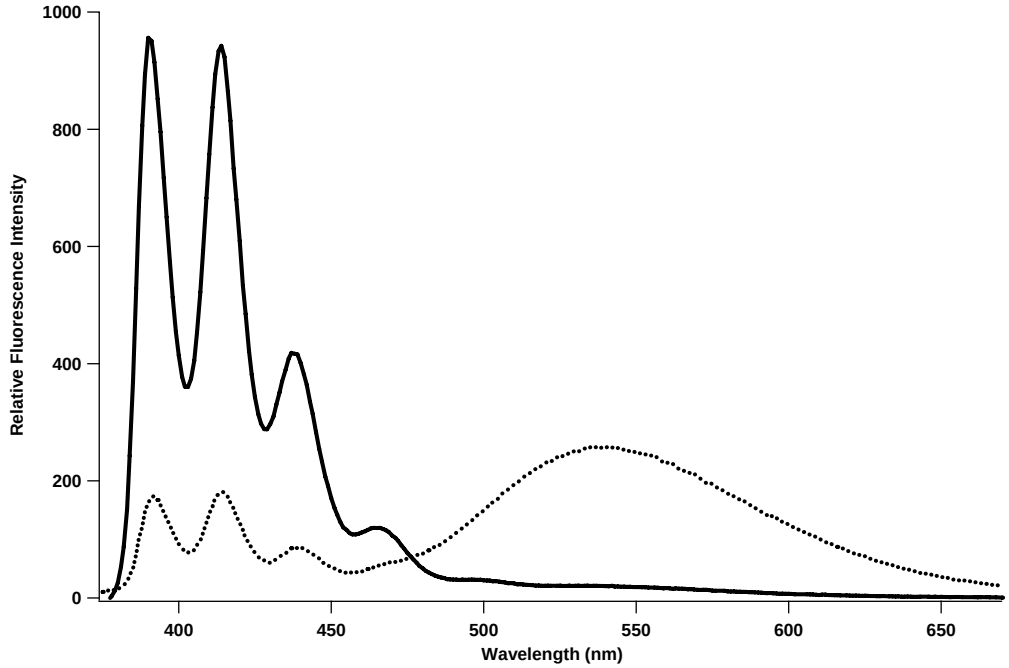

Figure 6.19 Fluorescence emission spectra of the ADMA-ACN-PgC_6 complex (solid), compared with the free ADMA in THF (dotted).

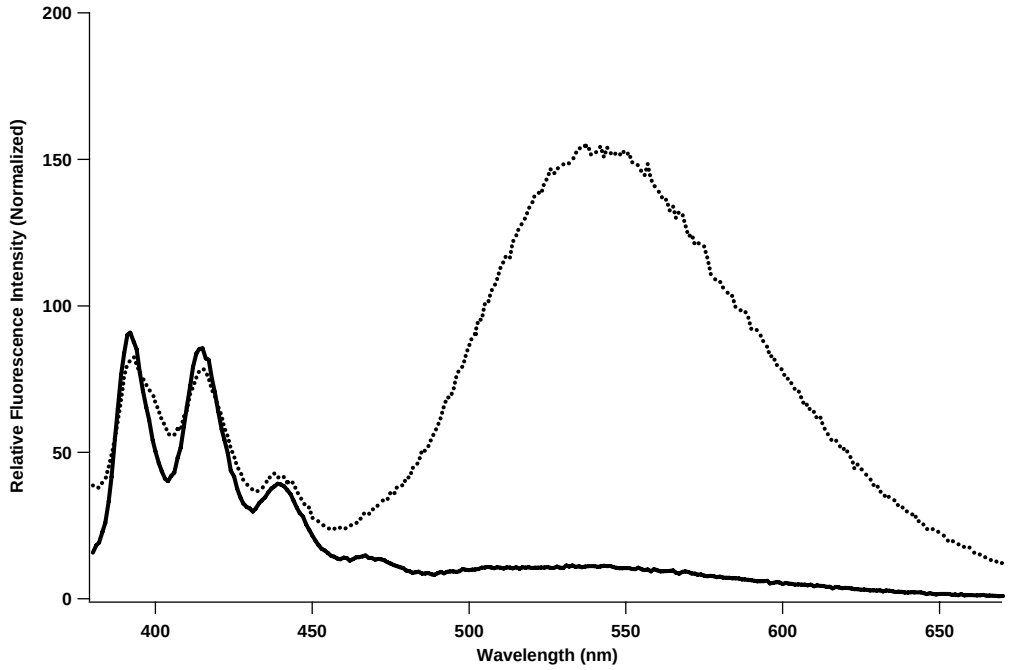

Figure 6.20 Fluorescence emission spectra of the ADMA-EA-PgC_{10} complex (dotted) compared to free ADMA (solid) in THF.

Steady state studies of ADMA-ACN-PgC_6 (Figure 6.19) and -PgC_{10} (Figure 6.20) complexes solutions show little, if any, exciplex emission. Similar results were obtained for both ADMA-EA-PgC_6 (Figure 6.21) and -PgC_{10} capsules (Figure 6.20). These data clearly indicate that ADMA is encapsulated. Moreover, compared to free ADMA, the fluorescence emission intensity of *endo*-ADMA is significantly enhanced (two-fold when encapsulated with EA and five-fold with ACN, Figure 6.21). This enhancement is expected for a fluorophore that is retained and/or constrained in a protective microenvironment. For example, for the ADMA-PgC_6 capsules containing ACN, the

emission intensity is similar to free ADMA in highly viscous mineral oil (Figure 6.13), as mentioned earlier.[10]

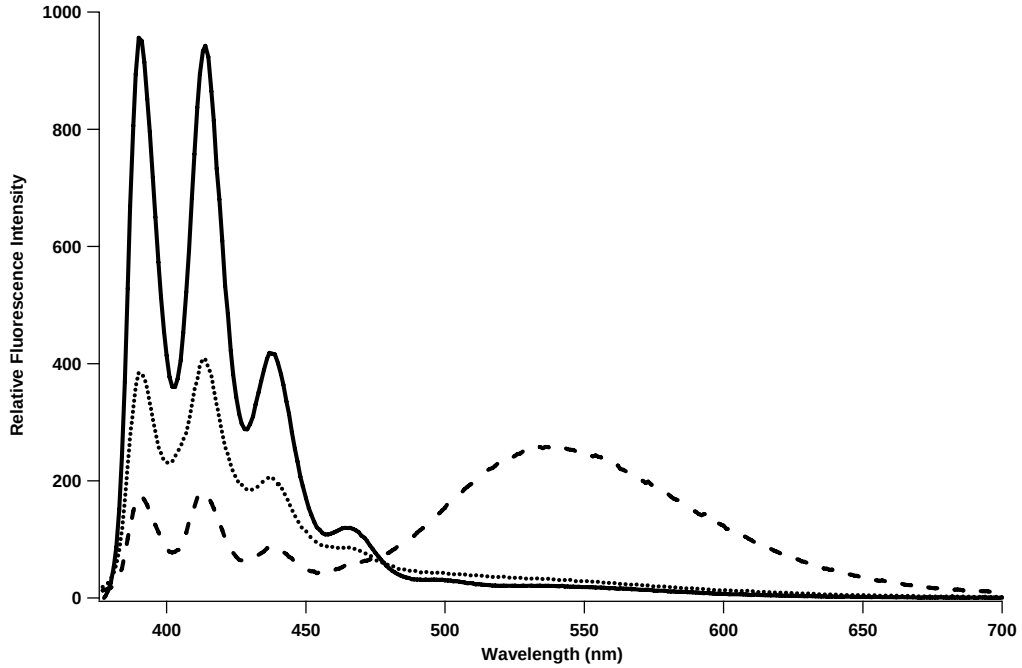

Figure 6.21 Fluorescence emission spectra of the ADMA-ACN-PgC_6 (solid) and ADMA-EA-PgC_6 complexes (dotted) compared to free ADMA (dashed) in THF.

The steady-state data and lifetime results indicate that the encapsulated ADMA is most likely in an extended conformation. For example, it is known that exciplex emission from free ADMA in EA results from a folded ADMA conformation,[12,13] and such emission is not seen for the ADMA-EA-PgC_6 complex (Figure 6.20). In the case where ACN is the solvent, non-emissive CT from free ADMA is energetically more favorable from the extended conformation.[10,13] It is the folded conformation that occasionally leads to CT emission being observed.[10,13]

The stability of the complex was also examined. In Figure 6.22, the intensity of the exciplex emission from the ADMA-ACN-PgC_6 complex is shown to change significantly (10% to 44%) after 12 days. This result indicates that ADMA leaches out of the capsules into the surrounding THF, where it adopts the expected folded conformation that results in exciplex emission. The possibilities of either THF leaching into the capsule, or ADMA folding while inside cannot be ruled out. However, given the environmental limitations of the capsule and the fact that this observation is only made after significant passage of time, this explanation is unlikely. Similar results were not obtained for time-lapse studies of ADMA-EA-PgC_6 complexes. The emission intensity due to the anthracene moiety decreased, without the excepted increase in the exciplex spectral region (*ca.* 540 nm), as seen with ADMA-ACN-PgP_6. Further investigation of free ADMA in EA also indicated anomalous behavior over time; therefore, additional studies of the photophysics of ADMA in EA are being carried out.

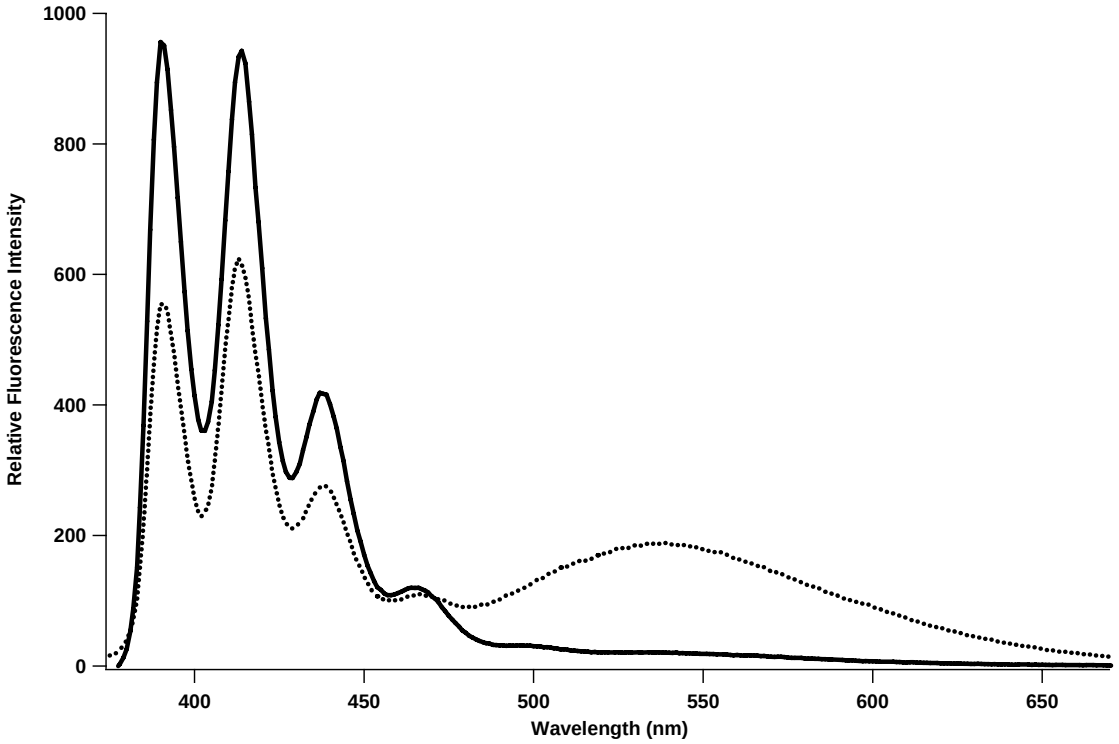

Figure 6.22 Fluorescence emission spectra of the ADMA-ACN-PgC_6 complex at day 0 (solid) and at day 12 (dotted) in THF.

V. Lifetime study:

In general, the fluorescence lifetime data and steady-state emission spectral profiles led to the same conclusion. As mentioned earlier in this Chapter, in THF and EA, the exciplex emission of free ADMA is prominent in both the spectra (Figure 6.12) and the lifetime distribution ($\alpha \approx 0.7$ for τ_3, Table 6.1). Despite there being occasional evidence of very weak exciplex formation in the emission spectrum for ADMA in

ACN,[7,13] no lifetime attributable to exciplex emission is recovered, consistent with the literature.[3,5,10-12,14,20-23]

However, the lifetime distribution of ADMA-ACN-PgC_6 complex (Figure 6.23) does reveal the presence of a minor amount of exciplex emission ($\alpha \approx 0.2$ for τ_3, Figure 6.1). Similar results were obtained for both ADMA-EA-PgC_6 and -PgC_{10} capsules,[30] these data clearly indicate that ADMA is encapsulated if the ADMA were *exo*-capsule, residing in the THF, it would result in a substantial emission (*ca.* 540 nm) and τ_3 lifetime contribution($\alpha \approx 0.70$).

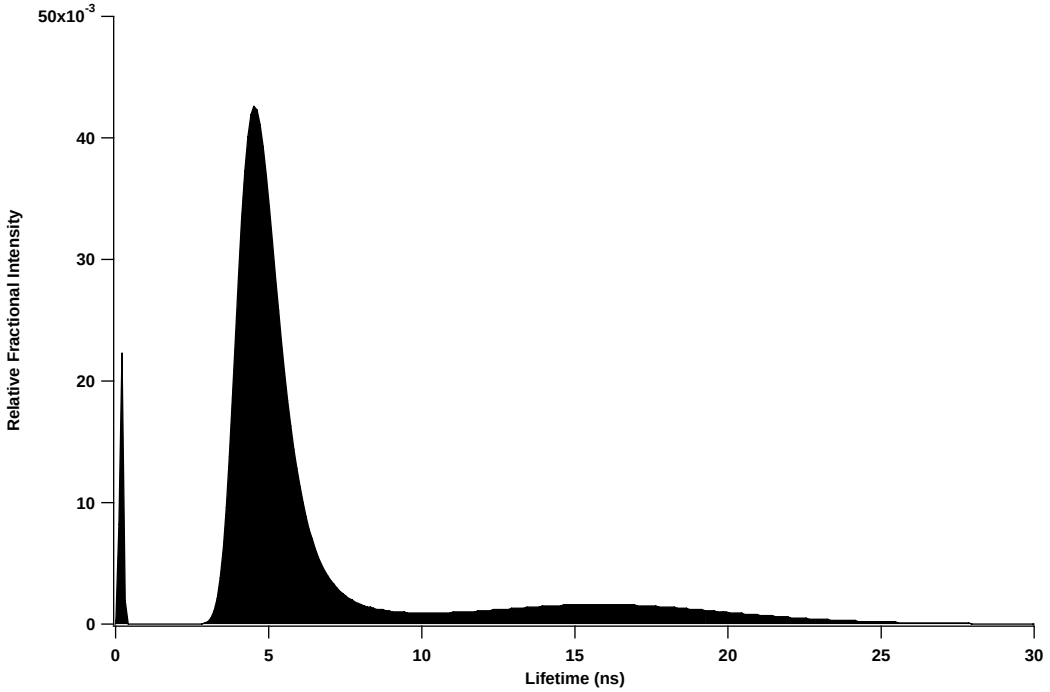

Figure 6.23 Representative MEM plot of the fluorescence lifetime distribution recovered for the ADMA-ACN-PgC_6 complex in THF.

The steady-state data and lifetime results indicate that the encapsulated ADMA is most likely in an extended conformation. for instance, it is known that exciplex emission from free ADMA in EA results from a folded ADMA conformation,[12,13] and such emission is not seen for the ADMA-EA-PgC_6 complex. In the case where ACN is the solvent, non-emissive CT from free ADMA is energetically more favorable from the extended conformation.[10,13] It is the folded conformation that occasionally leads to CT emission being observed.[10,13] The ADMA-ACN-PgC_6 lifetime measurements show a minor amount of exciplex emission, indicating that some population of the ADMA may be in a folded conformation either *endo*- or *exo*-capsule. The extremely small exciplex contribution seen in the emission spectra supports the *endo*-capsule model, as exciplex emission in THF (*exo*-capsule) would be rather pronounced. The general lack of exciplex emission from the ADMA-PgC_n complexes indicates that the majority of the *endo*-ADMA is trapped in the supramolecular assembly in a manner that does not favor folding.

VI. *Exo*-1-(9-anthryl)-3-(4-dimethylaniline) propane:

Occasionally, during the attempt to encapsulate ADMA, smaller and colorless crystals formed instead. Using single crystal X-ray measurement, we determine that ADMA molecules are sitting in between the capsules, intercalated in the channels in these particular crystals (Figure 6.24).[5,30,31] Therefore, the robustness of the assemblies

were interrogated in solution. Immediately after the crystals were dissolved in THF, fast UV-Vis absorption and fluorescence measurements were taken (Figure 6.25). The solution results are in agreement with the X-ray crystals predictions. The initial CT emission was not as intense as expected, and soon after sonication of the solution, the CT emission intensity increases, suggesting that the ADMA is kept in the channels of the crystals arrangement for a short-period of time. The sonication disrupted the aggregation, freeing the ADMA from the matrix, and the subsequent emission profile is similar to the solution of free ADMA in THF.

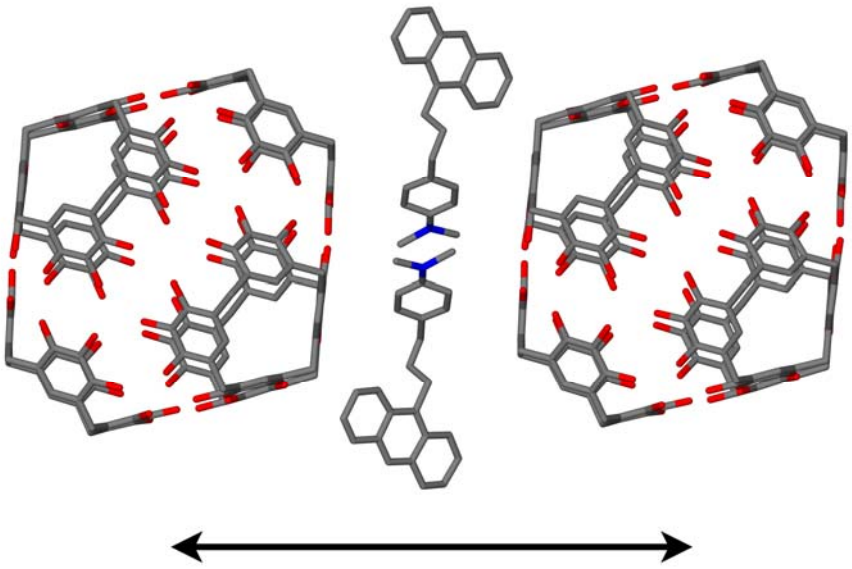

Figure 6.24 Structural illustrations of the *exo*-ADMA molecules intercalated between the nanocapsules spheroids.

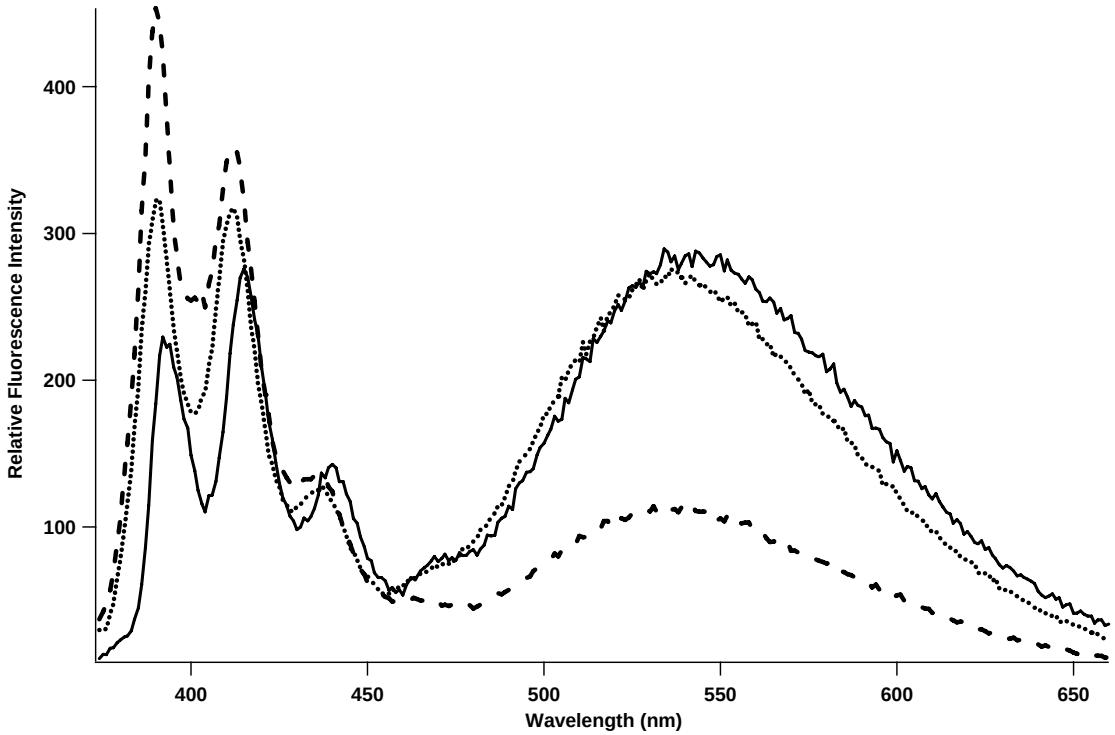

Figure 6.25 Fluorescence emission spectra of the *exo*-ADMA-PgC_6 complex pre-sonication (dashed) and post-sonication (dotted) compared to free ADMA in (solid) THF.

VII. Conclusion:

Solution and solid-state results agree and indicate that ADMA and the crystallization solvents (EA or ACN) are retained in the PgC_6 and PgC_{10} nanocapsules, with *endo*-ADMA in the more energetically favorable extended conformation.[32,33] Similar results were reported by Güsten *et al.* for an ADMA-like molecule in polymeric matrices, where the restricted internal rotation of ADMA prevented the formation of the sandwich conformation and exciplex emission.[34] It is clear, from the spectral data that

the nanocapsule provides a protective microenvironment for the ADMA guest molecule. However, the conformational flexibility of this probe compared to PBA appears to hinder the ease of encapsulation (lower occupancy rates), as well as the robustness (extent of leaching) of this supramolecular assembly.[30] The crystallizing solvent (ACN *vs.* EA) and the *exo*-capsule alkyl tail length (C_6 *vs.* C_{10}) appear to have little effect on the creation and overall nature of these assemblies. These research findings guide our future studies with other reporter molecules with the intent of gaining a better understanding of the versatility of these unique supramolecular assemblies and of directing future synthesis to harness their chemical and physical properties for specific applications.

VIII. References:

(1) Wasielewski, M. R. *Chem. Rev.* **1992**, *92*, 435-61.

(2) Bassil, D. B.; Kauffman, J. F. *Abstr. 38th Mid. Reg. Meet. Am. Chem. Soc.* **2003**, 22.

(3) Khajehpour, M.; Kauffman, J. F. *Chem. Phys. Lett.* **1998**, *297*, 141-146.

(4) Katusin-Razem, B.; Wong, M.; Thomas, J. K. *J. Am. Chem. Soc.* **1978**, *100*, 1679-86.

(5) Dalgarno, S. J.; Tucker, S. A.; Bassil, D. B.; Atwood, J. L. *Science* **2005**, *309*, 2037-2039.

(6) Chuang, T. J.; Cox, R. J.; Eisenthal, K. B. *J. Am. Chem. Soc.* **1974**, *96*, 6828-31.

(7) Crawford, M. K.; Wang, Y.; Eisenthal, K. B. *Chem. Phys. Lett.* **1981**, *79*, 529-533.

(8) Wang, Y.; Crawford, M. K.; Eisenthal, K. B. *J. Phys. Chem.* **1980**, *84*, 2696-2698.

(9) Yang, N.-C. C.; Neoh, S. B.; Naito, T.; Ng, L.-K.; Chernoff, D. A.; McDonald, D. B. *J. Am. Chem. Soc.* **1980**, *102*, 2806-10.

(10) Kauffman, J. F.; Khajehpour, M.; Saleh, N. i. *J. Phys. Chem. A* **2004**, *108*, 3675-3687.

(11) Khajehpour, M.; Kauffman, J. F. *J. Phys. Chem. A* **2000**, *104*, 9512-9517.

(12) Khajehpour, M.; Kauffman, J. F. *J. Phys. Chem. A* **2001**, *105*, 10316-10321.

(13) Okada, T.; Migita, M.; Mataga, N.; Sakata, Y.; Misumi, S. *J. Am. Chem. Soc.* **1981**, *103*, 4715-20.

(14) Saleh, N. i.; Kauffman, J. F. *J. Phys. Chem. A* **2004**, *108*, 7139-7146.

(15) *The molecular volume of ADMA was calculated using the X-Seed program (www.x-seed.net).*

(16) Syage, J. A.; Felker, P. M.; Zewail, A. H. *J. Chem. Phys.* **1984**, *81*, 2233-56.

(17) *X-ray data was collected by Gareth W. V. Cave, 2004.*

(18) Lakowicz, J. R. *Principles of Fluorescence Spectroscopy*; 2nd ed.; Kluwer Academic/Plenum Publishers: New York, 1999.

(19) McGown, L. B.; Hemmingsen, S. L.; Shaver, J. M.; Geng, L. *Appl. Spectrosc.* **1995**, *49*, 60-6.

(20) Gupta, D.; Basu, S. *J. Photochem.* **1975**, *4*, 307-8.

(21) Okada, T.; Fujita, T.; Kubota, M.; Masaki, S.; Mataga, N.; Ide, R.; Sakata, Y.; Misumi, S. *Chem. Phys. Lett.* **1972**, *14*, 563.

(22) Mataga, N.; Nishikawa, S.; Asahi, T.; Okada, T. *J. Phys. Chem.* **1990**, *94*, 1443-7.

(23) Wang, Y.; Crawford, M. C.; Eisenthal, K. B. *J. Am. Chem. Soc.* **1982**, *104*, 5874-5878.

(24) Larson, C. L.; Tucker, S. A. *Appl. Spectrosc.* **2001**, *55*, 679-683.

(25) Richter-Egger, D. L.; Landry, J. C.; Tesfai, A.; Tucker, S. A. *J. Phys. Chem. A* **2001**, *105*, 6826-6833.

(26) Richter-Egger, D. L.; Tesfai, A.; Tucker, S. A. *Anal. Chem.* **2001**, *73*, 5743-5751.

(27) Shaver, J. M.; McGown, L. B. *Anal. Chem.* **1996**, *68*, 611-20.

(28) Shaver, J. M.; McGown, L. B. *Anal. Chem.* **1996**, *68*, 9-17.

(29) Cave, G. W. V.; Antesberger, J.; Barbour, L. J.; McKinlay, R. M.; Atwood, J. L. *Angew. Chem. Int. Ed.* **2004**, *43*, 5263-5266.

(30) Dalgarno, S. J.; Bassil, D. B.; Tucker, S. A.; Atwood, J. L. *Angew. Chem., Int. Ed. Engl.* **2006**, *45*, 7019-7022.

(31) Dalgarno, S. J.; Power, N. P.; Antesberger, J.; McKinlay, R. M.; Atwood, J. L. *Chem. Commun.* **2006**, 3803-3805.

(32) Kizu, N.; Itoh, M. *J. Am. Chem. Soc.* **1993**, *115*, 4799-807.

(33) Takasu, R.; Kizu, N.; Itoh, M.; Shinoda, H. *J. Chem. Phys.* **1994**, *101*, 7364-71.

(34) Gusten, H.; Meinsner, R.; Schoof, S. *J. Photochem.* **1980**, *14*, 77.

Chapter 7: The Encapsulation of Related Probes

I. Encapsulation of perylene:

Perylene (Pe, Figure 7.1) was examined, as it is known to be an anisotropic reporter.[1,2] Therefore, this dye might give information on how freely the molecules tumbles inside the C-alkylpyrogallol[4]arenes, PgC_n, nanocapsules.

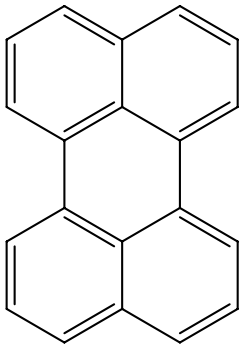

Figure 7.1 Molecular structure of Pe.

The absorbance profile of the free perylene in hexane, HEX (Figure 7.2), and the encapsulated perylene, Pe-PgC_6, dissolved in HEX show a similar phenomenon seen in the absorbance profile of pyrene butyric acid (PBA, Figure 5.4). The absorption spectrum of perylene entrapped in the spheroids displays the extra shoulder that was attributed to π-interaction with the interior wall of PgC_6.[3]

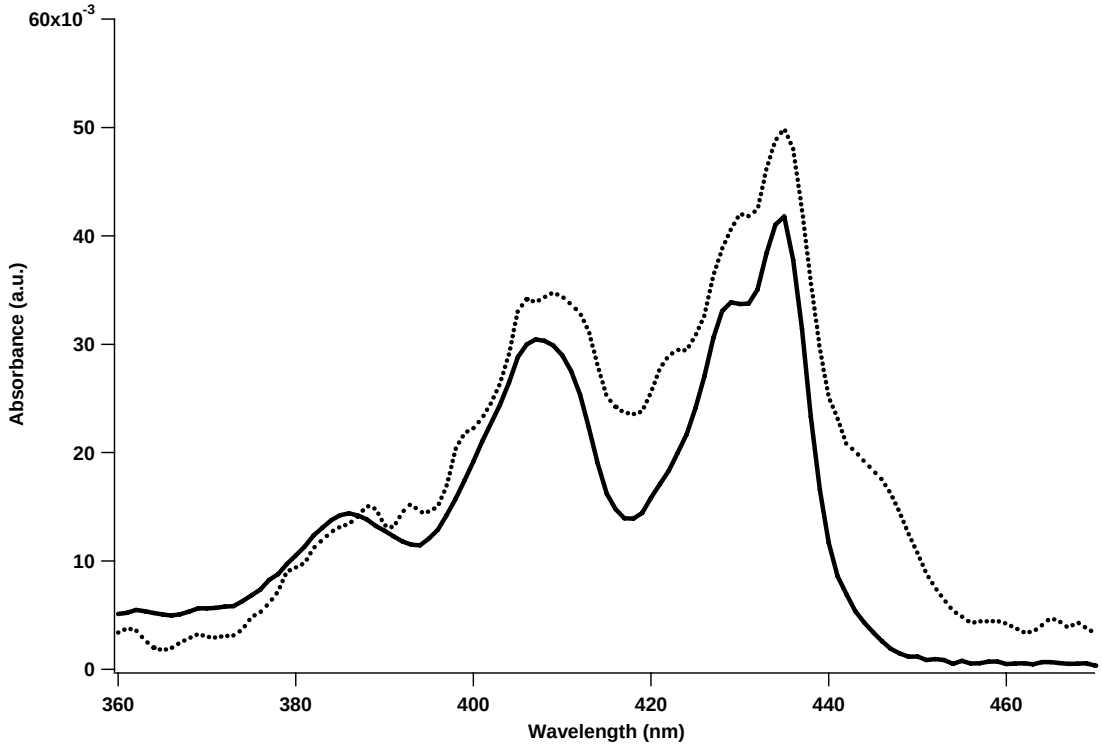

Figure 7.2 Absorbance spectra of free Pe (solid) and Pe-PgC_6 in HEX (dotted).

Initially, it appeared that Pe may encapsulate in a similar fashion to PBA, particularly given the single crystal X-ray determination, which also showed possible π-interaction with the interior PgC_6 wall. However, the fluorescence emission spectra (Figure 7.3) do not follow the expected trend. Indeed, the fluorescence emission intensity of Pe-PgC_6 is actually in the similar order of magnitude. Successful encapsulation with previous probes showed enhancement in the fluorescence emission intensity of the complex compared to the free probe. Additional quenching and anisotropy studies are also in agreement with the fluorescence emission data.

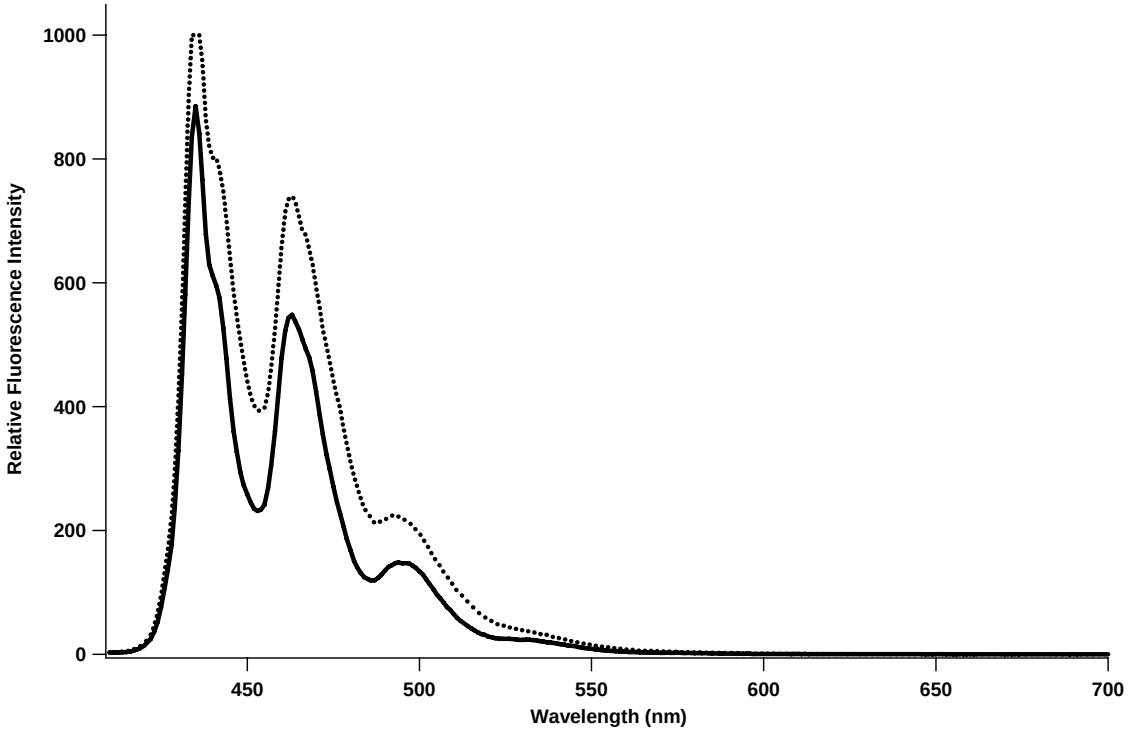

Figure 7.3 Fluorescence emission spectra of Pe-PgC_6 (dotted) and free Pe (solid) in HEX. (λ_{ex} = 408).

Quenching measurements were performed in three neat solvents (HEX, tetrahydrofuran, THF and acetonitrile, ACN) with two different quenchers (*N*,*N*-dimethylaniline, DMA, and triethylamine, TEA). The extent of quenching (40%) for both free Pe and Pe-PgC_6 was the same. The anisotropy values obtained under the same conditions for free Pe (r = 0.17 ± 0.01) and Pe-PgC_6 (r = 0.16 ± 0.01) were also identical. All fluorescence results indicate that the PgC_6 nanocapsule does not hold Pe inside, unlike with the previous probes. It is possible that the shoulder seen in the absorption spectrum is due to π-stacking with the probe and single pyrogallol moieties.

II. Encapsulation of benzo[a]pyrene:

Benzo[a]pyrene (B[a]P; Figure 7.4) is a larger polycyclic aromatic hydrocarbon, PAH, than pyrene, but still highly planar.[4,5] This carcinogenic PAH is one the most studied molecules because of its affect on the human health.[6,7] In theory, this molecule that has a length of almost ~11 Å does not have room to sit in the heart of a PgC_6 nanocapsule, but may sit along the diagonal. Therefore, would be surprising if we observe successful encapsulation retained in solution.[8]

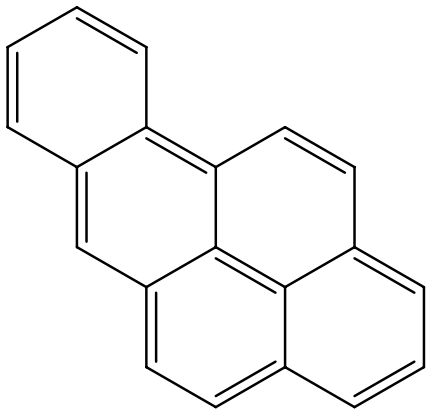

Figure 7.4 Molecular structure of B[a]P.

Figure 7.5 shows that emission spectra of both free and B[a]P-PgC_6 are similar except that for in the B[a]P-PgC_6 sample some of the fine structure is lost, as seen with the PBA.[3] There is also a small (5 nm) red shift within the B[a]P-PgC_6 emission spectrum.

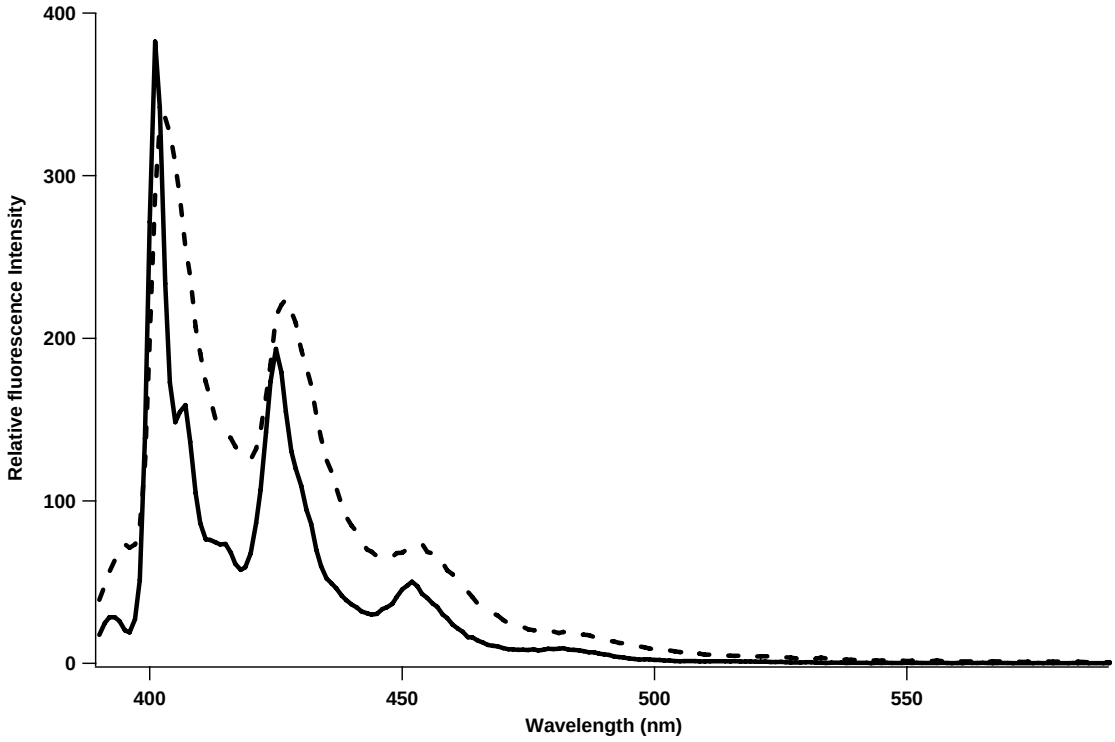

Figure 7.5 Fluorescence emission spectra of B[a]P-PgC_6 (dashed) and free B[a]P (solid) in HEX. (λ_{ex} = 384 nm).

Quenching studies were performed with quenchers TEA and DMA and B[a]P-PgC_6 was dissolved in ACN, THF, and HEX. Results are reported in HEX with DMA, where charge transfer, (CT) is emissive (*ca.* 470 nm). As seen in Figure 7.6 and 7.7, both free B[a]P and B[a]P-C_6 have similar fluorescence emission profiles and showed same extent of quenching (~60%). Fluorescence emission was also measured in presence and in the absence of oxygen a known quencher, by bubbling ultra-pure nitrogen through the cuvette for five minutes. The only change was the intensity that was enhanced three times for both samples: free B[a]P and B[a]P-PgC_6 in HEX.

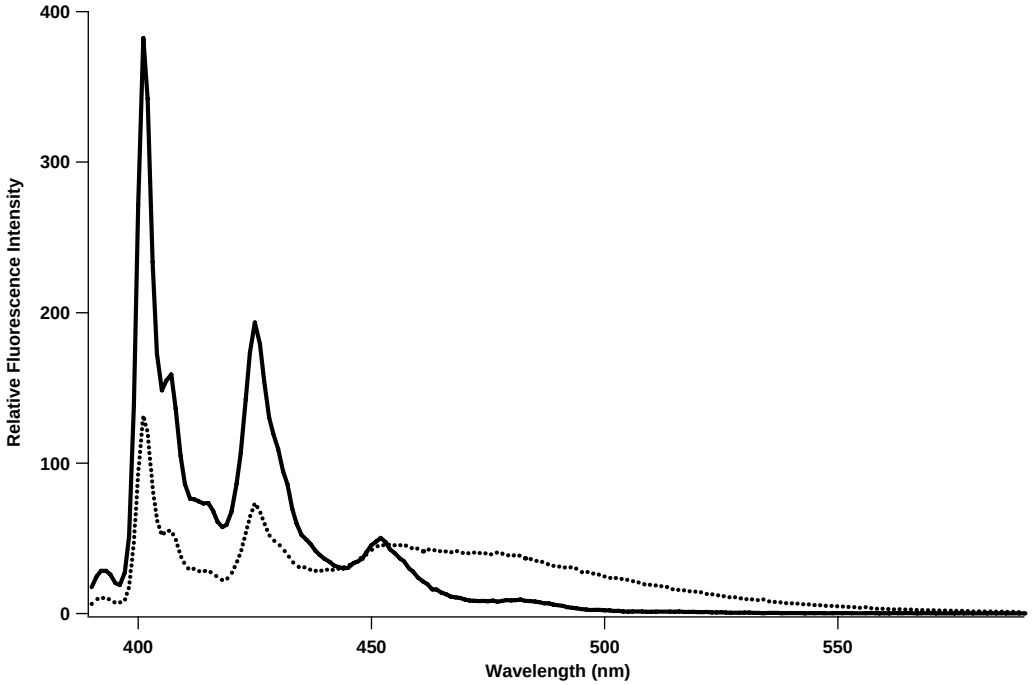

Figure 7.6 Fluorescence emission spectra of free B[a]P (solid) in HEX + 10 μL DMA (dotted). (λ_{ex} = 384 nm).

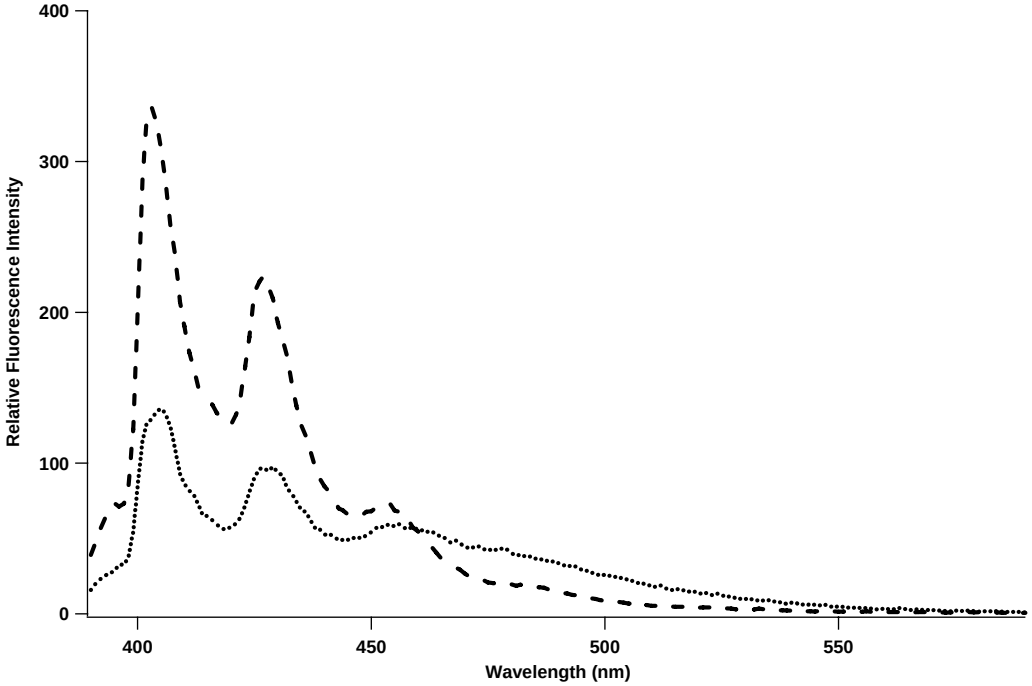

Figure 7.7 Fluorescence emission spectra of B[a]P-PgC_6 (dashed) + 10 μL DMA (dotted) in HEX. (λ_{ex} = 384 nm).

Fluorescence lifetime measurements were also taken and recorded values are in Table 7.1. Lifetime of B[a]P (~ 8 ns, Figure 7.8) are shorter than that reported in the literature,[9-11] because samples are not deoxygenated. Two lifetimes are recovered for B[a]P-PgC_6 samples (Figure 7.9). The shorter lifetime (~7 ns) appears to be free B[a]P in HEX and is the majority of the signal (~80%). The second lifetime (~25 ns) is significantly longer, indicating potential encapsulation, for a small amount (~20%) of B[a]P. However, DMA addition leads to nearly identical lifetime recoveries for both free B[a]P and B[a]P-PgC_6 (Figures 7.10 and 7.11): The ~8 ns lifetime attributed to unencapsulated B[a]P and ~ 2 ns lifetime to the exciplex emission, only accounting for ~5% of the signal.

Sample	τ_1	(α_1)	τ_2	τ_2	(α_2)	τ_3
B[a]P in HEX	-	-	-	-	8.03	(1.00)
B[a]P + DMA in HEX	-	-	1.61	(0.06)	8.03	(0.94)
B[a]P-PgC_6 in HEX	0.00	(0.08)	7.22	(0.81)	25.66	(0.19)
B[a]P-PgC_6 + DMA in HEX	0.21	(0.03)	2.21	(0.07)	8.03	(0.90)

a Using the 389-610 nm filter combination.

Table 7.1 Representative fluorescence lifetimes (τ) and fractional intensities (α) of free and B[a]P-PgC_6 recovered using MEM analysis.[a]

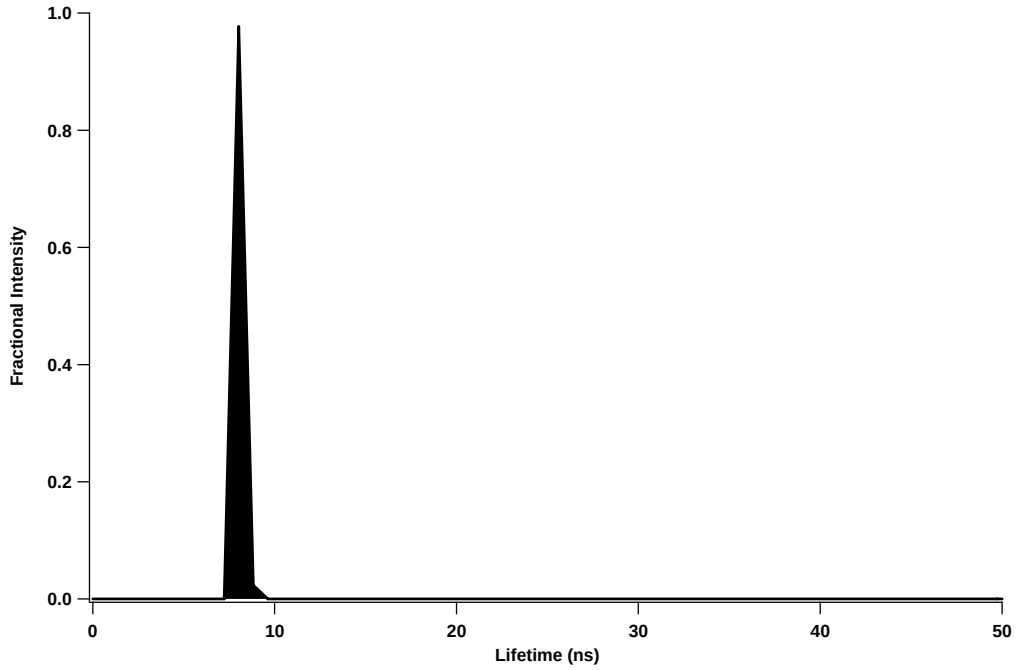

Figure 7.8 Representative MEM plot of the fluorescence lifetime distribution recovered for free B[a]P in HEX.

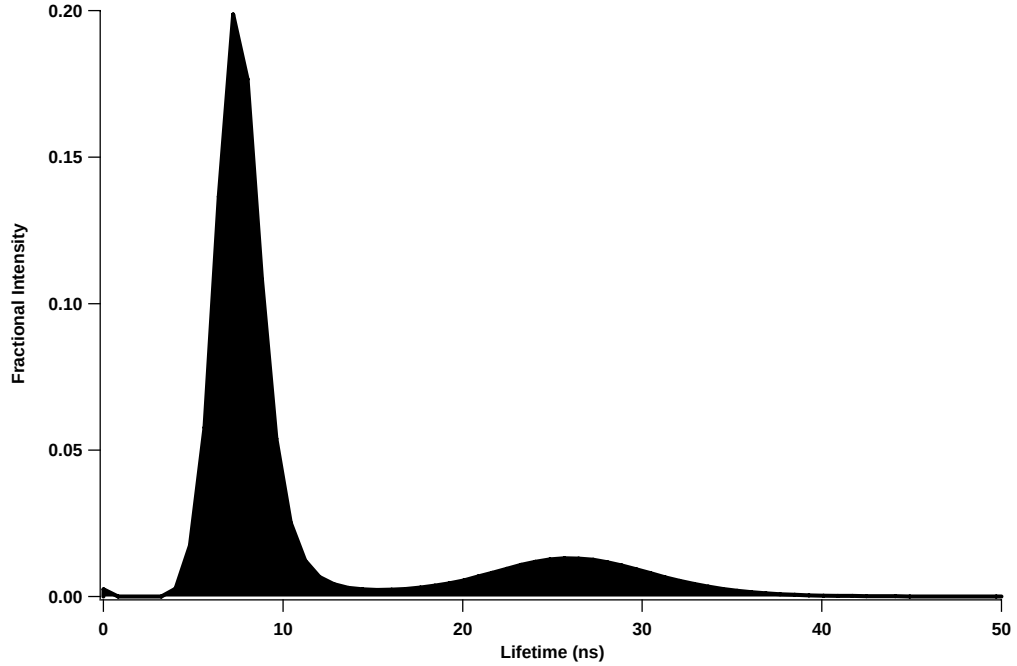

Figure 7.9 Representative MEM plot of the fluorescence lifetime distribution recovered for B[a]P-PgC_6 in HEX.

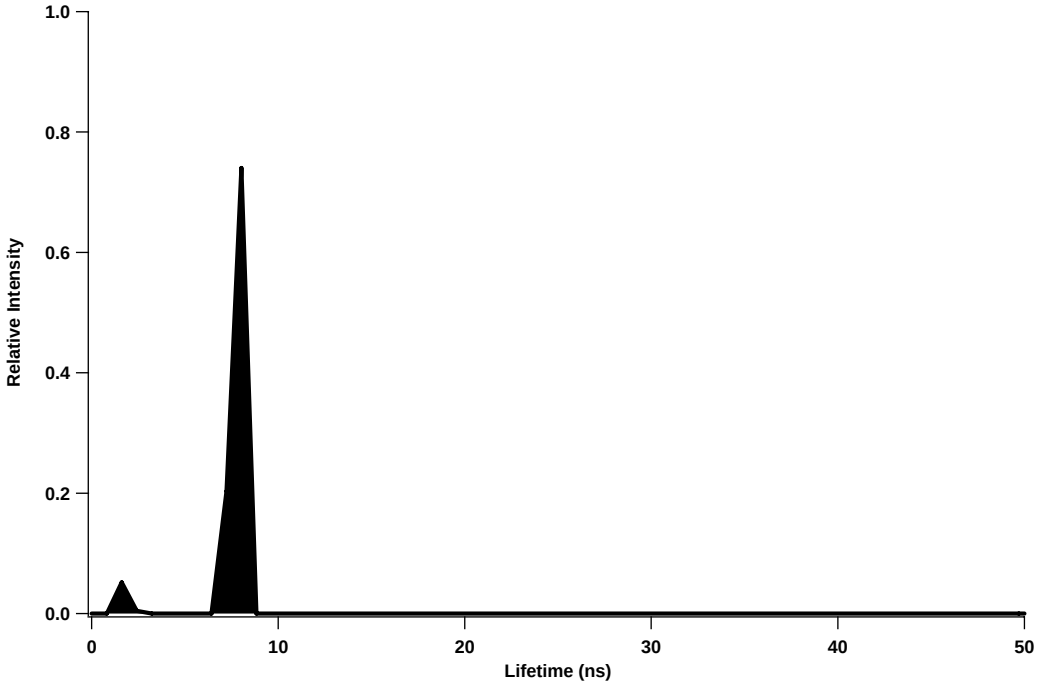

Figure 7.10 Representative MEM plot of the fluorescence lifetime distribution recovered for free B[a]P in HEX + 10 μL DMA.

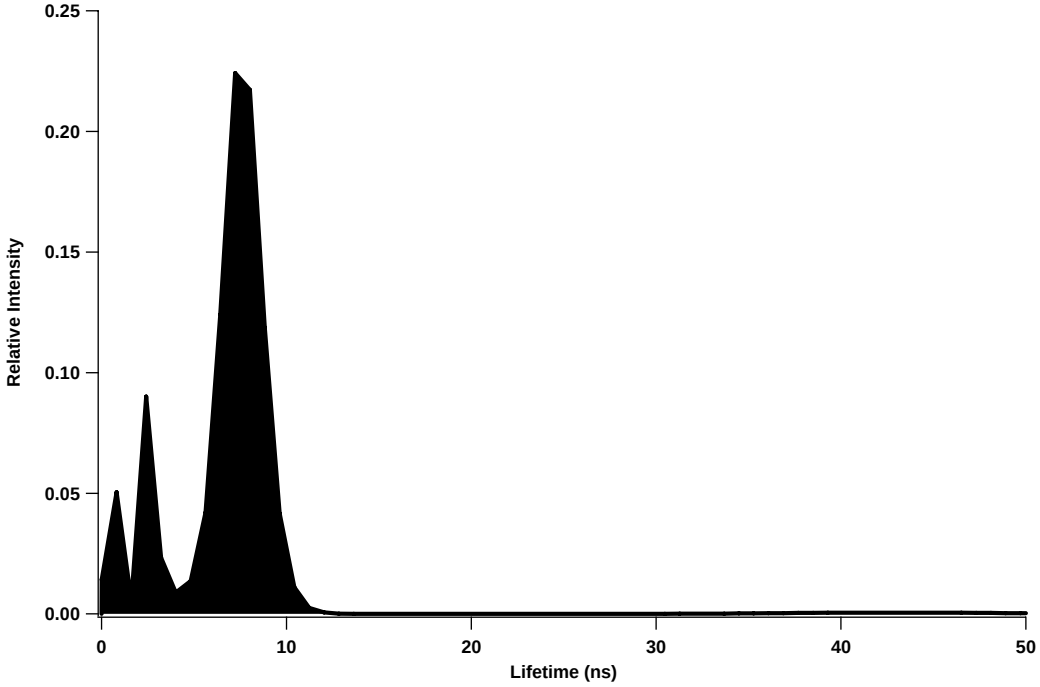

Figure 7.11 Representative MEM plot of the fluorescence lifetime distribution recovered for B[a]P-PgC_6 in HEX + 10 μL DMA.

Overall, we did not have any indication that B[a]P remains sequestered in solution. For example, the lifetime of B[a]P free (8.03 ns) is the same lifetime recovered for B[a]P-PgC_6 after adding DMA. Before the DMA addition, the longer lifetime (25.66 ns) for B[a]P-PgC_6 may have indicated encapsulation, but the addition of DMA. The longer lifetime for B[a]P-PgC_6 may actually be a B[a]P aggregate, as sparingly. Soluble polycyclic aromatic hydrocarbons are known to form higher ordered species and microcrystals.[12]

III. Encapsulation of pentacene and anthraquinone:

Pentacene (Pen, Figure 7.12) and anthraquinone (Aq, Figure 7.13) were examined since diversity in the probes was sought. Pentacene has a long linear structure, and Aq has additional chemical functionality. The encapsulation attempt of Pen and Aq was suggested to be successful in solid state. However, solution studies were inclusive. No spectral evidence showed that either probe was entrapped, and all results suggested that these reporters were not retained by the nanocapsules. UV-Vis absorbance, fluorescence emission, fluorescence lifetime and quenching experimental data were the same. The negative results might be due to the low solubility of Pen, and due to the carbonyl groups of Aq. In both cases, X-ray data indicated the geometrical constraints altered the hexameric spheroid preventing encapsulation.

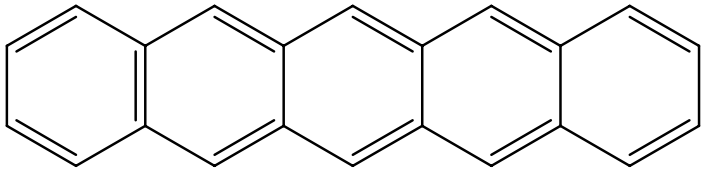

Figure 7.12 Molecular structure of Pen.

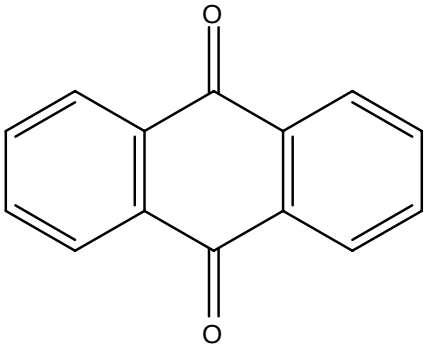

Figure 7.13 Molecular structure of Aq.

IV. Conclusion:

Perylene and B[a]P both show questionable encapsulation, especially in solution, where fluorescence studies showed the similar results for both the free form and encapsulated form. These two probes are planar and larger than the ones (PBA and ADMA) we successfully entrapped previously. We used Aq as a potential probe since it is not planar, and it had additional chemical functionality that might have promoted internal hydrogen bonding with the interior walls. However, the results were contradictory and no spectral evidence of entrapment was obtained. Pentacene, the

largest probe considered, was not encapsulated by PgC_n, as expected. This work illustrated that the nature of guest is a critical parameter in successful entrapment. Moreover, geometrical constraints of the host-guest interaction are also a key factor.

IV. References:

(1) Jiang, Y.; Blanchard, G. J. *J. Phys. Chem.* **1994**, *98*, 6436-6440.

(2) Lakowicz, J. R. *Principles of Fluorescence Spectroscopy*; Plenum Press: New York, 1983.

(3) Dalgarno, S. J.; Tucker, S. A.; Bassil, D. B.; Atwood, J. L. *Science* **2005**, *309*, 2037-2039.

(4) Carrell, C. J.; Carrell, T. G.; Carrell, H. L.; Prout, K.; Glusker, J. P. *Carcinogenesis* **1997**, *18*, 415-422.

(5) Huggins, C. B.; Pataki, J.; Harvey, R. G. *Proc. Natl. Acad. Sci.* **1967**, *58*, 2253-60.

(6) Li, Z.; Kim, H. Y.; Tamura, P. J.; Harris, C. M.; Harris, T. M.; Stone, M. P. *Biochemistry* **1999**, *38*, 14820-14832.

(7) Utesch, D.; Glatt, H.; Oesch, F. *Cancer Research* **1987**, *47*, 1509-15.

(8) *The molecular length of benzo[a]pyrene was calculated using Chem3D Ultra 10.0 (www.CambridgeSoft.com)*.

(9) Desilets, D. J.; Kissinger, P. T.; Lytle, F. E. *Anal. Chem.* **1987**, *59*, 1830-4.

(10) Nithipatikom, K.; McGown, L. B. *Appl. Spectrosc.* **1986**, *40*, 549-53.

(11) Iwata, T.; Hori, A.; Kamada, T. *Optical Review* **2001**, *8*, 326-330.

(12) Srikanth, M.; Vasudevan, N.; Matthias, K. *Appl. Microbiol. Biotechnol.* **2005**, *V67*, 569-576.

Chapter 8: Conclusions

This project put the collaboration of the Tucker group and the Atwood group ahead of many scientists who are trying to retrieve information from these nanocapsules in solution, where very little is known. The literature is rich in only solid state studies.[1-13]

The main achievement of this collaborative effort is that we were able to apply highly sensitive analytical technique to probe a self-assembled nanocapsules in solution.[14,15] Fluorescence measurements provided complementary information to the typical single-crystal X-ray crystallography data, especially when the low occupancy of the crystals gave an interior that was irresolvable.

Several host-guest parameters were explored in this work, such as the geometrical properties of the host and the guest (e.g. planar), the nature of host (e.g. tail length) and guest (e.g. chemical appendages) and the fit between host and guest. By attempting to encapsulate a diversity of probe types, we can now hypothesize and potentially predict up front successful of the entrapment.

This work indicates that the guest must be smaller that the host and have very little conformational flexibility or it will be difficult to entrap, as evidence by pyrene butyric acid (PBA) versus 1-(9-anthryl)-3-(4dimethylaniline) propane (ADMA) results. Furthermore, the successful, sustained entrapment appears to be significantly enhanced by the presence of chemical functionality capable of docking the molecules, as evidence by the PBA versus pyrene (Py) studies. The lack of a probe appendage or flexibility also

contributes to leaching from the capsules even after the appearance of initial entrapment as evident by the Py and ADMA data. While harder to monitor experimental data simply suggests that π-interaction with capsules interior walls are necessary for entrapment. This magnet-like arrangement also prevents leaching (PBA vs. ADMA results).

However, there were experimental factors that appear to have little affect on entrapment. The alkyl tail length on the exterior of the nanocapsules did not facilitate or prevent entrapment of ADMA, as experimental results were similar for hexyl and decyl tails. The crystallization solvent, which becomes entrapped with the guest, also does not appear to enhance or diminish encapsulation. For ADMA, both ethyl acetate and acetonitrile results were comparable.

This research is an ongoing project, and the goal is to gather additional data based on these concepts. For example, given the success of PBA, it is important to investigate the linker appendage. The length of the appendage (C_4) and chemical functionality (acid group) should be systematically changed to determine optimal guests.

Once a database is generated, one can begin to successfully predict encapsulation and gain a theoretical understanding of the encapsulation process, learning what the driving force is. Having a theoretical framework will be of great use in many applications of supramolecular chemistry.

References:

(1) Antesberger, J.; Cave, G. W. V.; Ferrarelli, M. C.; Heaven, M. W.; Raston, C. L.; Atwood, J. L. *Chem. Commun.* **2004**.

(2) Atwood, J. L.; Barbour, L. J.; Dalgarno, S. J.; Hardie, M. J.; Raston, C. L.; Webb, H. R. *J. Am. Chem. Soc.* **2004**, *126*, 13170-13171.

(3) Atwood, J. L.; Barbour, L. J.; Jerga, A. *Chem. Commun.* **2001**, 2376-2377.

(4) Atwood, J. L.; Barbour, L. J.; Jerga, A. *J. Supramol. Chem.* **2002**, *1*, 131-134.

(5) Atwood, J. L.; Barbour, L. J.; Jerga, A. *Proc. Natl. Acad. Sci.* **2002**, *99*, 4837-4841.

(6) Atwood, J. L.; Barbour, L. J.; Jerga, A. *Angew. Chem., Int. Ed.* **2004**, *43*, 2948-2950.

(7) Cave, G. W. V.; Antesberger, J.; Barbour, L. J.; McKinlay, R. M.; Atwood, J. L. *Angew. Chem. Int. Ed.* **2004**, *43*, 5263-5266.

(8) Cave, G. W. V.; Antesberger, J.; Barbour, L. J.; McKinlay, R. M.; Atwood, J. L. *Angew. Chem., Int. Ed.* **2004**, *43*, 5263-5266.

(9) Cohen, Y.; Avram, L.; Frish, L. *Angew. Chem., Int. Ed.* **2005**, *44*, 520-554.

(10) Dalgarno, S. J.; Power, N. P.; Antesberger, J.; McKinlay, R. M.; Atwood, J. L. *Chem. Commun.* **2006**, 3803-3805.

(11) Dietrich, B.; Lehn, J. M.; Sauvage, J. P. *Tet. Lett.* **1969**, 2885-8.

(12) MacGillivray, L. R.; Atwood, J. L. *Nature* **1997**, *389*, 469-472.

(13) Rebek, J., Jr. *Angew. Chem., Int. Ed.* **2005**, *44*, 2068-2078.

(14) Dalgarno, S. J.; Bassil, D. B.; Tucker, S. A.; Atwood, J. L. *Angew. Chem., Int. Ed. Engl.* **2006**, *45*, 7019-7022.

(15) Dalgarno, S. J.; Tucker, S. A.; Bassil, D. B.; Atwood, J. L. *Science* **2005**, *309*, 2037-2039.

VITA

Daniel B. Bassil was born on September 7, 1977, in Hadeth El-Joubbeh, Bshari; Lebanon, where he went to the "Mission Laïque Française" High School. He received his Bachelor of Science degree in chemistry in 2000 from the Lebanese University II, Beirut. He was awarded a scholarship from the International Centre for Advanced Mediterranean Agronomic Studies (Paris, France) and received his Master's degree in 2002 from their Institute (M.A.I.Ch.) in Chania, Greece. His thesis research involved the evaluation of the antioxidant properties of 2-*S*-cysteinylcaffeic acid. He joined the Department of Chemistry at the University of Missouri – Columbia in August 2002. He pursued his PhD in analytical chemistry under the supervision of Professor Sheryl A. Tucker. His research project was a collaboration with Professor Jerry L. Atwood in the Department. He completed his doctoral degree in February, 2007.